Conductivities of magnetic chains with (non-)magnetic impurities

Alexandros Metavitsiadis

Physics Department, University of Crete

Submitted in partial fulfillment of the requirements for the degree of

Doctor of Philosophy

Supervisor: Xenophon Zotos

July 2010

We approve the thesis of *Alexandros Metavitsiadis*

Signature

Christos Panagopoulos
Associate Professor of Condensed matter physics

Nikos Papanicolaou
Professor of Theoretical high energy physics

Ilias Perakis
Professor of Condensed matter physics

Peter Prelovšek
Professor of Condensed matter physics

George Tsironis
Professor of Condensed matter physics

Panagiotis Tzanetakis
Professor of Condensed matter physics

Xenophon Zotos
Professor of Condensed matter physics
Thesis Adviser, Chair of Committee

July 2 2010

Acknowledgments

This thesis would have never been accomplished unless many people have helped me in many different levels. It is a pleasure to devote a few lines to convey my appreciation.

First and foremost, I owe my sincerest gratitude to my supervisor, Professor Xenophon Zotos, for his supervision, guidance, and advice throughout all these years. I would also like to thank him for his patience and kindness, his trust, and for providing the best conditions to work undisturbed.

I am also indebted to Professor Peter Prelovšek for his advice and guidance, his elaborative responds to my questions and his overall crucial contribution to this work. Moreover, I would like to express my appreciation for his hospitality in Ljubljana. Our collaboration was a great honor for me.

I gratefully acknowledge my collaboration with Osor S. Barišić, his recommendations, our discussions and the exchange of ideas were very fruitful and beneficial for me.

It was a great pleasure to meet and collaborate with Anna Gorczyca; despite the short time our meeting lasted she had a great influence on me.

I would also like to thank Myron D. Kapetanakis for his help, advice, suggestions, and discussions, as well as for conveying his experience to me.

I am grateful to the personnel of the computer center of the physics department and the computer center of IESL institute at FORTH and especially D. Counalakis, A. Psyllaki and M. Giatromanolakis for their help and their immediate response to numerous problems occurred during these years.

I would also like to thank several people of my friendly and academic environment. I owe special thanks to my good friends Nondas, Dimitris, George, Georgia, Melina and Marina. Each and everyone of these people had a direct or indirect but in any case rather significant contribution to the accomplishment of this work. I should also individually acknowledge Marina's unique ability to spot bugs at a glance as well as her help to overcome many more difficulties. Last but not least, I would like to thank my family for their support and understanding.

Abstract

The field of low dimensional quantum systems remains active for decades for both theoretical and experimental research. This work is a contribution to the theoretical study of one-dimensional quantum magnets. In parallel with our theoretical study, several experimental teams all around the globe work to fabricate novel materials which are highly anisotropic and can be considered as good realizations of one-dimensional systems. Moreover, the unconventional transport properties of these systems makes them very promising candidates for technological applications.

We focus on the transport properties of one-dimensional quantum magnets described by the celebrated anisotropic Heisenberg Hamiltonian. In the pure spin-$\frac{1}{2}$ Heisenberg model, which is an integrable model, heat transport is really unique since the energy current is a constant of motion leading to ballistic heat transport. Thus, the interplay of integrability and defects is theoretically challenging and we attempt to shed light on various aspects of this issue employing primarily numerical diagonalization techniques.

First, we discuss the effect of static disorder accounting for the onset of Anderson localization. In a many body system interactions can delocalize the localized states leading the system to a diffusive state. The main conclusion is that the dc transport of the many body system is finite for any finite temperature. On the contrary, at zero temperature for the interacting system or at any temperature for the non-interacting one, spin and thermal dc conductivities vanish in the strong disorder regime.

Second, we consider the more subtle effect of a single non-magnetic impurity and whether this perturbation is capable to break the integrability of the system. We use as criteria for the breaking of integrability the level statistics of the system and the spin stiffness in the easy plane regime. Moreover, for a single impurity case it turns out that the thermal conductivity is a unique probe since the only scattering mechanism for the thermal transport comes from the impurity. We show that a single impurity in a many body system renders ballistic transport incoherent at high energies in contrast with the non-interacting case where the impurity only renormalizes the charge stiffness.

Third, is the effect of a single magnetic impurity of spin S disturbing the spin-$\frac{1}{2}$ Heisenberg chain. We consider the impurity to be located either out of the chain or to be embedded to it. In the former case, we find a universal scaling with both the lattice size, and the perturbation strength. On the other hand, the embedded impurity in the chain is a severe perturbation and dominates easily the behavior of the transport

quantities. Useful conclusions can be obtained by analytical arguments in the strong host-impurity coupling limit.

Last, as far as the temperature dependence is concerned for the single impurity cases, we seek cutting-healing phenomena. More particularly, for decreasing temperature we find that the chain is (cut)healed for (anti)ferromagnetic easy axis anisotropy for all types of single impurities—single weak link, local field, magnetic impurity out of the chain, magnetic impurity embedded in the chain. In the same concept is the (cutting)healing of the isotropic Heisenberg chain with decreasing temperature in the presence of (a single)two consecutive weak links.

Contents

The 1D world

Low dimensional quantum systems are of high theoretical interest since the reduced dimensionality, interactions, and quantum fluctuations assign fascinating properties to them in comparison with the normal, the three dimensional ones. Especially in one dimension (1D) strong quantum fluctuations modify the properties of these systems leading to new kinds of excitations. The ordinary quasiparticle Fermi liquid theory breaks down in 1D since the discontinuity at the Fermi surface vanishes and quasiparticles are not well defined. The counterpart of the Fermi liquid theory in 1D is the so-called Luttinger liquid (LL) [1–5]. Within LL the low energy excitations of fermionic systems are holons and spinons [6, 7] with the remarkable prediction of spin charge separation [8, 9]—the spin and charge degrees of freedom of an electron can be separated since the elementary excitations of each degree of freedom propagate with a different velocity.

There are several 1D effective lattice models proposed to describe various physical systems [10], but we choose to present here explicitly only three of them:[1] The anisotropic spin Heisenberg model,

$$\mathcal{H}_S = J \sum_l \left(S_l^+ S_{l+1}^- + S_l^- S_{l+1}^+ \right) + J_z \sum_l S_l^z S_{l+1}^z \, ,$$

with the isotropic point given for $J_z = 2J$. The t-V model, which describes interacting tight binding spinless fermions with an intersite interaction,

$$\mathcal{H}_{t-V} = -t \sum_l \left(c_l^\dagger c_{l+1} + c_{l+1}^\dagger c_l \right) + V \sum_l n_l n_{l+1} \, .$$

Note that the Heisenberg model and the t-V model are exact mapping of one another using the celebrated Jordan Wigner transformation which corresponds fermionic operators to spin operators and vice versa. Lastly, the Hubbard model, which describes interacting tight binding fermions with intrasite interactions,

$$\mathcal{H}_H = -t \sum_l \left(c_{l\sigma}^\dagger c_{l+1\sigma} + c_{l+1\sigma}^\dagger c_{l\sigma} \right) + U \sum_l n_{l\uparrow} n_{l\downarrow} \, .$$

[1] Let us for completeness describe here the notation. l denotes a lattice site and $\sigma, \uparrow, \downarrow$ the spin degrees of freedom. For the spin model, $\mathcal{H}_S$, $S^+(S^-)$ are raising(lowering) operators and S_z the z component of the spin operator. For the fermionic models, $\mathcal{H}_{t-V}$ and $\mathcal{H}_H$, $c^\dagger(c)$ creates(annihilates) a fermion and $n = c^\dagger c$.

The above models describe many body systems and their Hamiltonian consists of a kinetic term, the first term in each equation (proportional to J and t), and a term describing the interactions between the components of the system, the second term in each equation (proportional to J_z, V, U respectively). Besides the lattice models, there are also continuum models which focus on the low energy regime of the system and provide valuable information for the low lying excitations although they neglect the effect of the lattice; however, one can restore it by considering an external periodic potential.

All the systems mentioned above are integrable in the sense that they possess a macroscopic number of conservation laws, which are connected to the exact solubility of the model [11] and assign very interesting properties to them [12, 13]. First, the macroscopic number of conservation laws leads to level crossing [11] and consequently the energy spectrum obeys the Poisson distribution while non-integrable systems exhibit the Wigner Dyson due to level repulsion [14]. Moreover, these conservation laws may have a great impact on the transport properties of the system. For one thing, for the spin-$\frac{1}{2}$ Heisenberg model the energy current is a constant of motion—the current-current correlation does not decay in time despite the many body character of the Hamiltonian—leading to a divergence of thermal conductivity at zero frequency, namely ballistic heat transport. Even if a current (it could be any of the particle, spin, energy currents) is not conserved a finite overlap with the conservation laws of the system may prevent the decay of the current-current correlation, leading again to a divergence at zero frequency for the corresponding conductivity [15].

However, integrability does not ensure the existence of ballistic transport in the system. A striking example is the case where some modes of the system propagate ballistically while some others do not. Such an example is the Heisenberg model where in the gapless phase (easy plane), $J_z < 2J$, both the spin and thermal transport are ballistic, while in the gapped phase (easy axis), $J_z > 2J$, the spin transport is normal unlike the thermal transport which remains ballistic for any J_z [15, 16]. Moreover, the influence of defects, longer range interactions, scattering with other modes (e.g. phonons), and so on, and the interplay of these scattering mechanisms with the integrability is not always trivial [17–20]. Naturally, in real 1D systems many scattering mechanisms will be present, thus the theoretical study of the above pure models in the presence of defects is rather imperative. Despite the difficulty to solve analytically a many body problem in the presence of impurities there has been impressive progress leading to rigorous results for the properties of these systems for several kinds of impurities.

First, for a non-interacting 1D system in the presence of disorder all states are localized for any finite disorder [21]. However, on switching on the interactions between the components of the system the behavior of the system may change drastically delocalizing the localized states. Moreover, the temperature could play an important role since there could be a thermally activated dc transport above a critical temperature or at any finite temperature.

In the opposite regime, i.e., a single impurity in a pure system, it was shown that even a single non-magnetic impurity, a potential barrier or a weak link, in a LL with

repulsive interactions effectively obstructs dc transport leading to an insulating ground state [22]. On the contrary, for attractive interactions between the fermions the system is healed and becomes an ideal conductor at zero temperature (perfectly transmitting ground state) despite the presence of the impurity. This is in contrast to the non-interacting case where the impurity only renormalizes the transmission coefficient through the obstacle leading to a finite conductance (in a Landauer framework). Since $\mathcal{H}_{t-V}$ and $\mathcal{H}_S$ are exact mapping of one another, one can plausible seek the same behavior in a spin model. The role of the repulsive/attractive interactions V will play the antiferromagnetic/ferromagnetic easy axis anisotropy J_z. Indeed, this behavior is observed as well in spin models, described by the Heisenberg Hamiltonian where in the presence of magnetic or non-magnetic impurities the chain is either cut or healed according to the sign of the easy axis anisotropy (Ref. [23] and present work). Numerical calculations, using the thermal conductivity as a probe, performed on finite lattices and for finite temperatures verify the analytical predictions [24]. Hence, one can claim that the cutting-healing behavior of a 1D system in the presence of a single impurity is quite universal.

Despite the progress made in analytical techniques, providing the energy spectrum and the elementary excitations of the system, there is still plenty of open issues, controversies and debates. Thus, numerical techniques (like: Quantum Monte Carlo (QMC), Density Matrix Renormalization Group (DMRG) and numerical diagonalization techniques) can play an important role to these issues. However, as far as the numerical diagonalization techniques are concerned, the major problem one has to confront with is the rapid increase of the Hilbert space for a many body system. Thus, the development of new numerical techniques could be crucial in order to have more efficient numerical algorithms [25–27].

Besides the theoretical interest about low dimensional systems there is a revived experimental interest as well for systems which form magnetic structures with reduced dimensionality. These materials are normal three dimensional bulk materials with a high anisotropy in the magnetic moment interactions, forming quasi-one-dimensional spin systems (or quasi-two-dimensional systems). They attract the attention of two branches of condensed matter physicists since they are promising candidates for high T_c superconductivity as well as they exhibit exceptionally high and anisotropic thermal conductivity, due to the low dimensional magnetic structures.

There is a large number of such novel materials. A big category are the cuprates comprising compounds like the spin-$\frac{1}{2}$ zig-zag compound $SrCuO_2$, the chain compounds Sr_2CuO_3, $CaCu_2O_3$ and the two-leg spin-$\frac{1}{2}$ ladder compounds, $(Sr, Ca, La)_{14}Cu_{24}O_{41}$, $Ca_9La_5Cu_{24}O_{41}$, Fig. 1, [28–30]. The origin for the 1D structures is the superexchange coupling of the $Cu-O-Cu$ atoms [31] and they are described via the Heisenberg Hamiltonian. One can arrive to the Heisenberg Hamiltonian starting from the Hubbard Hamiltonian at half filling considering a large on-site repulsive interaction $U \gg t$. Within second order perturbation theory one arrives at the spin-$\frac{1}{2}$ Heisenberg Hamiltonian with $2J = J_z = \frac{4t^2}{U}$ [3, 10, 32].In order to obtain the anisotropic Heisenberg model with $J \neq 2J_z$ one has to take into account spin orbit coupling. The fact that

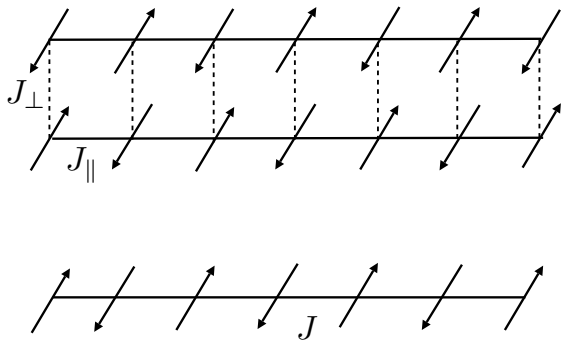

Figure 1: Schematic representation of a two-leg spin ladder(top) and a spin chain (bottom).

the Heisenberg Hamiltonian is obtained from the large U limit of the Hubbard model at half filling, which describes Mott insulators, indicates that materials which are described by the Heisenberg Hamiltonian are insulators, or poor conducting materials since there is a virtual hopping involved, cf. as well Ref. [31]. This feature makes these materials unique since on the one hand they are electric insulators and on the other hand they are very good heat conductors with a thermal conductivity along the chain/ladder direction of metallic order or even higher.

The theoretical prediction for the spin-$\frac{1}{2}$ Heisenberg Hamiltonian, as we have already mentioned, is that exhibits ballistic thermal transport. On the other hand for spin-1 chain compounds, like the $AgVP_2S_6$, or two-leg spin-$\frac{1}{2}$ ladder compounds the transport is normal, Refs. [33, 34] and [29]. Despite the theoretical predictions, in real materials there are numerous scattering mechanisms, like flaws in the production procedure, phonons, impurities, and so on, which would render even ballistic transport normal. Consequently the purity of these systems turns out to be crucial as it was realized recently [35]. Notwithstanding, the large exchange coupling, $(J, J_\parallel)/k_B \sim \mathcal{O}(10^3)$K, between neighboring spins accounts for an extraordinary high and anisotropic thermal conductivity. It should be noted that longer range interactions or interactions with the transverse directions are orders of magnitude smaller than the nearest neighbor in-chain interactions. The large anisotropy in thermal transport holds for a wide variety of temperatures, from a few decades of degrees—where magnetic contribution becomes significant—up to room temperature. However, we should also mention that there are materials which exhibit anisotropic heat transport due to magnetic excitations but with a much weaker exchange coupling, like the $CuGeO_3$ spin-Peierls compound.

To recapitulate, the study of low dimensional strongly correlated systems is a long standing problem. Besides its theoretical interest there is a revived experimental interest in the field due to developments like, fabrication of quasi-low dimensional quantum magnets, carbon nanotubes, quantum wires and so on. Finally, along with the fundamental research interest it turns out that there are very promising technological applications which can arise by exploiting the fascinating low dimensional physics.

Bibliography

[1] J. M. Luttinger, Journal of Mathematical Physics **4**, 1154–1162 (1963).

[2] F. D. M. Haldane, 'Luttinger liquid theory' of one-dimensional quantum fluids. I. Properties of the Luttinger model and their extension to the general 1D interacting spinless Fermi gas, Journal of Physics C: Solid State Physics **14**(19), 2585 (1981).

[3] V. J. Emery, Theory of the One-dimensional Electron Gas, in *Highly Conducting One-Dimensional Solids*, edited by J. Devreese, R. Evrard, and V. Doren, pages 247–303, Plenum Press, New York, 1979.

[4] H. Bruus and K. Flensberg, *Many-body quantum theory in condensed matter physics: an introduction*, Oxford Graduate Texts, Oxford University Press, Oxford, 2004.

[5] S. Doniach and E. Sondheimer, *Green's functions for solid state physicists*, Imperial College Press, 2004.

[6] L. D. Faddeev and L. A. Takhtajan, What is the spin of a spin wave?, Physics Letters A **85**(6-7), 375 – 377 (1981).

[7] D. A. Tennant, T. G. Perring, R. A. Cowley, and S. E. Nagler, Unbound spinons in the S=1/2 antiferromagnetic chain $KCuF_3$, Physical Review Letters **70**(25), 4003–4006 (Jun 1993).

[8] C. Kim, A. Y. Matsuura, Z.-X. Shen, N. Motoyama, H. Eisaki, S. Uchida, T. Tohyama, and S. Maekawa, Observation of Spin-Charge Separation in One-Dimensional $SrCuO_2$, Physical Review Letters **77**(19), 4054–4057 (Nov 1996).

[9] Y. Jompol, C. J. B. Ford, J. P. Griffiths, I. Farrer, G. A. C. Jones, D. Anderson, D. A. Ritchie, T. W. Silk, and A. J. Schofield, Probing Spin-Charge Separation in a Tomonaga-Luttinger Liquid, Science **325**(5940), 597–601 (2009).

[10] B. J. Powell, An introduction to effective low-energy Hamiltonians in condensed matter physics and chemistry, ArXiv e-prints (June 2009).

[11] H. K. Owusu, K. Wagh, and E. A. Yuzbashyan, The link between integrability, level crossings and exact solution in quantum models, Journal of Physics A: Mathematical and Theoretical **42**(3), 035206 (2009).

[12] X. Zotos and P. Prelovšek, Transport in one dimensional quantum systems, in *Strong interactions in low dimensions*, pages 347–382, Springer Netherlands, 2004.

[13] X. Zotos, Issues on the Transport of One Dimensional Quantum Systems, Journal of the Physical Society of Japan **74S**(Supplement), 173–180 (2005).

[14] D. Poilblanc, T. Ziman, J. Bellissard, F. Mila, and G. Montambaux, Poisson vs. GOE Statistics in Integrable and Non-Integrable Quantum Hamiltonians, EPL (Europhysics Letters) **22**(7), 537 (1993).

[15] X. Zotos, F. Naef, and P. Prelovsek, Transport and conservation laws, Physical Review B **55**(17), 11029–11032 (May 1997).

[16] X. Zotos, Finite Temperature Drude Weight of the One-Dimensional Spin- 1/2 Heisenberg Model, Physical Review Letters **82**(8), 1764–1767 (Feb 1999).

[17] J. Sirker, R. G. Pereira, and I. Affleck, Diffusion and Ballistic Transport in One-Dimensional Quantum Systems, Physical Review Letters **103**(21), 216602 (Nov 2009).

[18] P. Jung, R. W. Helmes, and A. Rosch, Transport in Almost Integrable Models: Perturbed Heisenberg Chains, Physical Review Letters **96**(6), 067202 (2006).

[19] M. Di Stasio and X. Zotos, Connection between Low Energy Effective Hamiltonians and Energy Level Statistics, Physical Review Letters **74**(11), 2050–2053 (Mar 1995).

[20] O. S. Barišić, P. Prelovšek, A. Metavitsiadis, and X. Zotos, Incoherent transport induced by a single static impurity in a Heisenberg chain, Physical Review B **80**(12), 125118 (Sep 2009).

[21] E. Abrahams, P. W. Anderson, D. C. Licciardello, and T. V. Ramakrishnan, Scaling Theory of Localization: Absence of Quantum Diffusion in Two Dimensions, Physical Review Letters **42**(10), 673–676 (Mar 1979).

[22] C. L. Kane and M. P. A. Fisher, Transport in a one-channel Luttinger liquid, Physical Review Letters **68**(8), 1220–1223 (Feb 1992).

[23] A. Furusaki and T. Hikihara, Kondo effect in XXZ spin chains, Physical Review B **58**(9), 5529–5538 (Sep 1998).

[24] A. Metavitsiadis, X. Zotos, O. S. Barišić, and P. Prelovšek, Thermal transport in a spin- $\frac{1}{2}$ Heisenberg chain coupled to a magnetic or nonmagnetic impurity, Physical Review B **81**(20), 205101 (May 2010).

[25] M. W. Long, P. Prelovšek, S. El Shawish, J. Karadamoglou, and X. Zotos, Finite-temperature dynamical correlations using the microcanonical ensemble and the Lanczos algorithm, Physical Review B **68**(23), 235106 (Dec 2003).

[26] J. Jaklič and P. Prelovšek, Finite-temperature properties of doped antiferromagnets, Advances in Physics **49**, 1–92 (2000).

[27] J. Kokalj and P. Prelovšek, Finite-temperature dynamics with the density-matrix renormalization group method, Physical Review B **80**(20), 205117 (Nov 2009).

[28] C. Hess, Heat conduction in low-dimensional quantum magnets, The European Physical Journal - Special Topics **151**, 73–83.

[29] A. V. Sologubenko, T. Lorenz, H. R. Ott, and A. Freimuth, Thermal Conductivity via Magnetic Excitations in Spin-Chain Materials, Journal of Low Temperature Physics **147**, 387–403 (2007).

[30] K. Katsumata, Low-dimensional magnetic materials, Current Opinion in Solid State and Materials Science **2**(2), 226 – 230 (1997).

[31] P. W. Anderson, New Approach to the Theory of Superexchange Interactions, Physical Review **115**(1), 2 (Jul 1959).

[32] K. A. Chao, J. Spalek, and A. M. Oles, Kinetic exchange interaction in a narrow S-band, Journal of Physics C: Solid State Physics **10**(10), L271 (1977).

[33] J. Karadamoglou and X. Zotos, Diffusive Transport in Spin-1 Chains at High Temperatures, Physical Review Letters **93**(17), 177203 (Oct 2004).

[34] X. Zotos, High Temperature Thermal Conductivity of Two-Leg Spin-1/2 Ladders, Physical Review Letters **92**(6), 067202 (Feb 2004).

[35] N. Hlubek, P. Ribeiro, R. Saint-Martin, A. Revcolevschi, G. Roth, G. Behr, B. Büchner, and C. Hess, Ballistic heat transport of quantum spin excitations as seen in $SrCuO_2$, Physical Review B **81**(2), 020405 (Jan 2010).

Chapter 1

Static disorder

1.1 Introduction

The concept of vanishing transport in condensed matter physics due to the localization of single particle states, was first introduced by Anderson [1] with a pathbreaking article in 1958. The phenomenon of localization in disordered systems has a big impact on physics research, although it was not immediately recognized [2]. Nowadays the phenomenon is observed not only in condensed matter systems but in a variety of other physical systems as well, involving matter, optical, acoustic or even seismic waves, extending from meso- to macro- scopic scales. The common attribute behind all these physical systems is their wave nature, where the incoherent scattering from the disordered medium localizes these waves, destroying transport.

The dc transport properties of non-interacting disordered electron systems are theoretically well understood using various techniques (such as: random matrix theory, renormalization group, diagrammatic analysis) and experimentally verified in many condensed matter systems [3]. The main idea is that disorder localizes the wavefunctions preventing diffusion. Actually it has been shown that in 1D any amount of disorder would localize all states leading to vanishing dc transport [4, 5]. In order to have non-vanishing dc transport in 1D, scattering mechanisms like electron-phonon or electron-electron interactions have to be introduced.

The effect of correlations on localized states is also a long standing problem [6] which still attracts both, theoretical [7] and experimental [8] interest. In contrast to the non-interacting case where all states are localized and dc transport vanishes at any temperature, the introduction of correlations could lead to different possible scenarios. First, at zero temperature, $T = 0$, numerical results for fermions with repulsive interactions in a disordered system reveal that localization persists in spite of correlations [9, 10] although some types of interactions might destroy the localized states driving the system to a normal diffusive state or even one with diverging low-frequency conductivity [11, 12]. Even if the system remains localized at $T = 0$, an arbitrary low temperature could delocalize it or a finite critical temperature [13, 14] might be needed to drive it to a normal state at high temperatures. There are also

indications that in the presence of large disorder even at high temperatures many-body states can appear effectively localized [15, 16].

1.2 Model

To explore the issue of transport in a system with correlations and disorder, we consider the anisotropic spin-1/2 Heisenberg Hamiltonian with nearest neighbor interactions either in the presence of a random configuration of magnetic fields (on-site disorder), or a random modification of the exchange coupling of nearest neighbors (bond disorder). The Hamiltonian for the pure system is given by the sum of local interaction energies between neighboring spins

$$H_0 = \sum_l h_l \,, \quad h_l = J(S_l^x S_{l+1}^x + S_l^y S_{l+1}^y + \Delta S_l^z S_{l+1}^z) \,, \tag{1.1}$$

which in the case of bond disorder is modified as

$$\mathcal{H} = \sum_l h_l \,, \qquad h_l = J_l \, (\mathbf{S}_l \cdot \mathbf{\Delta} \cdot \mathbf{S}_{l+1}) \,. \tag{1.2}$$

For the sake of brevity we have used a slightly different notation for the local energies h_l, with $\mathbf{S}_l$ being the vector for the local operator of the spin-1/2 at site l with components (S^x, S^y, S^z) and $\mathbf{\Delta}$ is the diagonal tensor of the anisotropy. Considering the interactions to be anisotropic only in the z-axis, as indicated by Hamiltonian (1.1) we have $\Delta_{x,y} = 1$, $\Delta_z = \Delta$, i.e. ,

$$\mathbf{\Delta} = \begin{pmatrix} 1 & 0 & 0 \\ 0 & 1 & 0 \\ 0 & 0 & \Delta \end{pmatrix} \,. \tag{1.3}$$

J_l is the exchange coupling between two adjacent spins at sites $l, l+1$ which in the absence of bond disorder is constant, with $J_l = J$.

Note that spin operators in the XY plane can be replaced by the raising S^+, lowering S^-, operators using the relation

$$S^{\pm} = S^x \pm i S^y \,, \tag{1.4}$$

which gives a kinetic interpretation of the $S^{x,y}$ terms.

Furthermore, the Jordan-Wigner transformation [17, 18] maps spin-1/2 operators into fermionic operators; the transformation relations are

$$S_l^z = c_l^\dagger c_l - \frac{1}{2} \,, \quad S_l^+ = e^{-i\phi_l} c_l^\dagger \,, \quad S_l^- = e^{i\phi_l} c_l \,, \quad \text{with} \quad \phi_l = \pi \sum_{\ell<l} c_\ell^\dagger c_\ell \,, \tag{1.5}$$

where $c_l(c_l^\dagger)$ annihilates(creates) a fermion at the l lattice site. Plugging (1.5) into (1.1) we arrive at

$$H_{t-V} = \sum_l \Big(- t\big(c_l^\dagger c_{l+1} + c_{l+1}^\dagger c_l\big) + V n_l n_{l+1} \Big) + \text{const.} \,, \tag{1.6}$$

where $t = -J/2$, $V = J\Delta$, and the constant is $-J\Delta(N_f - \frac{1}{4})$, with N_f the number of fermions in the system. Note that (1.6) is always correct to order $\mathcal{O}(1/L)$. Hamiltonian (1.6) describes the so-called t-V model. The previous mapping of the spin-1/2 operators indicates that $S^{x,y}$ are kinetic terms while the S^zS^z product denotes the interactions of the system, which are determined by the anisotropy parameter Δ.

For the bond disorder case the Hamiltonian is given by Eq. (1.2) with the neighboring exchange interactions J_l modified in a random way. On the other hand, on-site disorder is induced by a random distribution of local magnetic fields b_l, pointing at the z-direction, which yield the perturbation Hamiltonian

$$H_1 = \sum_l b_l S_l^z \,. \tag{1.7}$$

Thus the total Hamiltonian will be

$$H = \mathcal{H} + H_1 \,. \tag{1.8}$$

Spin $\jmath^s$ and energy $\jmath^\epsilon$ currents are obtained using the respective dipole operator [17]

$$P^s = \sum_l r_l S_l^z, \quad P^\epsilon = \sum_l r_l h_l \,,$$

with r_l being the corresponding coordinates while the local energies h_l are modified to take into account the possibility of on-site disorder ($h_l \to h_l + b_l S_l^z$). The spin, energy currents are obtained from the time derivative of the respective dipole operator,

$$\jmath^s = \frac{i}{\hbar}\sum_{l,m} r_l[h_m, S_l^z], \quad \jmath^\epsilon = \frac{i}{\hbar}\sum_{l,m} r_l[h_m, h_l] \,.$$

It is straightforward to see that the spin current operator will be given by

$$\jmath^s = \sum_l \jmath_l^s \,, \qquad \jmath_l^s = aJ_l \, (\mathbf{S}_l \times \mathbf{S}_{l+1}) \cdot \hat{e}_z \,, \tag{1.9}$$

where a is the lattice constant and $\hat{e}_z$ is the unit vector along the z-axis. The energy current consists of two terms in the presence of on-site disorder; the first one arises from Hamiltonian (1.2) and the second one from the magnetic field distribution, Eq. (1.7), where the latter involves the local spin current operators $\jmath_l^s$

$$\jmath^\epsilon = \sum_l \jmath_l^\epsilon + \frac{b_l}{2}(\jmath_{l-1}^s + \jmath_l^s) \,, \quad \jmath_l^\epsilon = aJ_{l-1}J_l \, \mathbf{S}_l \cdot \Big(\mathbf{\Delta} \cdot \mathbf{S}_{l+1} \times \mathbf{\Delta} \cdot \mathbf{S}_{l-1}\Big) \,. \tag{1.10}$$

The real parts of the dynamical spin σ and thermal κ, conductivities can be written in the linear response theory framework [19, 20] (cf. Appx. A) as,

$$\sigma'(\omega) = 2\pi D_s \delta(\omega) + \sigma(\omega) \,, \quad \kappa'(\omega) = 2\pi D_h \delta(\omega) + \kappa(\omega) \,. \tag{1.11}$$

$\delta(\omega)$ is the Dirac δ-function, and $D_s(D_h)$ is the corresponding spin(energy) stiffness, where a non-vanishing stiffness implies ballistic transport for the corresponding modes. However, in the presence of strong disorder coherent transport vanishes and the non-trivial quantities are the regular components of the conductivities $\sigma(\omega)$, $\kappa(\omega)$, which can be written using the respective current-current susceptibility as

$$\sigma(\omega) = \frac{1}{L}\Im \lim_{\eta\to 0^+} \frac{\chi_{\jmath^s\jmath^s}(z)}{z}\,, \quad \kappa(\omega) = \frac{1}{LT}\Im \lim_{\eta\to 0^+} \frac{\chi_{\jmath^\epsilon\jmath^\epsilon}(z)}{z}\,, \tag{1.12}$$

with $z = \omega + i\eta$. The susceptibility for the response of an observable $\hat{O}_p$ due to a perturbation which is coupled with an operator $\hat{O}_q$ is defined within standard linear response theory as

$$\chi_{\hat{O}_p\hat{O}_q}(z) = \frac{i}{\hbar}\int_0^\infty dt\, e^{izt}\,\langle[\hat{O}_p(t), \hat{O}_q]\rangle\,. \tag{1.13}$$

The angle brackets denote both the thermodynamic average,

$$\langle\hat{O}\rangle_{th} = \frac{Tr\; e^{-\beta H}\hat{O}}{Tr\; e^{-\beta H}}\,, \tag{1.14}$$

and an average over the random distribution of impurities. $\beta = 1/k_BT$, with k_B being the Boltzmann constant and T the temperature.

1.3 On-site disorder

Let us first consider the case of on-site disorder. In that case we restrict ourselves in a homogeneous exchange coupling, i.e., $J_l = J$ and $\mathcal{H} = H_0$ with H_0 the Heisenberg Hamiltonian for the pure anisotropic Heisenberg model (1.1). The disorder is induced in the pure Heisenberg model by considering a local magnetic field whose values are given by a uniform random distribution in the interval $-W/2 < b_l < +W/2$, with W being the strength of the disorder, Eq. (1.7).

1.3.1 Frequency moments

Before proceeding with numerical results, the analytical calculation of the first two frequency moments could offer quite rough, but rather valuable information for the spin and energy conductivity. Taking a short time expansion, one can write conductivities as a sum of powers of $1/\omega$, for $1/\omega \to 0$, (cf. Appx. A)

$$\sigma(\omega) \sim \frac{1}{\omega}\left(\tilde{\sigma}_0 + \frac{\tilde{\sigma}_2}{\omega^2} + \dots\right)\,, \quad \kappa(\omega) \sim \frac{1}{\omega}\left(\tilde{\kappa}_0 + \frac{\tilde{\kappa}_2}{\omega^2} + \dots\right)\,, \tag{1.15}$$

with the coefficients $\tilde{\sigma}_n, \tilde{\kappa}_n$ being the frequency moments which are given by

$$\tilde{\sigma}_n = \int_{-\infty}^{\infty} \omega^n\sigma(\omega)\, d\omega\,, \qquad \tilde{\kappa}_n = \int_{-\infty}^{\infty} \omega^n\kappa(\omega)\, d\omega\,. \tag{1.16}$$

In the high temperature limit, one can easily express the spin, energy moments as thermodynamic averages of the respective currents and their time derivatives,

$$\tilde{\sigma}_n = \pi\beta\hbar\sigma_n \,, \qquad \tilde{\kappa}_n = \pi k_B \hbar \beta^2 \kappa_n \,, \tag{1.17}$$

where for the two lowest moments we have

$$\sigma_0 = \frac{1}{L}\langle j^s j^s\rangle \,, \quad \sigma_2 = \frac{1}{L}\langle \dot{j}^s \dot{j}^s\rangle \,, \quad \dot{j}^s = \frac{i}{\hbar}[H, j^s] \,, \tag{1.18a}$$

$$\kappa_0 = \frac{1}{L}\langle j^\epsilon j^\epsilon\rangle \,, \quad \kappa_2 = \frac{1}{L}\langle \dot{j}^\epsilon \dot{j}^\epsilon\rangle \,, \quad \dot{j}^\epsilon = \frac{i}{\hbar}[H, j^\epsilon] \,. \tag{1.18b}$$

The operators $\dot{j}^s, \dot{j}^\epsilon$—the so-called force operators—are the time derivatives of the respective spin j^s, energy j^ϵ currents and signify the scattering processes that occur in a system, whether these processes originate from external perturbations or if they come from intrinsic scattering mechanisms of the system.

In order to calculate the thermodynamic averages in Eqs. (1.18), we will take the infinite temperature limit, $T \to \infty$, where the thermodynamic averages can be replaced by traces, $\langle \hat{O}\rangle_{th} \to Tr\ \hat{O}/Tr\mathbb{1}$, yielding for the spin, energy frequency moments

$$\sigma_0 = \frac{J^2}{8} \,, \tag{1.19a}$$

$$\sigma_2 = \frac{1}{16}\Big(J^4\Delta^2 + 4J^2\langle b^2\rangle\Big) \,, \tag{1.19b}$$

$$\kappa_0 = \frac{1}{32}\left[\Big(1 + 2\Delta^2\Big)J^4 + 2J^2\langle b^2\rangle\right] \,, \tag{1.19c}$$

$$\kappa_2 = \frac{J^4}{64}\Big(3 + 10\Delta^2\Big)\langle b^2\rangle + \frac{J^2}{16}\Big(\langle b^4\rangle - \langle b^2\rangle^2\Big) \,, \tag{1.19d}$$

where $\langle b^2\rangle = W^2/12$ and $\langle b^4\rangle = W^4/80$. In the above formulas we have omitted some awkward $\hbar$ factors. However, one can easily restore the correct dimensions by simply replacing the powers of J by $J^n \to J^n\hbar^{n+2}$.

Without disorder the anisotropic XXZ model is integrable using the Bethe ansatz method for any value of the anisotropy and it is known to show ideal spin (in the easy-plane) and thermal (for any anisotropy) conductivities at all temperatures [21]. This difference between spin and thermal conductivity is already implied in the infinite temperature calculation of the frequency moments. We can see that the finite dispersion $\delta^\epsilon = \sqrt{\kappa_2/\kappa_0}$ of $\kappa(\omega)$ is induced solely by a non zero value of W, whereas $\delta^s = \sqrt{\sigma_2/\sigma_0}$ remains finite even for $W = 0$. Moreover, the absence of a J^6 term in κ_2 reflects the fact that in the pure Heisenberg model the energy current is a constant of motion and the force operator vanishes.

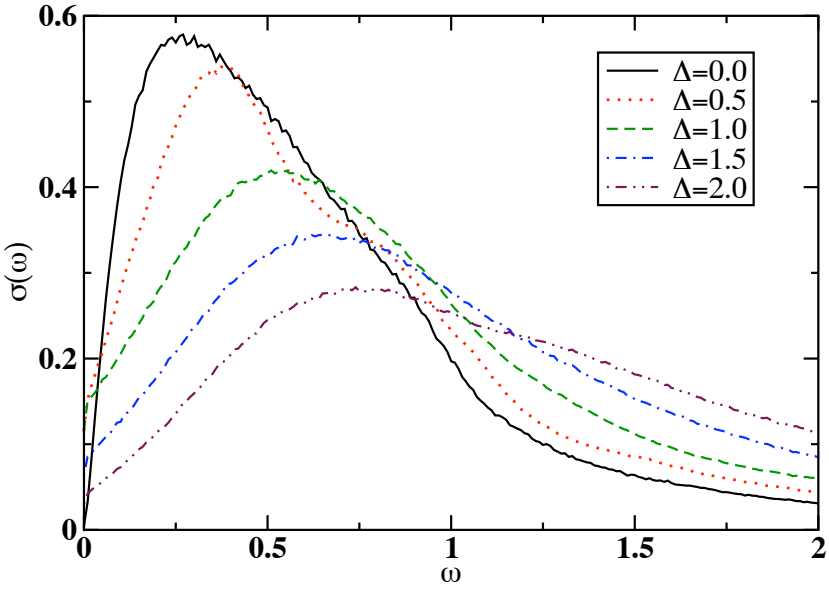

Figure 1.1: Dynamical spin conductivity $\sigma(\omega)$ at $T \to \infty$ for local disorder $W = 2$ and various Δ (curves normalized to unity) evaluated via ED ($L = 14$) .

1.3.2 Numerical results

Although the lowest-frequency moments can serve as a reference, they are insufficient to reveal the most challenging $\omega \to 0$ behavior. For the latter we have to rely on numerical calculations. The most favorable case for simulations on a finite-size lattice is the strong disorder limit where we expect the localization length ξ to be shortest. In the following we consider $W = 2$, where an estimate of $T = 0$ localization length ξ exists in the literature [10], which suggests that ξ is less than ten sites in the cases we are studying.

For this part, we will use state of the art numerical diagonalization techniques—the exact diagonalization (ED), the finite-temperature Lanczos method (FTLM) (Ref. [22]) and the microcanonical Lanczos method (MCLM)(Ref. [23])—to see what they can offer on this issue of disorder and correlations. While we will study the spin and thermal conductivity of the spin-1/2 anisotropic Heisenberg model, the spin conductivity maps directly to that of the charge conductivity of the t-V model. For the numerical results and from now on we use a system of units where $\hbar, k_B, a = 1$.

In Figs. 1.1 and 1.2 we present results for the spin $\sigma(\omega)$ and thermal $\kappa(\omega)$ conductivity, respectively, where curves are normalized to unity. The data for $L = 14$, with a Hilbert-space dimension of $\mathcal{D}_H = 3432$ states in the $S_z = 0$ subsector, were obtained by exact (full) diagonalization (ED). The peaks at the excitation frequencies are binned in windows $\delta\omega = 0.01$, which also gives the frequency resolution of the spectra. There is an average over $N_r = 10$ random-field configurations. In the same plots, we show the noninteracting case for $L = 1000$ and averaging $N_r = 1000$, where we expect the

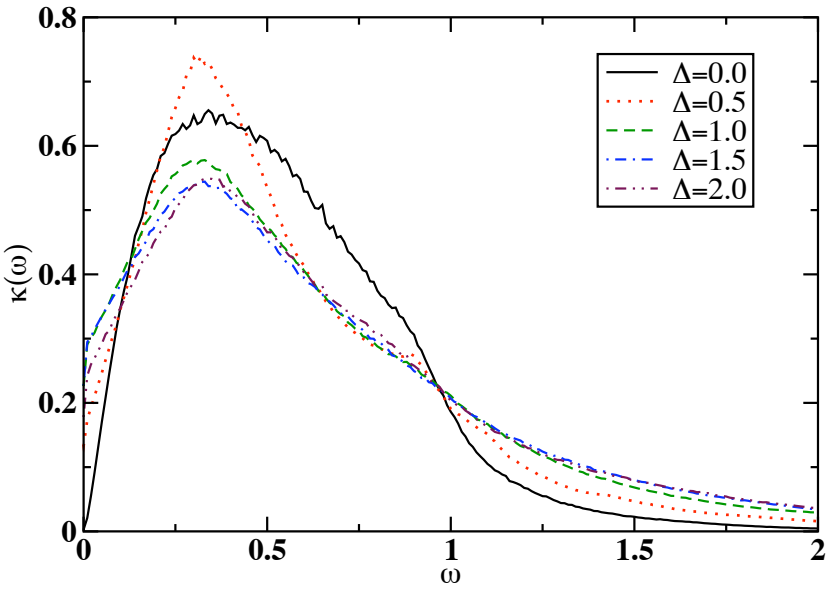

Figure 1.2: Dynamical thermal conductivity $\kappa(\omega)$ at $T \to \infty$ for local disorder $W = 2$ and various Δ (curves normalized to unity) evaluated via ED ($L = 14$).

dc conductivities $\sigma_{dc} = \sigma(\omega \to 0)$ and $\kappa_{dc} = \kappa(\omega \to 0)$ to vanish.

These results clearly reveal that apart from the XY limit, $\Delta = 0$, the system is conducting, i.e., both spin and thermal dc conductivities are finite. Nevertheless, due to the large disorder W the dynamics is non-Drude type since the maximum of $\sigma(\omega)$ as well as of $\kappa(\omega)$ appears at a finite $\omega^* > 0$, in analogy with the localization at $\Delta = 0$. Hence, at $\Delta > 0$ and large W we are dealing with pseudolocalized dynamics [15, 16]. Another feature of this regime appears to be a generic (nonanalytic) cusplike behavior at low frequencies, $\sigma(\omega) \simeq \sigma_{dc} + \alpha|\omega|$ and $\kappa(\omega) \simeq \kappa_{dc} + \gamma|\omega|$, for which so far we cannot offer an explanation. It might be attributed to long-time tail effects although, in such a case, the low-frequency drop of the conductivity was found to be only a few percent [24] and not as large as in our case. Such a frequency dependence is strongly reminiscent of the behavior in strongly disordered two-dimensional systems as has been analyzed theoretically and observed experimentally [25].

Apart from a qualitative similarity between $\sigma(\omega)$ and $\kappa(\omega)$ in Figs. 1.1 and 1.2 there are also some differences. $\sigma(\omega)$ is more sensitive to Δ, as it is already evident from the moments Eqs. (1.19) and the corresponding δ^s. The origin of these differences comes from the fact that even at $W = 0$ $\sigma(\omega \to 0)$ changes qualitatively at $\Delta = 1$ [26], not being the case for $\kappa(\omega \to 0)$ [21].

As our numerical simulations indicate, a similar qualitative behavior persists by decreasing the disorder to W = 1.0 (not shown). With decreasing W the pseudolocalized form gives way to a more Drude-like form with $\omega^* \to 0$ and strongly increased σ_{dc} and κ_{dc}. However, reducing the disorder further we are running to long localization lengths

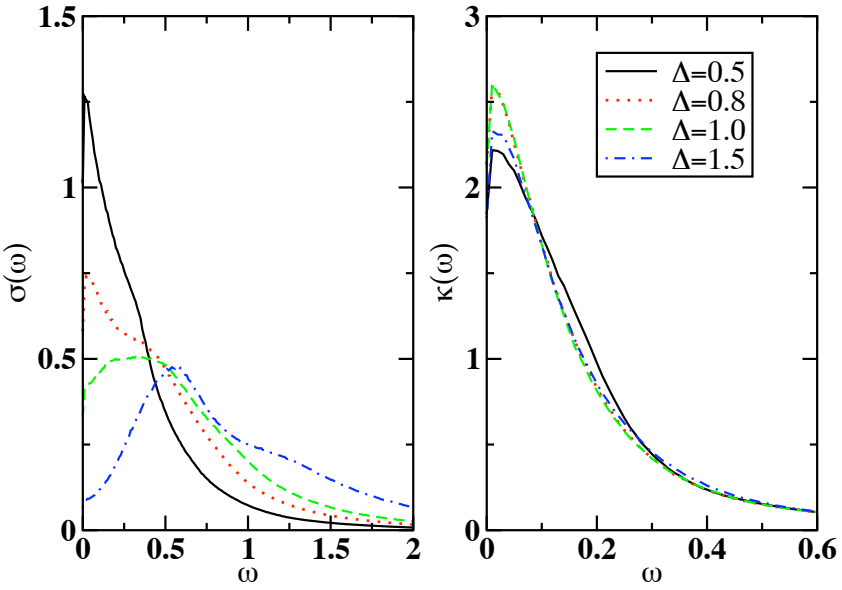

Figure 1.3: Dynamical spin $\sigma(\omega)$ (left) and thermal $\kappa(\omega)$ (right) conductivity evaluated via ED ($L = 14$), at $T \to \infty$ for a weak on-site disorder $W = 0.8$ and various values of the anisotropy Δ (curves are normalized to unity).

and in general less controllable finite-size effects preventing reliable conclusions.

Notwithstanding, to give a qualitative picture of the difference between spin and thermal conductivity, as far as their dependence on the anisotropy Δ is concerned, we present in Fig. 1.3 results for spin (left) and thermal (right) conductivity for a weak disorder $W = 0.8$ with a number of realizations $N_r = 10$ and for various values of the parameter Δ; curves are normalized to unity. In the XY regime ($\Delta < 1$) and for the pure Heisenberg model the spin conductivity exhibits a finite spin stiffness at any temperature, manifesting dissipationless dc transport, while it vanishes in the gapped phase ($\Delta > 1$). Thus, in the XY regime and for weak disorder it is expected that the spin conductivity will show a more Drude-like behavior. On the contrary for $\Delta > 1$ the spin conductivity shows a strongly non-monotonic behavior, present already in the absence of impurities. Thus, the low frequency behavior for $\Delta > 1$ shown in Fig. 1.3 (left) is attributed to the properties of the pure Heisenberg model in the gapped phase and not to the presence of the disorder—as it is implied by the low frequency non-linear behavior of $\sigma(\omega)$ as well. For the thermal conductivity, Fig. 1.3 (right), we observe that the Drude-like behavior is maintained for any value of the anisotropy parameter Δ, since the conservation of the energy current in the pure model leads to a finite thermal stiffness at any temperature and for any anisotropy.

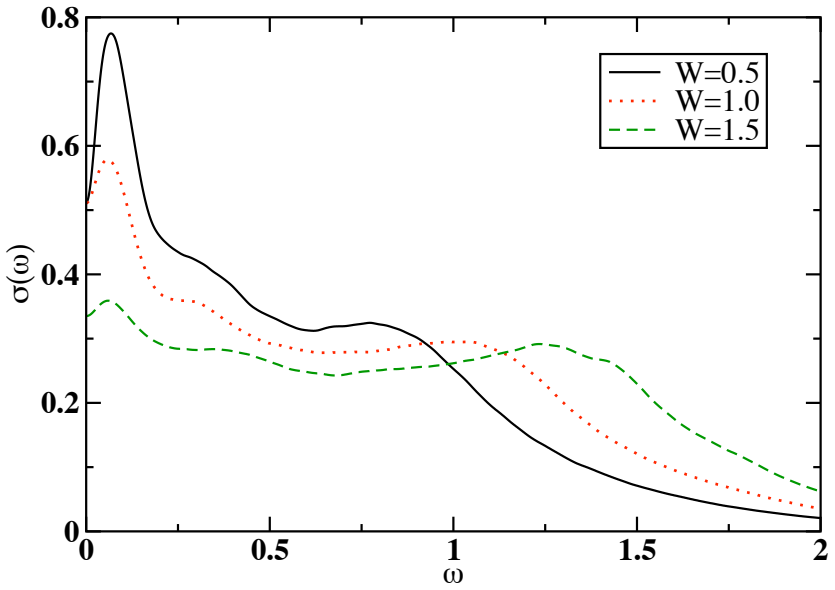

Figure 1.4: $T \to \infty$ results for $\sigma(\omega)$ and for $\Delta = 1$ and different bond disorder W (curves are normalized).

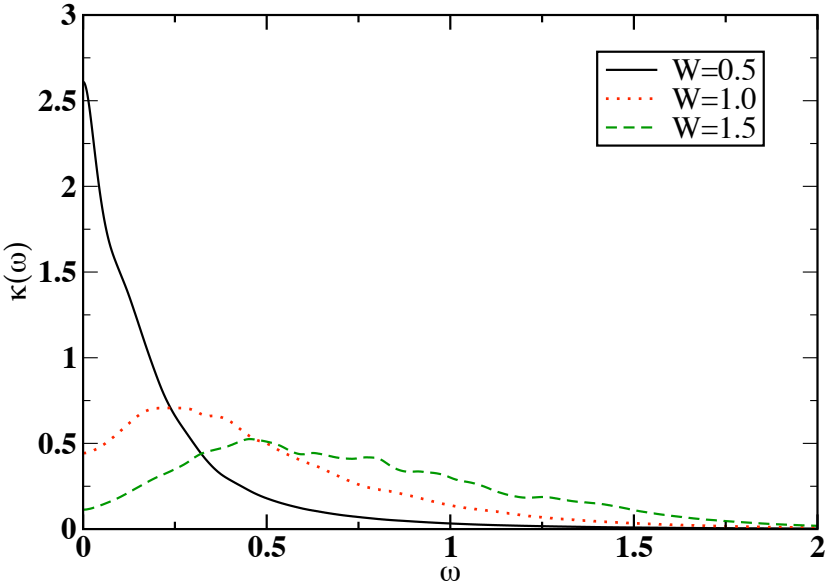

Figure 1.5: $T \to \infty$ results for $\kappa(\omega)$ and for $\Delta = 1$ and different bond disorder W (curves are normalized).

1.4 Bond disorder

In connection to existing 1D magnetic compounds [27] more relevant appears to be the spin-1/2 anisotropic Hamiltonian with bond disorder, i.e., disorder in exchange couplings. This is formulated by taking $J_l = J(1-s_l)$ in (1.2) where $-W/2 < s_l < W/2$ are uniformly distributed random numbers and $b_l = 0$ in Eq. (1.7). Such a disorder can be induced, e.g., by coupling to static lattice displacements [28]. An open question is whether a 1D spin chain with bond disorder [11, 12] behaves qualitatively different to the site disorder discussed above. Our results indicate that it is not the case.

In Figs. 1.4 and 1.5 we present $T \to \infty$ results for $\sigma(\omega)$ as well as $\kappa(\omega)$ for $\Delta = 1$ and different bond disorder strengths $W = 0.5, 1, 1.5$. Results were obtained using the MCLM method on $L = 20$ sites. Results for larger $W = 1, 1.5$ are well converged with size and clearly indicate that we are again dealing with finite dc limits $\sigma_{dc} > 0$ and $\kappa_{dc} > 0$. With respect to the site disorder case in Figs. 1.1 and 1.2 there are similarities and also differences as follows: (a) for bond disorder we are restricted to $W < 2$ to have a meaningful model without a possibility of a broken bond, (b) the pseudolocalization is less pronounced at least for $\sigma(\omega)$ and shows up only closer to $W = 2$, e.g., for $\kappa(\omega)$ at $W = 1.5$, (c) $\kappa(\omega)$ in Fig. 1.5 reveals a quite abrupt crossover with disorder strength from a Drude-type response at $W = 0.5$ to a localized-like one with $\omega^* > 0$ at $W = 1.0$, and (d) at least for $\sigma(\omega)$ two energy scales are evident in Fig. 1.4 which are not present in the random-field case, (e) for weak disorder, e.g., $W = 0.5$, in the XY regime ($\Delta < 1$) the spin conductivity resembles the behavior of the thermal conductivity which remains qualitatively similar for any value of the anisotropy Δ.

1.5 Temperature dependence

The next issue is the temperature dependence of the dynamical (in particular dc) conductivity and the eventual existence of a critical temperature T_c below which the system becomes insulating [13, 14]. To study this question we employed the FTLM for $L = 20$ with 400 Lanczos steps for high-frequency resolution and $N_r = 100$. The FTLM method, properly interpolating between the $T = 0$ (ground-state) Lanczos method and $T > 0$ behavior, is more reliable for small $T < 0.5$ due to larger L and denser low-energy spectra. Results for $\sigma(\omega)$ and $\kappa(\omega)$ in the isotropic case $\Delta = 1$ and at fixed $W = 2$ are shown in Figs. 1.6 and 1.7 for various $T = 0 - 2$ and $L = 20$ being essentially equal to the results obtained for $L = 16$. The data again indicate that σ_{dc} and κ_{dc} remain finite at all $T > 0$ and vanish only at $T = 0$. A rather abrupt drop of σ_{dc} appears at $T \sim 0.1$ which is however in the range of finite-size temperature T_{fs} for available $L = 20$ below which the FTLM results are not to be trusted [22]. These data suggest a zero critical temperature of localization-delocalization transition, although of course we cannot exclude an exponentially small one, which is beyond the reach of actual numerical simulations.

Note that the finite σ_{dc} in Fig. 1.6 is a result of the finite system size. On the other hand $\kappa_{dc} \simeq 0$ (Fig. 1.7) since $\kappa_{dc} \propto C_V$, where C_V is the specific heat, and vanishes

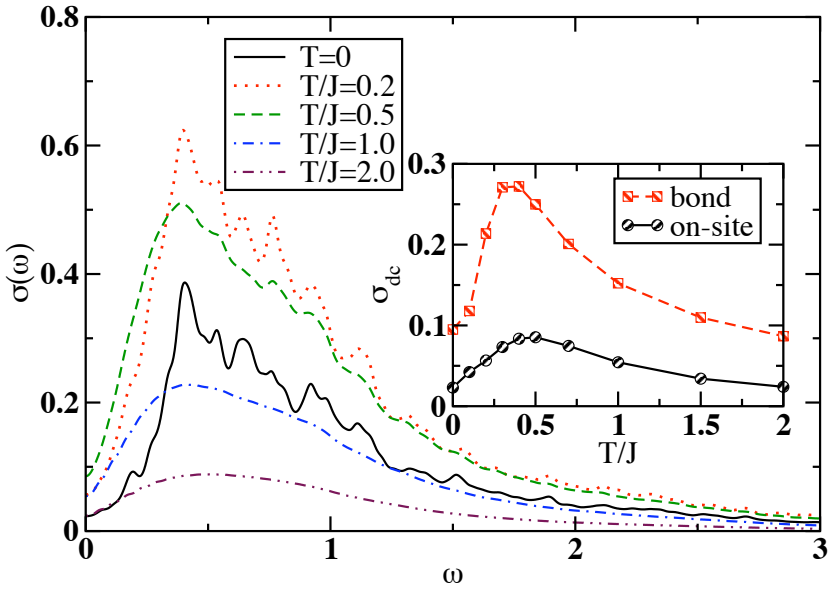

Figure 1.6: Spin conductivity $\sigma(\omega)$ for $\Delta = 1$ and $W = 2$ for various temperatures.

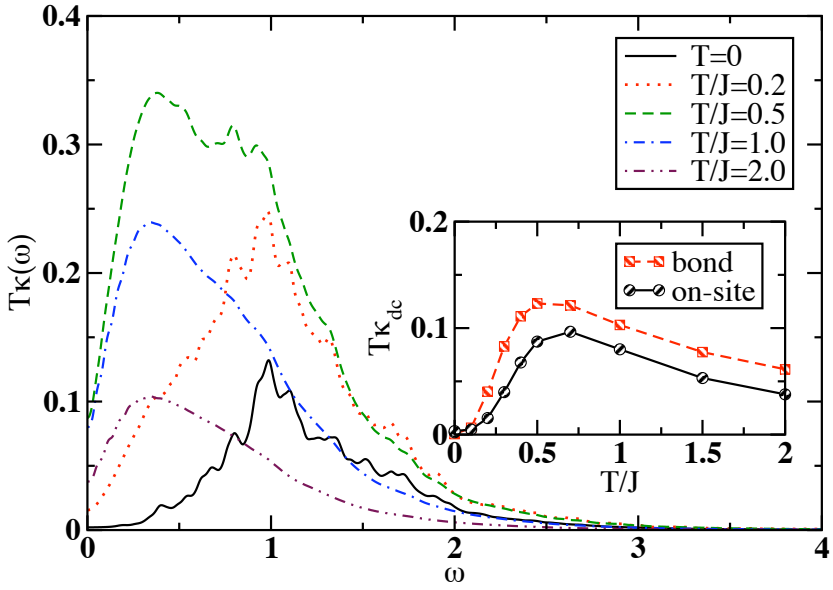

Figure 1.7: Thermal conductivity $\kappa(\omega)$ for $\Delta = 1$ and $W = 2$ for various temperatures.

independently of the localization length. More refined results are shown in Ref. [29].

1.6 Perturbative approximations - XY model

The next issue we would like to discuss is the weak perturbation regime for the non-interacting case, $\Delta = 0$. For weak disorder one expects localization effects to be insignificant—the localization length to be quite large so that conductivities exhibit a Lorentzian like form at high frequencies and a possible sharp drop at the very low ones. This provides the opportunity to discuss the problem using perturbative approximations to obtain the scattering time which will completely determine the high frequency behavior of the conductivities. This analysis applies only to the bulk of the conductivity before localization sets in at low frequencies. We exploit the memory function approach, cf. Ref. [30] or App. B, in order to discuss the effect of many impurities on the XY model. In addition we also use diagrammatic analysis to compare the charge, energy scattering rates with those obtained by the memory function approach.

As we have already mentioned the spin Heisenberg model can be mapped into a spin-less tight binding fermion one (1.6). Particularly for the XY model ($\Delta = 0$) the Jordan-Wigner transformation maps the spin system into a non-interacting ($V = 0$) spin-less tight binding fermionic system at half filling. Thus, starting from the XY model, Eq. (1.1) for $\Delta = 0$, we arrive at

$$H_0 = -t \sum_l c_l^\dagger c_{l+1} + \text{h.c.} \,, \tag{1.20}$$

where $t = -J/2$ is the hopping amplitude of the tight binding fermions and $c^\dagger(c)$ are creation (annihilation) operators. Using the Fourier transform

$$c_l^\dagger = \frac{1}{\sqrt{L}} \sum_p e^{-ilp} c_p^\dagger \,, \tag{1.21}$$

the Hamiltonian H_0 can be diagonalized to obtain

$$H_0 = \sum_p \epsilon_p c_p^\dagger c_p \,. \tag{1.22}$$

The eigenvalues of the pure model ϵ_p are given by

$$\epsilon_p = -2t \cos p \,, \quad \text{with} \quad p = \frac{2\pi}{L} n \,, \quad n = 0, \pm 1, \pm 2, \ldots, \pm(L/2-1), L/2 \,, \tag{1.23}$$

while since the chemical potential is $\mu = 0$ (half filling) the magnitude of the Fermi wavevector is $p_F = \pi/2$.

Applying the Jordan-Wigner transformation to the perturbation Hamiltonian, Eq. (1.7), we obtain

$$H_1 = \sum_l b_l n_l + \text{const.} \,, \quad n_l = c_l^\dagger c_l \,, \tag{1.24}$$

with b_l being the local field distribution. Although in the previous sections we modeled the on-site disorder with a continuum distribution of random fields here we will consider

a finite concentration $c_I = N_I/L$ (N_I is the number of impurities in the system) of identical impurities each of them which yields a scattering potential b. The perturbation Hamiltonian in the momentum space after using the Fourier transform (1.21) will be

$$H_1 = \sum_{p,p'} b_{pp'} c_p^\dagger c_{p'} \,, \qquad b_{pp'} \equiv \frac{1}{L} \sum_l b_l e^{-i(p-p')l} \tag{1.25}$$

and the total Hamiltonian will be given by the sum

$$H = H_0 + H_1 \,. \tag{1.26}$$

Despite the differences of the continuum distribution model to the finite concentration model, for weak perturbations the first few frequency moments would be sufficient to describe the behavior of the conductivities of the two models, at least at higher frequencies. Thus one could require the field distributions to have the same second moment which yields a constrain of the strength of the random distribution W, the concentration c_I and the local potential b, assumed for the finite concentration model. Choosing $b = W/\sqrt{12c_I}$, which satisfies the condition that the two distribution fields have the same second moment, we obtain numerically similar conductivities for the two models, in the weak perturbation regime.

In order to obtain the particle, energy current operators we proceed as in the XXZ model using the respective dipole operators,

$$P = \sum_l r_l n_l, \quad P^\epsilon = \sum_l r_l h_l \,, \tag{1.27}$$

where r_l are the corresponding coordinates and n_l, h_l the particle and the energy density operators respectively. Hence the particle, energy currents will be

$$\jmath = \sum_l \jmath_l, \qquad \jmath^\epsilon = \sum_l \jmath_l^\epsilon + \frac{b_l}{2}(\jmath_{l-1} + \jmath_l) \,, \tag{1.28}$$

where the local currents $\jmath_l, \jmath_l^\epsilon$ are given by

$$\jmath_l = -it(c_l^\dagger c_{l+1} - \text{h.c.}) \,, \quad \jmath_l^\epsilon = +it^2(c_{l-1}^\dagger c_{l+1} - \text{h.c.}) \,. \tag{1.29}$$

Using the Fourier transform (1.21) for the creation, annihilation operators which appear in $\jmath_l$, we have for the particle current

$$\jmath = \sum_p v_p c_p^\dagger c_p \,, \qquad \text{where} \,, \qquad v_p = 2t \sin p \,. \tag{1.30}$$

For the energy current where an extra term $\jmath_1^\epsilon$ has emerged due to the perturbation H_1, we will have using (1.21)

$$\jmath^\epsilon = \jmath_0^\epsilon + \jmath_1^\epsilon \,, \qquad \jmath_0^\epsilon = \sum_p \epsilon_p v_p c_p^\dagger c_p, \quad \jmath_1^\epsilon = \sum_{p,p'} \vartheta_{pp'} c_p^\dagger c_{p'} \tag{1.31}$$

with

$$\vartheta_{pp'} = \frac{v_p + v_{p'}}{2} b_{pp'} = 2t \, \sin\left(\frac{p+p'}{2}\right) \cos\left(\frac{p-p'}{2}\right) b_{pp'} \,. \tag{1.32}$$

1.6.1 Diagrammatic analysis - particle relaxation rate

The problem of scattering of non-interacting fermions on static impurities is presented in many standard many-particle textbooks [17, 31–33]. We follow here the diagrammatic approach to explore the scattering of the 1D tight binding fermions on static impurities. Although Eqs. (1.24), (1.25) were obtained directly from the spin model using the Jordan-Wigner transformation we would like to reformulate the scattering Hamiltonian in an equivalent way, which allows to be more compatible with the literature.

Let us consider a number N_I of impurities being present in the system and each of which yields an extended potential on which fermions are scattered. This can be formulated by writing the perturbation Hamiltonian $\mathcal{H}$ as

$$\mathcal{H} = \sum_{l'}{}' \sum_{l} b_{ll'} c_l^\dagger c_l \,, \tag{1.33}$$

which reduces to H_1, Eq. (1.25), for $b_{ll'} \sim \delta_{ll'}$. The prime at the first sum denotes that the sum does not extend through the whole system but only through the locations of the impurities l', while the sum without the prime extends through all system sites. The subscript ll' of the field b denotes the distance of a given point l of the lattice from the location l' of the impurity.

Using the Fourier transform (1.21), we arrive at the Hamiltonian

$$\mathcal{H} = \sum_{pp'} \tilde{b}_{pp'} c_p^\dagger c_{p'} \,, \tag{1.34}$$

where the scattering potential $\tilde{b}_{pp'}$ is given by

$$\tilde{b}_{pp'} \equiv \sum_{l}{}' e^{-i(p-p')l} b_{pp'} \,, \qquad b_{pp'} \equiv \frac{1}{L} \sum_{l} b_{ll'} e^{-i(p-p')(l-l')} \,. \tag{1.35}$$

Finally, in order to calculate the particle, energy current relaxation rates and in order to handle simultaneously both, we consider a current $\mathcal{J}$ of the form

$$\mathcal{J} = \sum_{p} \jmath_p c_p^\dagger c_p. \tag{1.36}$$

For charge transport $\jmath_p = v_p$ while for energy transport $\jmath_p = \epsilon_p v_p$, i.e., we neglect the extra non-diagonal term $\jmath_1^\epsilon$ of the energy current. The latter assumption can be justified using the memory function approach, cf. Sec. 1.6.3.

It is necessary before proceeding with the current relaxation rate to evaluate the single particle relaxation rate. We start with the definition of the one-particle retarded Green's function

$$G_{pp'}(t) \equiv -i\theta(t) \langle \{ c_p(t), c_{p'}^\dagger \} \rangle \tag{1.37}$$

where $\theta(t)$ is the step function and the braces denote the anticommutator of the enclosed fermionic operators. Writing the equation of motion for $G_{pp'}(t)$ and taking the Fourier transform we obtain the following equation

$$G_{pp'}(z) = \delta_{pp'} G^0_p(z) + G^0_p(z) \sum_q \tilde{b}_{pq} G_{qp'}(z) \,, \tag{1.38}$$

where $z = \varepsilon + i\eta$ ($\eta > 0$); the Fourier transform and the inverse Fourier transform for a function g are given by

$$g(t) = \int_{-\infty}^{\infty} \frac{d\varepsilon}{2\pi} e^{-i\varepsilon t} g(\varepsilon) \,, \qquad g(\varepsilon) = \int_{-\infty}^{\infty} dt e^{+i\varepsilon t} g(t) \,, \tag{1.39}$$

$\delta_{pp'}$ is the Kronecker $\delta-$function and G^0_p is the Green's function (1.37) calculated in the unperturbed system

$$G^0_p(z) = \frac{1}{z - \epsilon_p} \,. \tag{1.40}$$

Eq. (1.38) can be expanded in an infinite series of terms where only the free propagator G^0 will be involved. Writing only up to second order terms of this expansion, with respect to the Born scattering $\tilde{b}$, the full propagator $G_{pp'}$ can be written

$$\begin{aligned} G_{pp'}(z) = \delta_{pp'} G^0_p(z) \quad &+ \quad G^0_p(z)\, \tilde{b}_{pp'}\, G^0_{p'}(z) \\ &+ \quad G^0_p(z) \sum_q \tilde{b}_{pq} G^0_q(z) \tilde{b}_{qp'}\, G^0_{p'}(z) + \dots \quad . \end{aligned} \tag{1.41}$$

We will now implement the standard trick of averaging over the random distributions of impurities. To become more concrete, assume the averaged Green's function $\overline{G}_{pp'}$, where the line over the Green's function denotes an average over the possible random distributions of impurities. $G^0_p(z)$ is the propagator in the pure system and consequently it does not depend on the impurity distribution. Thus, the only quantity in Eq. (1.41) that depends on the impurity distribution is the scattering potential $\tilde{b}$. Performing the average over the random configurations of impurities for a term where a single $\tilde{b}_{pp'}$ field appears the exponential factor of the potential $\tilde{b}_{pp'}$ (1.35) will be [17, 31]

$$\overline{{\sum_l}' e^{-i(p-p')l}} = N_I \; \overline{e^{-i(p-p')l}} = N_I \delta_{pp'} \,.$$

In second order with respect to the scattering potential, terms which involve the product of two such exponential factors have to be averaged, i.e. ,

$$\overline{{\sum_l}' e^{-i(p-p')l} + {\sum_{l \neq l'}}' e^{-i(q-p)l - i(p'-q)l'}} \simeq N_I \delta_{pp'} + N_I^2 \delta_{qp} \delta_{p'q} \,,$$

and so on for the highest order terms. Omitting the line for the averaged propagator, $\overline{G} \to G$, we will have from Eq. (1.41)

$$\begin{aligned} G_{pp'}(z) \quad &= \quad \delta_{pp'} G^0_p(z) + G^0_p(z) \cdot N_I b_{pp'} \delta_{pp'} \cdot G^0_{p'}(z) \\ &+ \quad G^0_p(z) \cdot \sum_q b_{pq} G^0_q(z) \left(N_I \delta_{pp'} + N_I^2 \delta_{qp} \delta_{p'q} \right) b_{qp'} \cdot G^0_{p'}(z) + \dots \,. \end{aligned} \tag{1.42}$$

From the above, it is clear that the averaging over the impurity distributions makes the Green's function diagonal to the indices pp', $G_{pp'}(z) \to G_p(z)$.

Eq. (1.42) can be represented in a diagrammatic way

$G_p(z) \;=$ 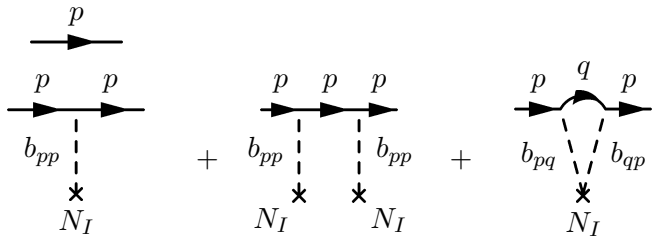

(1.43)

where each solid line with an arrow denotes a free propagator G^0 (1.40) with the corresponding labeled momentum, the dashed lines denote a factor of the impurity scattering potential as defined in Eq. (1.35) while each cross multiplies a diagram with a factor N_I. Finally, a sum over all the internal momenta (which are not equal with the external) should be taken. Considering a dilute concentration of impurities a significant simplification occurs. In this approximation high order in concentration c_I diagrams can be neglected. Thus in the dilute concentration limit diagrams with only one cross will contribute to the retarded Green's function, since these will be the only ones linear in the concentration c_I. This means that diagrams like the one in the middle of the bottom line of Eq. (1.43) will be neglected. On the other hand the first and the third diagrams of the bottom line of Eq. (1.43) are linear in concentration c_I although they might be of different order with respect to the scattering potential b.

Furthermore, introducing the concept of the irreducible[1], retarded self energy $\Sigma_p(z)$, one can write the Dyson's equation for the propagator $G_p(z)$ [31, 34]

$$G_p(z) = G_p^0(z) + G_p^0(z)\Sigma_p(z)G_p(z) \quad \Rightarrow \quad G_p(\varepsilon) = \frac{1}{\varepsilon - \epsilon_p - \Sigma_p(\varepsilon)}\,. \tag{1.44}$$

The diagrams which contribute to the self energy are the same with those of the Green's function except that the external lines have been removed. Hence, for the self energy we will have (presenting diagrams $\mathcal{O}(b^3)$)

$\Sigma_p(z) \;\simeq$ 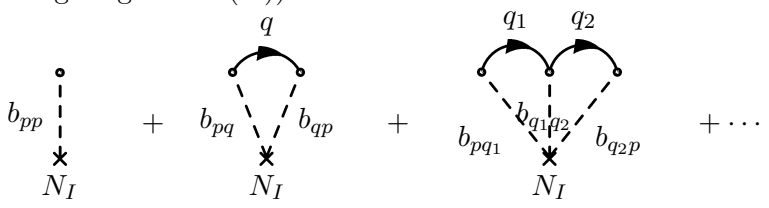

(1.45)

If we assume a weak scattering potential then we will be interested in terms up to second order in Born scattering, i.e., we should take into account only the first two diagrams of the self energy (1.45). However, let us not truncate the series of the self

[1] As a matter of fact, since we have kept the lowest order diagrams in concentration all the self energy diagrams that have to be taken into account are irreducible.

energy but instead consider the contribution of a self energy diagram which corresponds to an arbitrary order of the perturbation theory with respect to the scattering potential. That diagram would be

$\Sigma_p^{(n+1)}(z)$ = 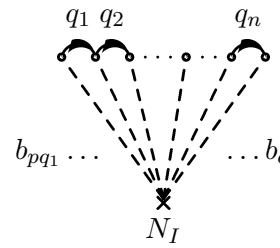

, $n \geq 1$. (1.46)

Let us mention once again that even though this diagram represents an arbitrary order of perturbation with respect to the scattering potential b it is only linear to the concentration of impurities c_I. The contribution of this term to the self energy will be

$$\Sigma_p^{(n+1)}(z) = N_I \sum_{q_1,\ldots,q_n} \frac{b_{pq_1} b_{q_1 q_2} \ldots b_{q_n p}}{(z-\epsilon_{q_1})(z-\epsilon_{q_2})\ldots(z-\epsilon_{q_n})} \,. \tag{1.47}$$

Taking the potential scattering to be of the form $b_{ll'} = b\delta_{ll'}$ we revert to the initial form for the scattering potential (1.24), (1.25) where the distribution of fields consists of N_I constant fields $b_l = b$ distributed in a random way. Thus the scattering potential will be constant in the momentum space which simplifies farther the problem and permits the calculation of the sum of Eq. (1.47). Summations in Eq. (1.47) will decouple, hence

$$\Sigma_p^{(n+1)}(z) = c_I b \left(\frac{1}{L} \sum_q \frac{b}{z-\epsilon_q} \right)^n \,. \tag{1.48}$$

In the thermodynamic limit the summation can be replaced by an integral over the first Brillouin zone. The (n+1) term of the self energy will be proportional to the nth power of this integral $\mathcal{I}$, $\Sigma_p^{(n+1)} \propto \mathcal{I}^n$, which will be of the form

$$\mathcal{I} = \int_{-\pi}^{\pi} \frac{dq}{\alpha - \cos q} \,, \tag{1.49}$$

with α being a complex constant. It is easy calculate this integral in the complex plane with the suitable change of variable $w = \exp(iq)$ after which the integral becomes

$$\mathcal{I} = 2i \oint_C \frac{dw}{w^2 - 2\alpha w + 1} \,,$$

where the contour of integration C is the unit circle. Apparently only one of the two roots $w_\pm$ of the polynomial in the denominator of the integrand will be inside the contour of integration. Hence using the residue theorem the result will be

$$\mathcal{I} = \pm \frac{-4\pi}{w_+ - w_-} \,,$$

with the sign chosen regarding to which root is in the contour. The roots of the polynomial are

$$w_{\pm} = \alpha \pm \sqrt{\alpha^2 - 1}\,,$$

and the one which is in the circle is the w_-. Finally, the integral will be

$$\mathfrak{I} = \frac{2\pi}{\sqrt{\alpha^2 - 1}}\,, \tag{1.50}$$

and Eq. (1.48) becomes

$$\Sigma_p^{(n+1)}(z) = c_I b \left(\frac{b}{2t} \frac{1}{\sqrt{\left(\frac{z}{2t}\right)^2 - 1}} \right)^n \,. \tag{1.51}$$

Result (1.51) is the contribution to the self energy up to an arbitrary (n+1) order with respect to the potential scattering b.

The quantity in the parenthesis of Eq. (1.51) resembles the density of states per volume for the pure one dimensional tight binding model which is given by

$$\rho(\varepsilon) = \frac{1}{2\pi t} \frac{1}{\sqrt{1 - \left(\frac{\varepsilon}{2t}\right)^2}}\,. \tag{1.52}$$

Using (1.45), (1.51) and (1.52) we obtain for the self energy in the lowest order of the concentration c_I

$$\Sigma_p(z) = c_I b \left(1 + \sum_{n=0}^{\infty} \left(-i\pi b \rho(z)\right)^n \right)\,, \tag{1.53}$$

which according to the previous is independent of the index p. In Ref. [31] a similar formula for the self energy is obtained, evaluated in second order but independently of the particular model or its dimensionality.

Considering a quasi particle picture the scattering relaxation rate can be defined from the retarded self energy as [17, 18, 31]

$$\frac{1}{\tau} \equiv -2\Im\Sigma_p(\varepsilon)\Big|_{\varepsilon \to 0}\,. \tag{1.54}$$

Within second order Born approximation we obtain

$$\frac{1}{\tau} = 2c_I \left(\frac{b^2}{2t} \right)\,, \tag{1.55}$$

while if we sum up all the terms for the self energy we have

$$\tau_\infty = \tau \left(1 + \left(\frac{b}{2t} \right)^2 \right)\,. \tag{1.56}$$

1.6.2 Diagrammatic analysis - transport relaxation rate

The next step is to evaluate the particle and thermal conductivities in the presence of impurities using the diagrammatic technique. The regular parts of the particle, energy conductivities are related to the corresponding susceptibility, Eqs. (1.12), (1.13). It is clear that the current-current susceptibility is the retarded current-current Green's function

$$-\chi_{\mathcal{J}\mathcal{J}}(t) = G_{\mathcal{J}\mathcal{J}}(t) \equiv -i\theta(t)\langle[\mathcal{J}(t),\mathcal{J}]\rangle\,, \tag{1.57}$$

where this time the commutator of the two operators is involved since we are dealing with a two-particle Green's function. Recall that the current $\mathcal{J}$ is given by Eq. (1.36).

However, instead of proceeding with the retarded Green's function we choose to work with the thermal Green's function, defined as

$$-\chi^{T}_{\mathcal{J}\mathcal{J}}(\lambda) = \mathcal{G}_{\mathcal{J}\mathcal{J}}(\lambda) \equiv -\langle\mathcal{T}(\mathcal{J}(\lambda)\mathcal{J})\rangle\,. \tag{1.58}$$

The time ordering operator $\mathcal{T}$ for two operators $\hat{O}_p, \hat{O}_q$ is defined as

$$\mathcal{T}(\hat{O}_p(\lambda)\hat{O}_q) \equiv \theta(\lambda)\hat{O}_p(\lambda)\hat{O}_q \pm \theta(-\lambda)\hat{O}_q\hat{O}_p(\lambda)\,; \tag{1.59}$$

the sign is chosen appropriately for bosonic (+) or fermionic (−) operators. The imaginary time evolution of an operator $\hat{O}$ is obtained by

$$\hat{O}(\lambda) = e^{\lambda H}\hat{O}\; e^{-\lambda H}\,. \tag{1.60}$$

Finally the retarded Green's function will be obtained from the thermal one by implementing an analytical continuation in the frequency domain.

It is useful to define here the imaginary time Fourier transform

$$g(\lambda) = \frac{1}{\beta}\sum_{n=-\infty}^{\infty} e^{-i\omega_n\lambda} g(i\omega_n)\,, \qquad g(i\omega_n) = \int_0^\beta d\lambda e^{+i\omega_n\lambda} g(\lambda)\,, \tag{1.61}$$

where the Matsubara frequencies ω_n are given by

$$\omega_n = \begin{cases} \dfrac{2n\pi}{\beta}\,, & \text{bosonic} \\ \dfrac{(2n+1)\pi}{\beta}\,, & \text{fermionic} \end{cases} \qquad \text{with} \quad n \in \mathbb{Z}\,. \tag{1.62}$$

Starting from the definition of the current-current thermal Green's function (1.58) one can express the two-particle Green's function as a product of two one-particle Green's functions

$$\mathcal{G}_{\mathcal{J}\mathcal{J}}(\lambda) = \sum_{pp'} \jmath_p \jmath_{p'}\,, \mathcal{G}_{pp'}(\lambda)\mathcal{G}_{p'p}(-\lambda)\,, \tag{1.63}$$

with the single-particle thermal Green's function defined as

$$\mathcal{G}_{pp'}(\lambda) \equiv -\langle \mathcal{T}(c_p(\lambda)c^\dagger_{p'})\rangle \,. \tag{1.64}$$

The Fourier component of the thermal Green's function in the frequency domain $\mathcal{G}_{\mathcal{J}\mathcal{J}}(i\omega_n)$ will be given by

$$\mathcal{G}_{\mathcal{J}\mathcal{J}}(i\omega_n) = \frac{1}{\beta}\sum_{pp'} \jmath_p \jmath_{p'} \sum_m \mathcal{G}_{pp'}(i\omega_n + i\omega_m)\mathcal{G}_{p'p}(i\omega_m) \,. \tag{1.65}$$

Our aim now is to expand the one-particle thermal Green's function $\mathcal{G}_{pp'}(i\omega_n)$ in a series which contains products of the one-particle Green's function which is calculated in the unperturbed system,

$$\mathcal{G}^0_{pp'}(i\omega_n) = \delta_{pp'}\mathcal{G}^0_p(i\omega_n) \,, \qquad \mathcal{G}^0_p(i\omega_n) = \frac{1}{i\omega_n - \epsilon_p} \,, \tag{1.66}$$

similarly with the procedure we followed for the the evaluation of the single particle relaxation rate. Eqs. (1.38), (1.41) which were obtained for the one-particle retarded Green's function hold as well for the thermal one, with $G \to \mathcal{G}$ and $z \to i\omega_n$. We plug the corresponding for the thermal Green's functions Eq. (1.41) into Eq. (1.65) and consider again an average over the random distribution of impurities. The result of this procedure can be described by the following equation

$\beta\mathcal{G}_{\mathcal{J}\mathcal{J}}(i\omega_n) \quad =$ 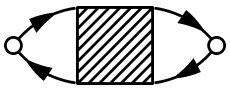 , (1.67)

where the shaded box denotes all the diagrams which contribute to the thermal Green's function, the solid lines with the arrows denote the single particle free propagators $\mathcal{G}^0_p(i\omega_l)$, where ω_l is either $\omega_l = \omega_m + \omega_n$ or $\omega_l = \omega_m$, the empty circles denote the current matrix element $\jmath_p$, while the indices of the left and the right free propagators are not necessarily the same.

We can classify the diagrams that contribute to $\mathcal{G}_{\mathcal{J}\mathcal{J}}$ into two categories. The one-particle scattering diagrams, which are diagrams where the upper propagators are not connected with the lower ones, for instance

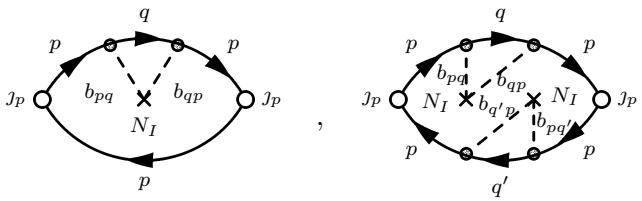

.

The second category consists of diagrams where the two particles are scattered from the same impurity, i.e., the upper lines are connected with the lower ones, for example

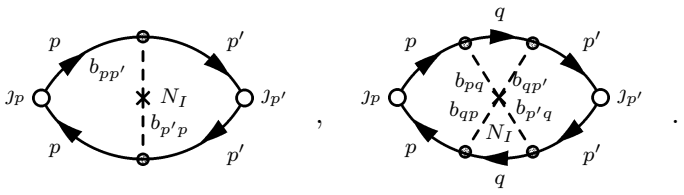

The reason we made the previous discrimination is that the single particle scattering diagrams can be summed by replacing the bare propagators $\mathcal{G}^0$ with the corresponding one-particle dressed propagators $\mathcal{G}$. Thus, we end up in summing only diagrams which connect the upper and the lower lines but the cost we have to pay is that we are not dealing any more with the free propagators. Now we have an infinite series of diagrams which have to be summed up and each of these diagrams will be a two-particle diagram but the scattering events are connected with the full one-particle propagators. In the lowest order approximation with respect to the concentration of impurities and to the scattering potential the current-current thermal Green's function will be given by the infinite sum of ladder diagrams [31–33]

$$\beta \mathcal{G}_{\mathcal{J}\mathcal{J}}(i\omega_n) = \tag{1.68}$$

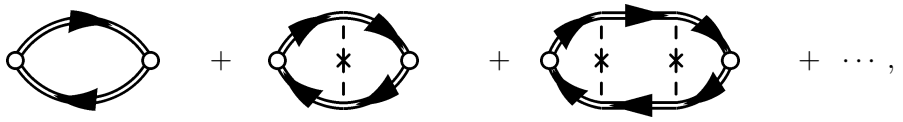

where the double lines represent the full single particle propagators $\mathcal{G}_p$. Eq. (1.68) can be written with the aid of the vertex function Γ as

$$\beta \mathcal{G}_{\mathcal{J}\mathcal{J}}(i\omega_n) = \tag{1.69}$$

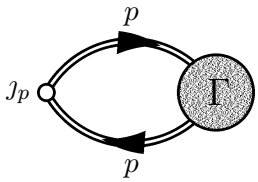

$$\equiv -\sum_p \sum_m \Gamma_p^0 \, \mathcal{G}_p(i\omega_m + i\omega_n)\mathcal{G}_p(i\omega_m)\Gamma_p(i\omega_m + i\omega_n, i\omega_m)$$

where $\Gamma_p^0 = \jmath_p$ and the vertex function $\Gamma_p = \Gamma_{pp}$ is given by

$$= \Gamma_p^0 + N_I \sum_q |b_{pq}|^2 \, \mathcal{G}_q(i\omega_m + i\omega_n)\mathcal{G}_q(i\omega_m)\Gamma_q(i\omega_m + i\omega_n, i\omega_m) \tag{1.70}$$

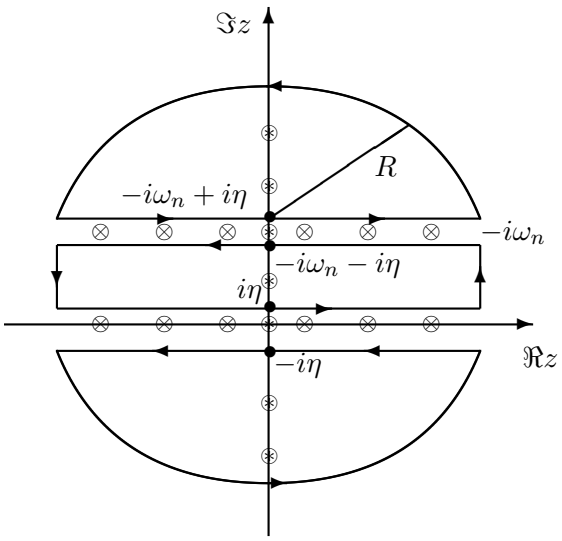

Figure 1.8: The contour of integration which is used to evaluate the sum in Eq. (1.73). The poles of f are denoted with $\circledast$, poles of g are denoted with $\otimes$ while the points where the contour intersects the imaginary axis are denoted with $\bullet$.

Hence, the current-current thermal Green's function will be given by Eq. (1.69) where the Γ-function will be given by Eq. (1.70).

Let us now proceed with the evaluation of the current-current Green's function and start with the sum over the Matsubara frequencies. The sum over the Matsubara frequencies is performed by a contour integration in the complex plane. Consider the generic function $g(i\omega_m + i\omega_n, i\omega_m)$ and the summation over the Matsubara frequencies $\mathcal{S}(i\omega_n)$, corresponding to the summation that appears in Eq. (1.69), given by

$$\mathcal{S}(i\omega_n) = \frac{1}{\beta}\sum_m g(i\omega_m + i\omega_n, i\omega_m)\,. \tag{1.71}$$

Using the Fermi-Dirac distribution $f(\varepsilon)$,

$$f(\varepsilon) = \frac{1}{e^{\beta\varepsilon}+1}\,, \tag{1.72}$$

one can show that the sum $\mathcal{S}$ will be given by the integral

$$\mathcal{S}(i\omega_n) = -\int_C \frac{dz}{2\pi i} f(z) g(z + i\omega_n, z)\,. \tag{1.73}$$

The contour of integration C is depicted in Fig. 1.8. It consists of two semicircles of radius R, one in the upper and one in the lower complex plane, and a rectangle of length R. The poles of the generic function g are denoted with the symbol $\otimes$ while

those of f with $\circledast$. The symbol $\bullet$ stands for the points where the contour intersects the imaginary axis (except those with $z \sim iR$.) Taking the limit $R \to \infty$ and at the end performing an analytical continuation of the frequency variable $i\omega_n \to \omega + i\eta$ we arrive at

$$\mathcal{S}(\omega + i\eta) = i \int_{-\infty}^{\infty} \frac{d\varepsilon}{2\pi} \Big[(f(\varepsilon + \omega) - f(\varepsilon)) g(\varepsilon + \omega + i\eta, \varepsilon - i\eta) + f(\varepsilon) g(\varepsilon + \omega + i\eta, \varepsilon + i\eta) - f(\varepsilon + \omega) g(\varepsilon + \omega - i\eta, \varepsilon - i\eta) \Big] . \tag{1.74}$$

Since we are interested in the low frequency behavior of the conductivity, we can expand the Fermi-Dirac distribution with respect to the frequency ω, set $\omega = 0$ in the function g and using Eqs. (1.12), (1.13), (1.57) we obtain for the conductivity of the current $\mathcal{J}$

$$\sigma^{\mathcal{J}}(\omega \to 0) = -\frac{1}{L} \Re \sum_p \jmath_p \int_{-\infty}^{\infty} \frac{d\varepsilon}{2\pi} f'(\varepsilon) |G_p(\varepsilon)|^2 \Gamma_p(\varepsilon + i0^+, \varepsilon + i0^-) . \tag{1.75}$$

Terms which are proportional to G_p^2 have been thrown away in the formula for the conductivity above (see discussion in Ref. [33]) and f' denotes the derivative of the Fermi-Dirac distribution with respect to ε. The retarded Green's function can be written using the retarded self energy (1.44). Furthermore exploiting the property for the magnitude of any complex number w

$$\left| \frac{1}{w} \right|^2 = \frac{1}{\Im w^*} \Im \frac{1}{w} , \tag{1.76}$$

the magnitude of the retarded Green's function will be

$$|G_p(\varepsilon)|^2 = \tau A_p(\varepsilon) . \tag{1.77}$$

The scattering time τ is defined in Eq. (1.54), its value is given in second order by (1.55) and $A_p(\varepsilon)$ is the spectral function which is defined as

$$A_p(\varepsilon) \equiv i(G_p(\varepsilon) - G_p^*(\varepsilon)) = -2\Im G_p(\varepsilon) . \tag{1.78}$$

Hence the dc conductivity will become

$$\sigma_{dc}^{\mathcal{J}} = -\tau \frac{1}{L} \sum_p \jmath_p \int_{-\infty}^{\infty} \frac{d\varepsilon}{2\pi} f'(\varepsilon) A_p(\varepsilon) \Gamma_p(\varepsilon + i0^+, \varepsilon + i0^-) . \tag{1.79}$$

The simplest way to evaluate the integral giving the conductivity is to neglect the vertex corrections, i.e. take $\Gamma_p \simeq \Gamma_p^0 = \jmath_p$ and approximate the spectral function with its unperturbed form, $A_p(\varepsilon) \simeq 2\pi\delta(\varepsilon - \epsilon_p)$. Taking the thermodynamic limit, the conductivity of the current $\mathcal{J}$ will be

$$\sigma_{dc}^{\mathcal{J}} \sim \tau \left(\frac{\chi_0^{\mathcal{J}}}{L} \right) , \qquad \chi_0^{\mathcal{J}} = \beta \langle \mathcal{J}\mathcal{J} \rangle , \tag{1.80}$$

implying that the relaxation rate of the current $\mathcal{J}$ is the same one as the particle relaxation rate, given by Eq. (1.55). Another important conclusion is that the relaxation rate depends only on the general form that was initially assumed for the current $\mathcal{J}$ (1.36). In other words the relaxation rate of the charge and the energy current will be the same, which is consistent with the well known Wiedemann-Franz law

$$\tau^{\epsilon} = \tau \,, \qquad \text{with} \qquad \frac{1}{\tau} = 2c_I \left(\frac{b^2}{2t}\right) \,, \tag{1.81}$$

while charge and thermal conductivity will be given by

$$\sigma_{dc} = \tau \left(\frac{\chi_0}{L}\right) \,, \qquad T\kappa_{dc} = \tau \left(\frac{\chi_0^{\epsilon}}{L}\right) . \tag{1.82}$$

The assumption we have made that there is only elastic scattering on the impurities accounts for the fact that we arrive at the same scattering time for the particle and the energy currents.

If we do not neglect the vertex corrections, we can still proceed with the evaluation of the integral in the low temperature limit. At low temperatures the Fermi-Dirac distribution can be approximated with a step function as $f(\varepsilon) \simeq 1 - \theta(\varepsilon)$ and the integral in Eq. (1.79) becomes

$$\sigma_{dc}^{\mathcal{J}} = \frac{\tau}{4\pi^2} \int_{-\pi}^{\pi} \jmath_p A_p(0) \Gamma_p(i0^+, i0^-) dp \ . \tag{1.83}$$

Using Eq. (1.70) the Γ-function will be given by

$$\Gamma_p(i0^+, i0^-) = \jmath_p + c_I \tau b^2 \int_{-\pi}^{\pi} \frac{dq}{2\pi} A_q(0) \Gamma_q(i0^+, i0^-) \,. \tag{1.84}$$

Approximating again the spectral function with a δ-function we can see that the vertex corrections vanish for $p = \pm p_F$. Thus, for this particular model in the low temperature limit vertex corrections do not contribute to the transport scattering rate.

1.6.3 Scattering time via memory function approach

After evaluating the dc conductivities via the diagrammatic analysis in the previous paragraphs we would like to perform the same calculation using this time the memory function (MF) approach [30]. We choose to repeat this calculation in order to compare and test the memory function approach since it will be used in cases where analytical calculations are not possible. The gist of the memory function approach is that one can evaluate the scattering time, in the lowest order with respect to the concentration of impurities c_I, assuming that only a single impurity is present in the system. To obtain the scattering rate in the presence of N_I impurities one should multiply the scattering rate of the single impurity with the concentration c_I. The perturbative memory function (scattering rate) is calculated from the force-force susceptibility where the particle j

and the energy $\dot{j^\epsilon}$ force operators (dots over the current operators denote the derivative with respect to time) are given from (neglecting second order in concentration terms)

$$j = \sum_{p,p'} \phi_{pp'} c_p^\dagger c_{p'}, \quad \phi_{pp'} = i(v_p - v_{p'}) b_{pp'} \,, \tag{1.85a}$$

$$\dot{j^\epsilon} = \sum_{p,p'} \phi^\epsilon_{pp'} c_p^\dagger c_{p'} \,, \quad \phi^\epsilon_{pp'} = i(\epsilon_p v_p - \epsilon_{p'} v_{p'}) b_{pp'} - (\epsilon_p - \epsilon_{p'}) \vartheta_{pp'} \,. \tag{1.85b}$$

The imaginary part of the respective particle M_0 and energy N_0 memory functions (Eq. B.11) are given by

$$M_0''(\omega) = \pi \frac{c_I}{(\chi_0/L)} \frac{1 - e^{-\beta\omega}}{\omega} \sum_{p,p'} |\phi_{pp'}|^2 f_p (1 - f_{p'}) \delta(\epsilon_{p'} - \epsilon_p - \omega) \,, \tag{1.86a}$$

$$N_0''(\omega) = \pi \frac{c_I}{(\chi^\epsilon_0/L)} \frac{1 - e^{-\beta\omega}}{\omega} \sum_{p,p'} |\phi^\epsilon_{pp'}|^2 f_p (1 - f_{p'}) \delta(\epsilon_{p'} - \epsilon_p - \omega) \,, \tag{1.86b}$$

where the subscript 0 denotes that memory functions are calculated in the unperturbed system and f_p is the Fermi-Dirac distribution

$$f_p = \frac{1}{e^{\beta\epsilon_p} + 1} \,.$$

Since only one impurity is considered to be present in the system we can choose to place it at the origin of the system, i.e. $b_l = b\delta_{l,0}$. The scattering potential in momentum space $b_{pp'}$ will be constant, $b_{pp'} = b/L$. After evaluating the corresponding memory functions the particle and energy conductivities are obtained using Eq. (B.3)

$$\tilde{\sigma}(z) = \frac{i(\chi_0/L)}{z + M_0(z)} \,, \quad \tilde{\kappa}(z) = \frac{1}{T} \frac{i(\chi^\epsilon_0/L)}{z + N_0(z)} \,, \tag{1.87}$$

where we use the symbols $\tilde{\sigma}, \tilde{\kappa}$ for the complex particle and thermal conductivities respectively.

The corresponding τ, τ^ϵ scattering rates are obtained by taking the limit $\omega \to 0$ in Eqs. (1.86) as imposed by Eq (1.87) (see also discussion in Appx. B which ends up in Eqs. (B.4), (B.6)), hence,

$$\frac{1}{\tau} = M''(\omega \to 0) = \pi\beta \frac{c_I}{(\chi_0/L)} \sum_{p,p'} |\phi_{pp'}|^2 f_p (1 - f_{p'}) \delta(\epsilon_{p'} - \epsilon_p) \,, \tag{1.88a}$$

$$\frac{1}{\tau^\epsilon} = N''(\omega \to 0) = \pi\beta \frac{c_I}{(\chi^\epsilon_0/L)} \sum_{p,p'} |\phi^\epsilon_{pp'}|^2 f_p (1 - f_{p'}) \delta(\epsilon_{p'} - \epsilon_p) \,. \tag{1.88b}$$

Taking the thermodynamic limit and using the property of the δ-function which has as an argument a function $g(p)$ with roots p_i,

$$\delta(g(p)) = \sum_i \frac{\delta(p-p_i)}{|g'(p_i)|}\,, \qquad g'(p) = \frac{d}{dp}\, g(p)\,,$$

we conclude that from the integral over the momentum p' only two values will contribute, the $p' = \pm p$. Looking at the force operators' matrix elements (1.85) we can conclude that only terms with $p' = -p$ will contribute to the memory function for both the particle and the energy current. Furthermore for the case of the energy current it is easy to observe that the term which is proportional to ϑ vanishes for $p' = \pm p$ (1.32), (1.85b). This leads to the conclusion that the perturbative current $\jmath_1^\epsilon$, Eq. (1.31), which had emerged due to the perturbation does not contribute to the scattering time, supporting the result for the energy scattering rate with the diagrammatic analysis where it was considered only the diagonal term of the energy current. Finally, at low temperatures only transitions from states around $p = \pm p_F$ will occur. Expanding the energy eigenvalues ϵ_p and the velocity v_p around the points $p = \pm p_F$ we will have

$$\epsilon_p \simeq \pm v_F p\,, \quad v_p \simeq \pm v_F\,, \quad v_F = 2t \tag{1.89}$$

Performing the integrals (1.88) in addition with the low temperature assumptions we arrive at

$$\frac{1}{\tau} = \pi\beta \frac{c_I}{(\chi_0/L)} \left(b^2 \frac{2}{\pi^2} T \right)\,, \quad \frac{1}{\tau^\epsilon} = \pi\beta \frac{c_I}{(\chi_0^\epsilon/L)} \left(\frac{2}{3} b^2 T^3 \right) \tag{1.90}$$

with

$$\chi_0 = \frac{v_F}{\pi} L\,, \qquad \chi_0^\epsilon = \frac{\pi}{3} v_F L T^2\,. \tag{1.91}$$

Combining Eqs. (1.90), (1.91) we are led to the scattering time which was obtained by the quite bothersome diagrammatic analysis Eq. (1.81)

$$\tau^\epsilon = \tau\,, \qquad \text{with} \qquad \frac{1}{\tau} = 2c_I \left(\frac{b^2}{2t} \right)\,,$$

while for the Wiedemann-Franz law we will have (cf. Ref. [35]).

$$\frac{\kappa(T)}{\sigma(T)} = \frac{\pi^2}{3} T\,. \tag{1.92}$$

Scattering times can also be evaluated via memory function in the high temperature regime ($\beta \to 0$). Starting from Eq. (B.11) we have for the imaginary part of the corresponding memory functions

$$M_0''(\omega) = \pi \frac{c_I}{(\chi_0/L)} \sum_{p,p'} |\phi_{pp'}|^2 \frac{f_p - f_{p'}}{\omega} \delta(\epsilon_{p'} - \epsilon_p - \omega)\,, \tag{1.93a}$$

$$N_0''(\omega) = \pi \frac{c_I}{(\chi_0^\epsilon/L)} \sum_{p,p'} |\phi_{pp'}^\epsilon|^2 \frac{f_p - f_{p'}}{\omega} \delta(\epsilon_{p'} - \epsilon_p - \omega)\,. \tag{1.93b}$$

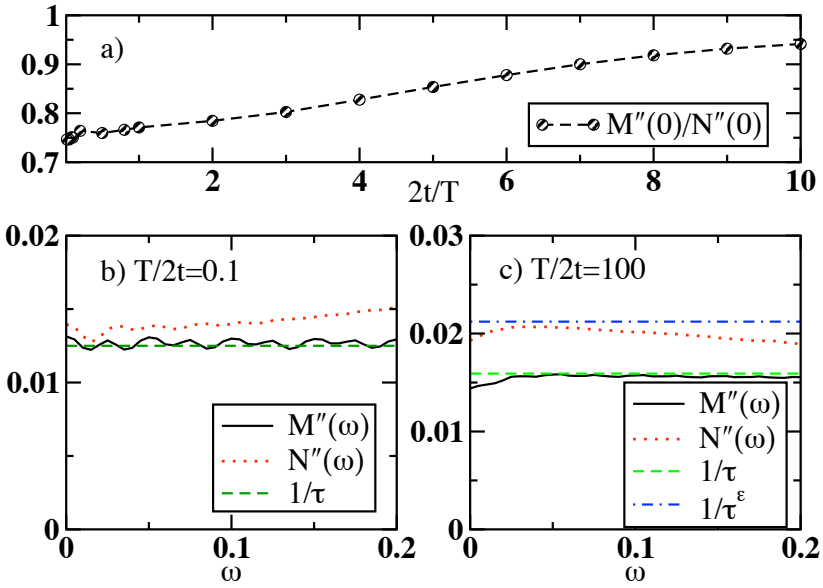

Figure 1.9: a) The ratio of the imaginary part of the particle over the energy memory function at zero frequency as a function of the inverse temperature $2t/T$. Frequency dependence of the particle, energy memory function for a low (b), high (c) temperature. The analytical results for the corresponding scattering rates are presented as well. The parameters of the system are $t = 0.5$, $L = 1000$, $b/t = 0.5$, $c = 10\%$.

Expanding the Fermi-Dirac distribution with respect to β and keeping only linear terms we arrive at

$$M_0''(\omega) = \pi \frac{\beta}{4} \frac{c_I}{(\chi_0/L)} \sum_{p,p'} |\phi_{pp'}|^2 \delta(\epsilon_{p'} - \epsilon_p - \omega) \,, \tag{1.94a}$$

$$N_0''(\omega) = \pi \frac{\beta}{4} \frac{c_I}{(\chi_0^\epsilon/L)} \sum_{p,p'} |\phi_{pp'}^\epsilon|^2 \delta(\epsilon_{p'} - \epsilon_p - \omega) \,. \tag{1.94b}$$

The static limit ($\omega \to 0$) of Eqs. (1.94) will be in the thermodynamic limit ($L \to \infty$),

$$\frac{1}{\tau} = \frac{8}{\pi} \, c_I \, \frac{b^2}{2t} \,, \qquad \frac{1}{\tau^\epsilon} = \frac{32}{3\pi} \, c_I \, \frac{b^2}{2t} \,, \tag{1.95}$$

and the ratio of the scattering rates is not 1 but

$$\frac{1/\tau}{1/\tau^\epsilon} = \frac{3}{4} \,. \tag{1.96}$$

In Fig. 1.9 we present the imaginary part of the particle, energy memory function for two temperatures, $T/2t = 0.1$ Fig. 1.9(b), and $\beta \to 0$ Fig. 1.9(c), in the low frequency regime. In the same figures the scattering rates evaluated from the analytical

calculations (1.81), (1.95) are also shown. The parameter for the particular system, shown in Fig. 1.9 are: $t = 0.5$, $L = 1000$, $b/t = 0.5$, $c = 10\%$. Moreover we bin the δ-functions in windows of width $\delta\omega = 0.005$ and we smooth our results with an extra broadening paramterer η, where $\eta = 0.01$. For the high temperature as well for the low one we observe that numerical results are in good agreement with the analytical calculations. From Fig. 1.9(a) we can see that at high temperatures the ratio of the two scattering rates, as obtained from the numerical results using the memory function approach, is consistent with the analytical evaluation $M''(\omega \to 0)/N''(\omega \to 0) \simeq 0.75$. For decreasing temperature the ratio increases towards ~ 1 with its value for the lowest available temperature to be ~ 0.95. Numerical limitations prevent us from presenting results for even lower temperatures, however, the behavior of the ratio of the two scattering rates with temperature makes plausible the conjecture that at very low temperatures it will be ~ 1 as it was analytically derived (Eq. (1.81)) using diagrammatic analysis and the memory function approach.

Although the transport scattering rates are not equal at high temperatures this does not necessarily mean that the Wiedemann-Franz law does not hold. Instead it could signify that our approximations failed at some point of the evaluation of the scattering rates. On the other hand for the lower temperature we obtain a ratio of the two scattering rates which is closer to unity as it was also predicted from the low temperature analytical calculation.

In order to test the perturbative approximations we present in Figs. 1.10, 1.11 results for particle and for the thermal conductivity as well, obtained either by extracting them from the respective memory function, Eqs. (1.86), (1.87), labeled as "perturbative" or calculated by diagonalizing the full Hamiltonian H (1.26); exact results are labeled as "exact". The formulas for the conductivities obtained for the full system are (cf. Appx. A, Eqs. (A.17a), (A.19a))

$$\sigma(\omega) = \frac{\pi}{L}\mathcal{P}\left(\frac{1}{\omega}\right)\sum_{p,p'}|\jmath_{pp'}|^2(f_p - f_{p'})\delta(\varepsilon_{p'} - \varepsilon_p - \omega)\,, \tag{1.97a}$$

$$\kappa(\omega) = \frac{\pi}{TL}\mathcal{P}\left(\frac{1}{\omega}\right)\sum_{p,p'}|\jmath^{\epsilon}_{pp'}|^2(f_p - f_{p'})\delta(\varepsilon_{p'} - \varepsilon_p - \omega)\,. \tag{1.97b}$$

where the ε_p are the eigenvalues of the full Hamiltonian and are obtained by numerical diagonalization and the matrix elements for the current operators can be obtained using Eqs. (1.28), (1.29) and (A.16). We have used a system of $L = 1000$ sites, a concentration $c_I = 5\%$, $T/t = 0.1$(Fig. 1.10) and $c_I = 10\%$, $T/t = 1$(Fig. 1.11) and $N_r = 1000$ configurations, while $t = 0.5$, $b/t = 0.5$.

From Figs. 1.10, 1.11 we can infer that the structureless low frequency behavior of the memory functions leads to Drude-type behavior for the conductivities which exhibit a Lorentzian form. The perturbative memory function approximation reproduces with good accuracy the high frequency behavior of the conductivities for both values of the concentration $c_I = 5\%, 10\%$. Nevertheless, a discrepancy between perturbative approximation and exact results comes up at low frequencies for $c_I = 10\%$, Fig. 1.11.

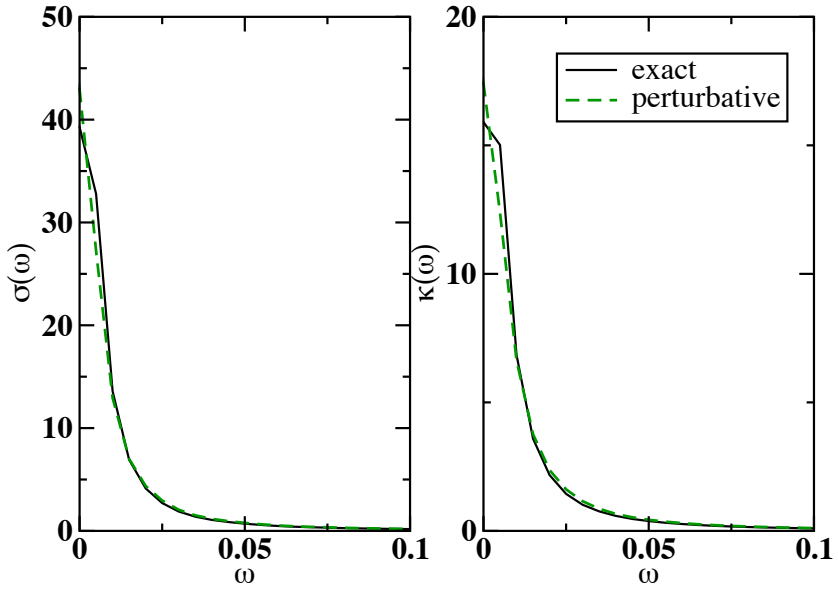

Figure 1.10: Frequency dependence of the particle (left) and thermal (right) conductivity calculated using the exact formulas (1.97), labeled as "exact" and extracted from the corresponding memory functions Eqs. (1.86),(1.87), labeled as "perturbative". The data were obtained for a system of $L = 1000$ sites, $t = 0.5$, $b/t = 0.5$, $c_I = 5\%$, $N_r = 1000$ and $T/t = 0.1$.

Weak localization effects cause a sharp drop in conductivities at low frequencies and cannot be revealed by the memory function approach which does not take into account correlations among the impurities and consequently cannot reveal localization phenomena. On the other hand for the lower concentration $c = 5\%$ we observe that localization phenomena are not present and consequently the memory function approach is in very good agreement with the exact numerical results. The conclusion is that a dilute concentration of impurities and a weak scattering potential is needed, for a non-interacting system, to be well described by the perturbative approximations we presented in the previous sections.

For a stronger field b localization phenomena become even stronger and even for the dilute case of a impurity concentration, $c_I = 5\%$, there will be a sharp drop on the low frequency behavior of particle and thermal conductivity. Moreover, we propose that the particle and thermal conductivities will obey a universal scaling with respect to the concentration of impurities c_I with the concentration independent quantity to be $c_I\sigma(\omega/c_I)$ and similarly for the thermal conductivity. The proposed scaling is expected to be valid in the absence of localization phenomena where conductivities exhibit a Drude-type form or in the strong localization regime where the sharp reduction at low frequencies is present. For intermediate cases the shape of conductivities will change with increasing/decreasing concentration c_I and the sharp reduction at low frequencies

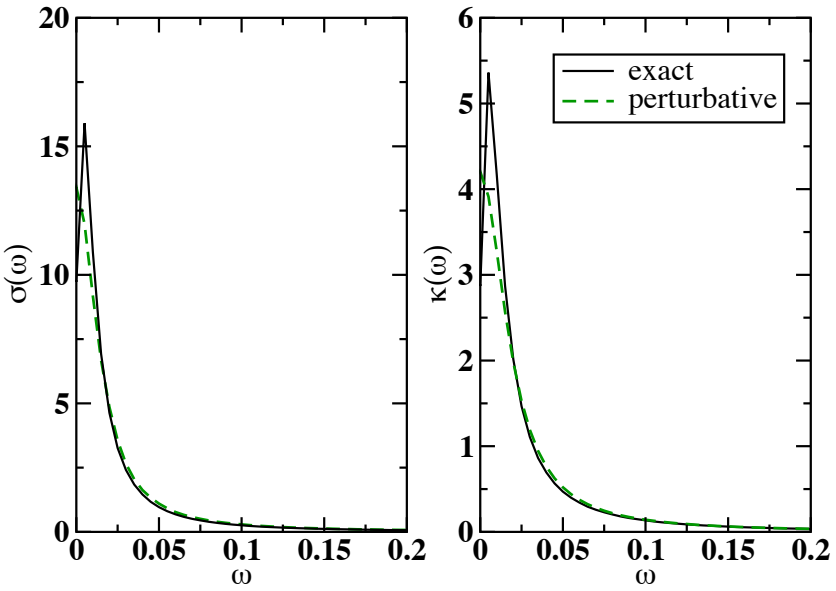

Figure 1.11: Frequency dependence of the particle (left) and thermal (right) conductivity calculated using the exact formulas (1.97), labeled as "exact" and extracted from the corresponding memory functions Eqs. (1.86),(1.87), labeled as "perturbative". The data are obtained for a system of $L = 1000$ sites, $t = 0.5$, $b/t = 0.5$, $c_I = 10\%$, $N_r = 1000$ and $T/t = 1$.

may appear/disappear and the proposed scaling cannot be valid. In Fig. 1.12 we plot the particle conductivity scaled as $c_I\sigma(\omega/c_I)$ for a field $b/t = 1$ ($t = 0.5$), a lattice size of $L = 1000$ sites and various concentrations of impurities $c_I = 5\%, 10\%, 20\%$. Moreover, we plot the scaled particle conductivity for two more lattice sizes $L = 500, 2000$ and a concentration $c_I = 10\%$. A random configuration sampling $N_r = 1000$ was taken while the temperature is $T/2t = 1$. The numerical results shown in Fig. 1.12 verify the proposed scaling with the concentration while they show that results are well converged with the lattice size. Similar are the results for the thermal conductivity as well. For weak impurities where conductivities are expected to have a Drude-type form this scaling is rather trivial since the behavior of the corresponding conductivity is determined only by one parameter, the scattering rate, which is proportional to the impurity concentration c_I.

1.7 Conclusions

In conclusion, our results of numerical simulations on the interplay of disorder and correlations in the spin and thermal transport within Heisenberg spin chains can be summarized by the following scenario:

- Finite random-field disorder $W > 0$ induces localization and vanishing dc trans-

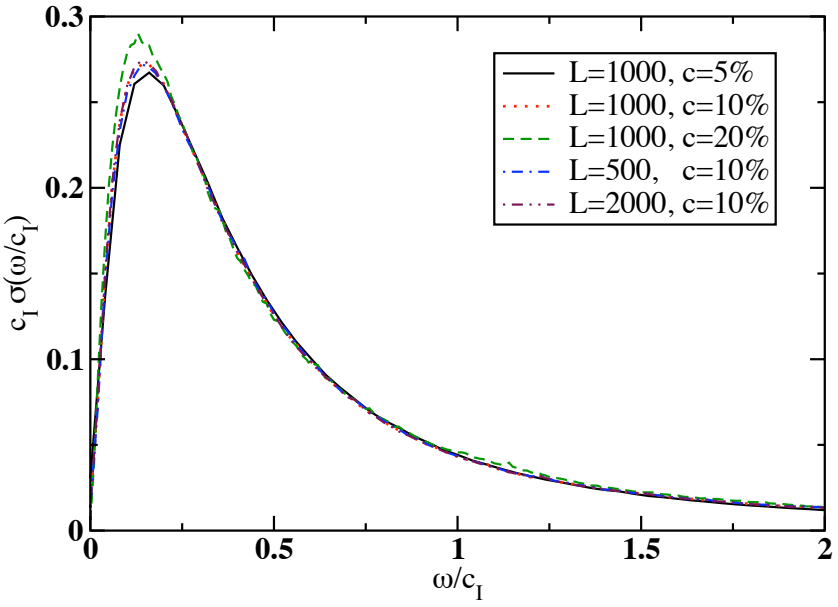

Figure 1.12: Frequency dependence of the scaled particle conductivity $c_I\sigma(\omega/c_I)$ obtained via ED for $L = 1000$ and various concentrations $c_I = 5\%, 10\%, 20\%$ while for a concentration $c_I = 10\%$ the lattice sizes $L = 500, 2000$ are shown as well. The rest of the parameters are $t = 0.5$, $b/t = 1$, $N_r = 1000$ and $T/2t = 1$.

port at any T in the XY limit, corresponding to noninteracting fermions [5].

- In the weak disorder regime we are led to Lorentzian-like forms, at least at high frequencies, for the particle, thermal conductivities. The high frequency behavior is determined by the scattering rate, evaluated analytically at low and high temperatures.

- In the absence of localization phenomena or in the presence of strong localization we obtain a universal scaling with the concentration of impurities for the conductivities as $c_I\sigma(\omega/c_I)$, $c_I\kappa(\omega/c_I)$.

- Vanishing dc transport is induced in the XXZ model ($\Delta > 0$), as well, by the finite random disorder ($W > 0$), but only at $T = 0$ Refs. [9] [10].

- Apart from the two limits, $\Delta = 0$ any T or $T = 0$ and any Δ, the system appears to behave as a normal conductor with finite $\sigma_{dc} > 0$ and $\kappa_{dc} > 0$ both for various $\Delta > 0$ and $T > 0$; in particular, we do not find any evidence for a phase transition by varying T or W.

- Dynamical transport at least for larger disorder reveals a generic cusplike nonanalytic behavior, analogous to long-time tails in classical dynamical systems in low-dimensional [36] or 2D strongly disordered systems.

- With increasing disorder the system reveals a crossover from the Drude-type to a pseudolocalized dynamics with very low σ_{dc} and κ_{dc} (Ref. [16]).
- Similar conclusions seem to hold for the bond disorder.

Clearly, several caveats are in order. The considered cases mostly correspond to substantial disorder, where the finite-size effects are well under control and results converged within available L, at least for $T > T_{fs}$ and not too small $\Delta > 0$. Also, numerical results cannot exclude the localization on a very long scale $\xi \gg L$ although we do not find any signature of such a development.

Bibliography

[1] P. W. Anderson, Absence of Diffusion in Certain Random Lattices, Physical Review **109**(5), 1492–1505 (Mar 1958).

[2] A. Lagendijk, B. v. Tiggelen, and D. S. Wiersma, Fifty years of Anderson localization, Physics Today **62**, 24–29 (August 2009).

[3] B. Kramer and A. MacKinnon, Localization: theory and experiment, Reports on Progress in Physics **56**(12), 1469 (1993).

[4] N. F. Mott and W. D. Twose, The theory of impurity conduction, Advances in Physics **10**, 107–163 (1961).

[5] E. Abrahams, P. W. Anderson, D. C. Licciardello, and T. V. Ramakrishnan, Scaling Theory of Localization: Absence of Quantum Diffusion in Two Dimensions, Physical Review Letters **42**(10), 673–676 (Mar 1979).

[6] L. Fleishman and P. W. Anderson, Interactions and the Anderson transition, Physical Review B **21**(6), 2366–2377 (Mar 1980).

[7] I. L. Aleiner, B. L. Altshuler, and G. V. Shlyapnikov, Finite temperature phase transition for disordered weakly interacting bosons in one dimension, cond-mat/0910.4534, 2009.

[8] M. E. Gershenson, Y. B. Khavin, A. G. Mikhalchuk, H. M. Bozler, and A. L. Bogdanov, Crossover from Weak to Strong Localization in Quasi-One-Dimensional Conductors, Physical Review Letters **79**(4), 725–728 (Jul 1997).

[9] C. A. Doty and D. S. Fisher, Effects of quenched disorder on spin-1/2 quantum XXZ chains, Physical Review B **45**(5), 2167–2179 (Feb 1992).

[10] P. Schmitteckert, T. Schulze, C. Schuster, P. Schwab, and U. Eckern, Anderson Localization versus Delocalization of Interacting Fermions in One Dimension, Physical Review Letters **80**(3), 560–563 (Jan 1998).

[11] K. Damle, O. Motrunich, and D. A. Huse, Dynamics and Transport in Random Antiferromagnetic Spin Chains, Physical Review Letters **84**(15), 3434–3437 (Apr 2000).

[12] O. Motrunich, K. Damle, and D. A. Huse, Dynamics and transport in random quantum systems governed by strong-randomness fixed points, Physical Review B **63**(13), 134424 (Mar 2001).

[13] D. Basko, I. Aleiner, and B. Altshuler, Metal-insulator transition in a weakly interacting many-electron system with localized single-particle states, Annals of Physics **321**(5), 1126 – 1205 (2006).

[14] I. V. Gornyi, A. D. Mirlin, and D. G. Polyakov, Interacting Electrons in Disordered Wires: Anderson Localization and Low-T Transport, Physical Review Letters **95**(20), 206603 (Nov 2005).

[15] V. Oganesyan and D. A. Huse, Localization of interacting fermions at high temperature, Physical Review B **75**(15), 155111 (2007).

[16] M. Žnidarič, T. Prosen, and P. Prelovšek, Many-body localization in the Heisenberg XXZ magnet in a random field, Physical Review B **77**(6), 064426 (Feb 2008).

[17] G. D. Mahan, *Many-particle physics*, Plenum Press, New York, 1981.

[18] G. C. Psaltakis, *Quantum Many-Particle Systems*, Crete University Press, November 2008, (published in greek).

[19] R. Kubo, Statistical-Mechanical Theory of Irreversible Processes. I. General Theory and Simple Applications to Magnetic and Conduction Problems, Journal of the Physical Society of Japan **12**(6), 570–586 (1957).

[20] J. M. Luttinger, Theory of Thermal Transport Coefficients, Physical Review **135**(6A), A1505–A1514 (Sep 1964).

[21] X. Zotos, F. Naef, and P. Prelovsek, Transport and conservation laws, Physical Review B **55**(17), 11029–11032 (May 1997).

[22] J. Jaklič and P. Prelovšek, Finite-temperature properties of doped antiferromagnets, Advances in Physics **49**, 1–92 (2000).

[23] M. W. Long, P. Prelovšek, S. El Shawish, J. Karadamoglou, and X. Zotos, Finite-temperature dynamical correlations using the microcanonical ensemble and the Lanczos algorithm, Physical Review B **68**(23), 235106 (Dec 2003).

[24] J. Wilke, A. D. Mirlin, D. G. Polyakov, F. Evers, and P. Wölfle, Zero-frequency anomaly in quasiclassical ac transport: Memory effects in a two-dimensional metal with a long-range random potential or random magnetic field, Physical Review B **61**(20), 13774–13784 (May 2000).

[25] A. Gold, S. J. Allen, B. A. Wilson, and D. C. Tsui, Frequency-dependent conductivity of a strongly disordered two-dimensional electron gas, Physical Review B **25**(6), 3519–3528 (Mar 1982).

[26] X. Zotos, Finite Temperature Drude Weight of the One-Dimensional Spin- 1/2 Heisenberg Model, Physical Review Letters **82**(8), 1764–1767 (Feb 1999).

[27] C. Hess, Heat conduction in low-dimensional quantum magnets, European Physical Journal Special Topics **151**, 73–83 (Dec 2007).

[28] K. Louis, P. Prelovsek, and X. Zotos, Thermal conductivity of one-dimensional spin-1/2 systems coupled to phonons, Physical Review B **74**(23), 235118 (2006).

[29] A. Karahalios, A. Metavitsiadis, X. Zotos, A. Gorczyca, and P. Prelovšek, Finite-temperature transport in disordered Heisenberg chains, Physical Review B **79**(2), 024425 (2009).

[30] W. Götze and P. Wölfle, Homogeneous Dynamical Conductivity of Simple Metals, Physical Review B **6**(4), 1226–1238 (Aug 1972).

[31] S. Doniach and E. Sondheimer, *Green's functions for solid state physicists*, Imperial College Press, 2004.

[32] E. N. Economou, *Green's Functions in Quantum Physics*, Springer, July 2006.

[33] H. Bruus and K. Flensberg, *Many-body quantum theory in condensed matter physics: an introduction*, Oxford Graduate Texts, Oxford University Press, Oxford, 2004.

[34] S. F. Edwards, A new method for the evaluation of electric conductivity in metals, **3**, 1020–1031 (1958).

[35] N. W. Ashcroft and N. D. Mermin, *Solid State Physics*, HRW International Editions, 1976, Printed in Hong Kong 1988.

[36] J.-P. Boon and S. Yip, *Molecular Hydrodynamics*, New York : Dover Publications, 1980.

Chapter 2

Single non-magnetic impurity

2.1 Introduction

Transport properties of one dimensional systems are of particular interest due to their unusual transport properties [1–4]. For one thing, in a one dimensional model with only nearest neighbor interactions, a broken bond in a spin chain, or the vanishing of one hopping amplitude in a particle system, leads to vanishing dc transport despite the fact that the defect is only one in a macroscopic system. On the other hand, pure one dimensional systems could be ideal electric, spin or heat conductors, a fact which arises from the integrability of these systems, i.e., the existence of a macroscopic number of conservation laws [5–7]. For an integrable model, even if a current is not a constant of motion and its autocorrelation decays in time the coupling of this particular current with the existing conservation laws might lead to infinite dc transport of the corresponding modes [8, 9]. Furthermore, the coexistence of both, diffusive and ballistic transport channels [10] or even the divergence of a conductivity at zero frequency in the presence of perturbations incapable to break the integrability of the system [11] is discussed in the literature. Finally, we would like to mention the exotic "cutting-healing" behavior of one dimensional many body systems in the presence of defects [12–16]. For a Luttinger liquid [17] it was shown that in the presence of a single barrier or a weak link the transmission through the defect renormalizes to (zero)one, at zero temperature, for (repulsive)attractive interactions [12, 13]. Similarly, for spin chains in the presence of magnetic impurities the cutting(healing) behavior is observed for antiferromagnetic(ferromagnetic) easy axis anisotropy [14, 15]. In the same context, for the spin-1/2 isotropic Heisenberg model, the cutting, healing behavior was shown for a single, two consecutive weak links, respectively [16].

According to the above, the effect of a single non-magnetic impurity in a finite system is of high theoretical interest. The problem of a single impurity could also be appealing for experiments as well—although not so directly relevant—considering a dilute concentration of impurities so that there would not be any correlations among the impurities.

2.2 Model

To explore the issues mentioned previously, we consider a one dimensional (1D) spin-1/2 system of L sites in the presence of a single non-magnetic impurity. The pure anisotropic Heisenberg model (AHM), in the absence of any impurities (external local fields or weak links), is described by the Hamiltonian

$$H_0 = \sum_l h_l \,, \quad h_l = J_l(S_l^x S_{l+1}^x + S_l^y S_{l+1}^y + \Delta S_l^z S_{l+1}^z) \qquad (J_l = J) \,, \tag{2.1}$$

where, $S^\alpha, \alpha = x, y, z$, are spin-1/2 operators, J is the anti-ferromagnetic ($J > 0$) exchange coupling and Δ the anisotropy parameter, which is taken either anti-ferromagnetic ($\Delta > 0$) or ferromagnetic ($\Delta < 0$) in order to investigate the "cutting-healing" effects, while we consider periodic boundary conditions ($\mathbf{S}_L = \mathbf{S}_0$).

Considering a local magnetic field b_0 applied at the zeroth site coupled with the spin z-component, we are led to the local perturbation Hamiltonian

$$H_1 = b_0 S_0^z \,. \tag{2.2}$$

On the other hand, for the single weak link perturbation one could take the couplings J_l of the spins at sites $l, l+1$ in Eq. (2.1) to be $J_{l\neq 0} = J$ and $J_0 = J'$.

One can obtain the spin $\jmath^s$ and the energy $\jmath^\epsilon$ currents from relations (1.9), (1.10) of Ch. 1 for the disordered chains; we repeat them here,

$$\jmath^s = \sum \jmath_l^s \,, \qquad \jmath_l^s = J_l \left(\mathbf{S}_l \times \mathbf{S}_{l+1}\right) \cdot \hat{e}_z \,, \tag{2.3a}$$

$$\jmath^\epsilon = \sum_l \jmath_l^\epsilon + \frac{b_l}{2}\left(\jmath_{l-1}^s + \jmath_l^s\right) \,, \quad \jmath_l^\epsilon = J_{l-1} J_l \; \mathbf{S}_l \cdot \left(\mathbf{\Delta} \cdot \mathbf{S}_{l+1} \times \mathbf{\Delta} \cdot \mathbf{S}_{l-1}\right) \,. \tag{2.3b}$$

For the single impurity case the distributions b_l, J_l will be: $b_l = b_0 \delta_{l,0}$ and $J_l = J$, for the local field case, *or* $b_l = 0$ and $J_l = J - (J - J')\delta_{l,0}$, for the single weak link case . Let us recall that $\mathbf{\Delta}$ is the anisotropy tensor, $\hat{e}_z$ the unit vector along the z-axis while we work in a system of units where $a, \hbar, k_B = 1$.

2.3 Level statistics

The distinction between integrable and non-integrable models is closely related to the statistics of many-body levels [18], which follow the Poisson level distribution for an integrable system and the Wigner-Dyson (WD) distribution for a generic non-integrable one [19]. In the absence of the impurity the AHM, Eq. (2.1), is integrable and its level statistics follows the Poisson level distribution (cf. Ref. [19])

$$P_{\rm P}(s) = \exp(-s) \,, \qquad s = \frac{\epsilon_{n+1} - \epsilon_n}{\delta\epsilon} \,, \tag{2.4}$$

where s is the dimensionless parameter proportional to the energy difference of consecutive eigenvalues and $\delta\epsilon$ is the average (energy) level spacing. Broken integrability is

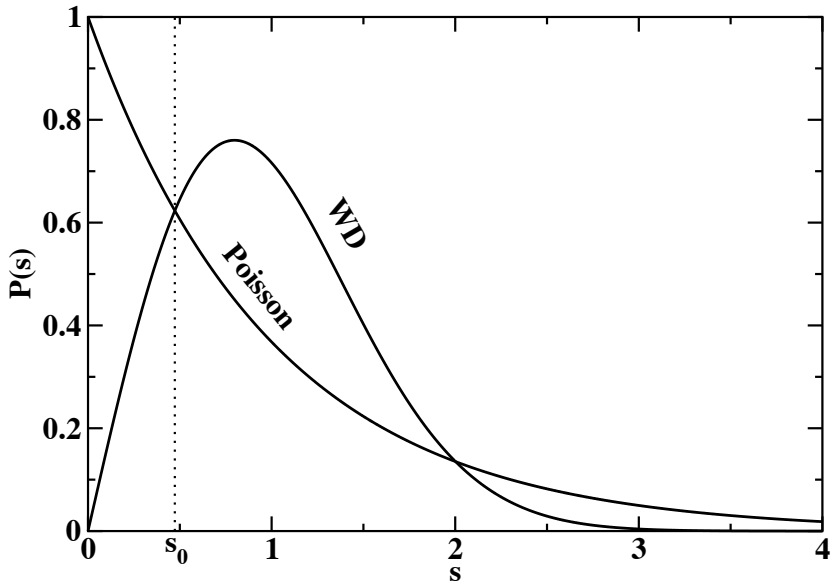

Figure 2.1: Poisson and Wigner-Dyson distributions. $s_0 = 0.473$ is the point of the intersection of the two curves.

expected to change the level statistics from Poisson to Wigner-Dyson (WD) distribution, given by

$$P_{\rm WD}(s) = \frac{\pi s}{2} \exp\left(-\frac{\pi s^2}{4}\right). \tag{2.5}$$

One can immediately notice one of the most important differences of the two distributions by taking the limit, $s \to 0$. While in the Poisson distribution the probability exhibits its maximum value for $s = 0$, the WD one vanishes. In other words, in the WD distribution it is unlikely to have a degenerate spectrum (because of level repulsion) in contrast to the Poisson distribution (level crossing) [20].

The perturbation of a next nearest neighbor interaction has been discussed in the literature for both integrable systems, the fermionic $t - V$ model (cf. Ch. 1)[21] and the spin Heisenberg model [11, 19, 22]. In Refs. [21, 22] the next nearest neighbor interactions were considered only at the diagonal terms, i.e., terms of the form $J' S^z_l S^z_{l+2}$, $V' n_l n_{l+2}$ were included respectively. While in both works it was observed that there is a crossover behavior from Poisson to WD level statistics, in Ref. [21] it was also observed that even in the presence of the next nearest term, for some parts of the spectrum there were deviations from the WD distribution indicating the existence of an integrable effective Hamiltonian. In Refs. [11, 19] the next nearest neighbor interactions were taken in the kinetic as well as in the diagonal terms. Using the level statistics analysis in Ref. [19] it was concluded that the perturbation breaks integrability, rendering the consecutive level spacing distribution of the WD form. On the other hand in Ref. [11], using the memory function framework to determine thermal transport coefficients, the next nearest neighbor perturbation was shown to be insufficient to break integrability

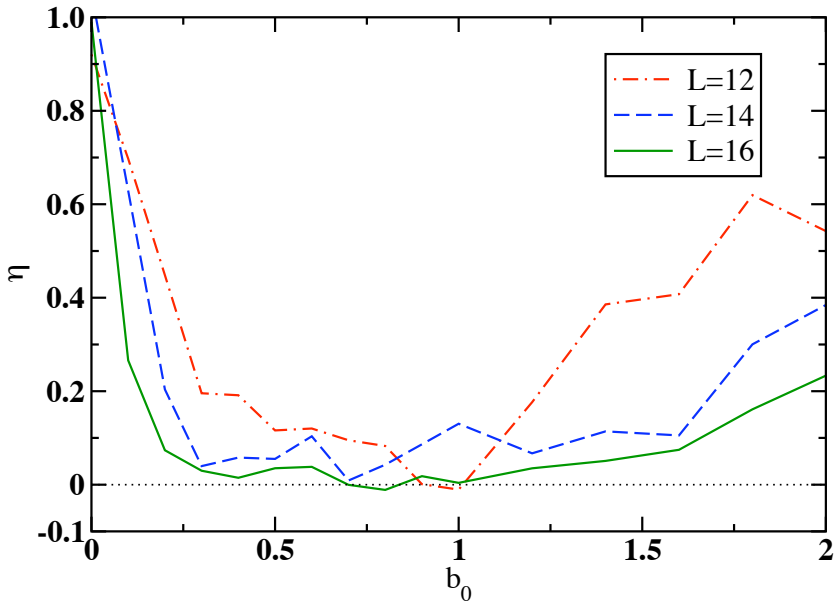

Figure 2.2: Parameter η for the deviation from the WD level distribution vs impurity field b_0 for $\Delta = 0.8$ and various L.

in leading order of the perturbation parameter J'/J. From the previous discussion it can be seen that breaking the integrability is not as trivial as someone would expect, making the effect of a single non magnetic impurity on a chain of L sites to be far from obvious.

In order to investigate the effect of a single static impurity, Eq. (2.2), in the pure 1D anisotropic Heisenberg model (AHM) within the level statistics framework we use the (full) exact diagonalization (ED) technique. We diagonalize system with lattice size $L = 10 - 16$, obtaining the full energy spectrum in the $S^z_{\rm tot} = 0$ subsector, where the dimension of the Hilbert space varies from $\mathcal{D}_H \sim 10^2 - 10^4$ states and the corresponding average level spacing $\delta\epsilon \sim 2 \times 10^{-2} - 5 \times 10^{-4}$.

η-parameter

To be concrete we present here two standard tests for the closeness of the RMT. The first one is the parameter η [23, 24] measuring the normalized distance to the WD distribution,

$$\eta = \frac{\int_0^{s_0} \Big(P(s) - P_{\rm WD}(s) \Big) ds}{\int_0^{s_0} \Big(P_{\rm P}(s) - P_{\rm WD}(s) \Big) ds} \,, \tag{2.6}$$

where $P(s)$ is the actual level distribution and $s_0 = 0.473$ is chosen to be the intersection of $P_{\rm P}(s)$ and $P_{\rm WD}(s)$. In order to stay within the regime of homogeneous density of states we analyze only one half of the intermediate many-body states, as relevant for the high temperature ($T \gg J$) properties discussed here. In Fig. 2.2 we present ED results for

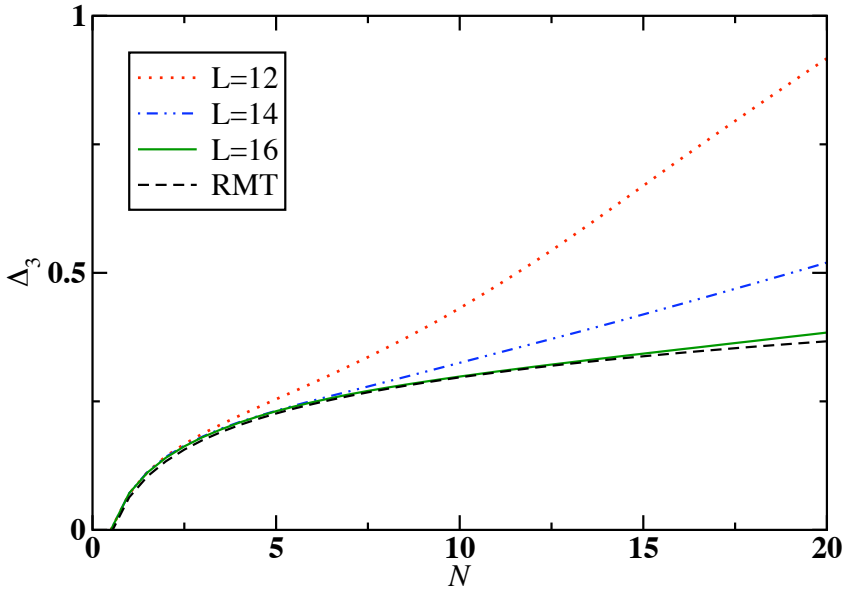

Figure 2.3: Level fluctuation parameter $\Delta_3(N)$ for fixed $\Delta = 0.8$ and $b_0 = 0.8$ and different system length L. For comparison the RMT result is presented (dashed line).

the parameter η as a function of b_0 for chosen intermediate $\Delta = 0.8$ (metallic regime) and for different $L = 12 - 16$. To avoid the effect of higher degeneracy of levels at $S^z_{\rm tot} = 0$, $b_0 = 0$ presented results in Fig. 2.2 are for $S^z_{\rm tot} = 1$. In the absence of impurity ($b_0 = 0$) we obtain $\eta = 1$ since $P(s) = P_{\rm P}(s)$ due to the integrability of the pure AHM. The most important conclusion is that a rather weak impurity $b_0 \sim 0.2$ in the largest $L = 16$ causes a fast drop to $\eta \sim 0$, i.e., to $P(s) \sim P_{\rm WD}(s)$. The threshold value of b_0 is decreasing with L so that for the largest $L = 16$ reachable with ED we get $P(s) \sim P_{\rm WD}(s)$ in the range $0.2 < b_0 < 1.5$. On the other hand, it is quite remarkable that η starts to recover toward $\eta \sim 1$ for large b_0. This can be easily explained by noting that a large b_0 effectively cuts the ring and leads to the AHM with open ends which is again an integrable model.

Δ_3-parameter

Even stronger probe of the level statistics is the correlation Δ_3 measuring the level fluctuations beyond the nearest neighbor levels [25, 26]. In fact Δ_3 is the mean square deviation of the number of states $\mathcal{N}(\varepsilon)$, with energy up to ε, from a linear fit $(A\varepsilon + B)$ without any constraints for A, B

$$\Delta_3 = \frac{1}{2N} \min_{A,B} \int_{-N}^{N} \Big(\mathcal{N}(\varepsilon) - A\varepsilon - B\Big)^2 d\varepsilon \,, \qquad \varepsilon = \frac{\epsilon}{\delta\epsilon} \,. \tag{2.7}$$

Δ_3 should behave as $\Delta_3 \sim N/15$ for Poisson distribution, and asymptotically as $\Delta_3 \sim \ln N/\pi^2$ within the RMT [25, 27].

In Fig. 2.3 we present results for $\Delta_3(N)$ for fixed $\Delta = 0.8$ and $b_0 = 0.8$ as obtained for different $L = 12 - 16$. A comparison with the result expected from the RMT shows that $\Delta_3(N)$ approaches the latter very accurately in an interval $N < N^*(L)$ with N^* exponentially increasing with L, while the deviation into a Poisson-like linear dependence $\Delta_3 \propto N$ appears for $N > N^*(L)$. Such a generic crossover has been observed also in other systems [21] and one can discuss the relevance of the related crossover energy scale $\varepsilon^* = N^* \cdot \delta\epsilon$. Fast increase in $N^*(L)$ can be understood by noting that the perturbation, being L independent, mixes up many-body levels [23, 24] within the interval ε^* whereby separation between many-body levels decreases as $\delta\epsilon \propto \exp(-L)$. We can estimate $b_0/4L$ within the XY ($\Delta = 0$) model which gives right order of magnitude for observed N^* in Fig. 2.3. More detailed analysis in analogy to other systems [23, 24] is difficult due to the complicated nature of states at intermediate Δ.

2.4 Spin stiffness

It has been shown [6, 7] that pure 1D integrable models of interacting fermions exhibit in spite of umklapp scattering at any $T > 0$ dissipationless ballistic transport manifested, for example, in a finite charge stiffness $D(T > 0) > 0$. Closely related to the onset of the WD distribution by a single impurity is the vanishing of the $T > 0$ coherent (ballistic) transport characteristic for integrable systems.

The real part of spin and thermal conductivities can be written as the sum of a non-dissipative term denoting the free acceleration of the corresponding fluxes and a dissipative term, which represents transport due to transitions between states with different energy [28, 29],

$$\sigma'(\omega) = 2\pi D_s \delta(\omega) + \sigma_{\rm reg}(\omega), \quad \kappa'(\omega) = 2\pi D_h \delta(\omega) + \kappa_{\rm reg}(\omega) \, . \tag{2.8}$$

The stiffnesses D_s, D_h manifest coherent transport, namely, whether ballistic transport exists in a system or not. For an integrable system, with a macroscopic number of conservation laws, the corresponding stiffness of a particular current could be finite either because this current coincides with one of these conservation laws, or because it has a finite coupling with the conservation laws of the system [7–9] . In Appx. A it is shown that the spin, energy stiffness are given by the imaginary part of the corresponding conductivity, σ'', κ'', using the relations

$$D_s = \frac{1}{2} \lim_{\omega \to 0} \omega \sigma''(\omega) \, , \qquad D_h = \frac{1}{2} \lim_{\omega \to 0} \omega \kappa''(\omega) \, . \tag{2.9}$$

For the pure AHM the spin stiffness remains finite, at a finite temperature, in the metallic regime $0 < |\Delta| < 1$, despite the fact that the spin current is not conserved for $\Delta \neq 0$. On the other hand, for the heat transport, where the energy current is conserved for any Δ, the corresponding stiffness remains finite at any temperature [6, 7]. The measure of the coherent dissipationless component for the spin transport $D_s(T)$, equivalent to the charge stiffness for the related fermionic model, can be defined

via the gauge phase ϕ into the spin-flip terms in Eq. (2.1), using Eq. (1.4) as well, i.e.,

$$S_l^x S_{l+1}^x + S_l^y S_{l+1}^y \;\longrightarrow\; e^{i\phi} S_l^+ S_{l+1}^- + \text{h.c.} \quad .$$

Subsequently, the spin stiffness can be expressed at finite temperatures ($T > 0$) by the derivative of the Hamiltonian eigenvalues with respect to the flux ϕ [6] via,

$$D_s = \frac{1}{2L} \sum_n p_n \frac{\partial^2 \epsilon_n}{\partial \phi^2} \tag{2.10}$$

$$\frac{\partial^2 F}{\partial \phi^2} = 0 \quad \Rightarrow \quad D_s \sim \frac{\beta}{2L} \sum_n p_n \left(\frac{\partial \epsilon_n}{\partial \phi} \right)^2 \tag{2.11}$$

where β is the inverse temperature, $\beta = 1/T$, p_n are the corresponding Boltzmann weights

$$p_n = \exp(-\beta \epsilon_n)/Z \,, \qquad \text{with} \qquad Z = \sum_n \exp(-\beta \epsilon_n) \,, \tag{2.12}$$

and F the free energy, $F = -T \ln Z$. The relation for the spin stiffness (2.11) becomes an equality provided that the susceptibility for persistent currents vanishes (for finite systems at large enough temperatures). On the other hand, D_s still depends on the value of ϕ where derivatives in Eq. (2.11) are taken.

XY model

For the XY model ($\Delta = 0$) the spin Hamiltonian can be mapped via the Jordan-Wigner transformation into tight-binding non-interacting (NI) fermions since $V \propto \Delta = 0$ in Eq. (1.6). Implementing the same transformation for the perturbation Hamiltonian (2.2), the S_z operator is replaced by $S^z \to c^\dagger c - 1/2$, we arrive at the Hamiltonian

$$H = -t \sum_l |l\rangle\langle l+1| + |l\rangle\langle l-1| + \varepsilon_0 |0\rangle\langle 0| \;\; + \;\; \text{const.} \quad , \tag{2.13}$$

where $|l\rangle$ are the localized states of the lattice sites, t is the hopping amplitude and $\varepsilon_0 = b_0$ the local potential at the zeroth site. Taking the eigenvalue equation for Hamiltonian (2.13) and expanding its eigenstates as linear combination of the localized sates $|l\rangle$ with corresponding weights $\psi_n(l)$ (eigenfunctions) we obtain the equation

$$\psi_n(l+1) + \psi_n(l-1) + \frac{\epsilon_n - \varepsilon_l \delta_{l,0}}{t} \psi_n(l) = 0 \,. \tag{2.14}$$

For vanishing impurity, $\varepsilon_0 = 0$, the energy eigenvalues are given by (cf. sec. 1.6)

$$\epsilon_n = -2t \cos p_n \,, \qquad p_n = \frac{2\pi}{L} n \,, \quad n = 0, \pm 1, \pm 2, \ldots \,. \tag{2.15}$$

Assuming a standard scattering process where plane waves are scattered on the impurity which is located at site $l = 0$ we can write for the eigenfunctions

$$\psi_p(l) = \begin{cases} t_p e^{+ipl} \,, & \text{for} \quad l \geq 0 \\ e^{+ipl} + r_p e^{-ipl} \,, & \text{for} \quad l \leq 0 \end{cases} \quad , \tag{2.16}$$

where $|r_p|^2, |t_p|^2$ are the reflection and transmission coefficients respectively while we omit the integer index n, i.e., $p_n \to p$. Using (2.14), (2.16) we calculate the transmission coefficient to be

$$|t_p|^2 = \frac{4t^2 \sin^2 p}{4t^2 \sin^2 p + \varepsilon_0^2} \,. \tag{2.17}$$

One can establish the relation with the transmission through the barrier, as used also in connection with the evaluation of the 1D conductance at $T = 0$ [30]. For general $T > 0$ one gets in the case of NI fermions in accordance with [6] that charge (spin) stiffness is given by

$$D = \frac{1}{2L} \sum_p f_p \frac{\partial^2 \epsilon_p(\phi)}{\partial \phi^2} \,, \tag{2.18}$$

where f_p is the Fermi-Dirac distribution at half filling ($\mu = 0$) and ϵ_p now are the single particle eigenvalues for the Hamiltonian in the presence of the flux

$$f_p = \frac{1}{e^{\beta \epsilon_p} + 1} \,, \quad \epsilon_p(\phi) = -2t \cos(p + q(\phi)) \,. \tag{2.19}$$

Assuming the absence of persistent currents in the thermodynamic limit we obtain

$$\frac{\partial^2 \Omega}{\partial \phi^2} \simeq 0 \qquad \Rightarrow \qquad D \simeq \frac{\beta}{2L} \sum_p f_p (1 - f_p) \left(\frac{\partial \epsilon_p(\phi)}{\partial \phi} \right)^2 \,. \tag{2.20}$$

Following Ref. [31] we calculate the derivative of the eigenvalues with respect to the flux, that appears in Eq. (2.20), to be

$$\left(\frac{\partial \epsilon_p(\phi)}{\partial \phi} \right)^2 = 4t^2 g_p \sin^2 p \,, \qquad g_p = \frac{|t_p|^2 \sin^2(L\phi)}{1 - |t_p|^2 \cos^2(L\phi)} \,. \tag{2.21}$$

Numerically we recover the behavior $D(\phi)$ as follows from Eqs. (2.17), (2.20) and (2.21) for arbitrary b_0 as far as $\Delta \to 0$.

XXZ model

For $\Delta > 0$ the dependence on ϕ remains qualitatively similar, although irregular due to the strong dependence on L. In the following we calculate $D_s(L)$ for fixed $\phi = \pi/2L$. Results for $\Delta > 0$ are nontrivial for any temperature. Since results of ED are better at high temperatures, we restrict ourselves here to the limit $\beta \to 0$. It has been shown for the pure model that D_s/β remains finite and nontrivial in the thermodynamic limit $L \to \infty$ due to the integrability of the model [7].

In Fig. 2.4 we show results for D_s/β vs $1/L$ for chosen $\Delta = 0.8$ and for four cases $b_0 = 0, 0.5, 1, 2$. It is evident from Fig. 2.4 that $b_0 > 0$ cases are qualitatively different from the $b_0 = 0$ where D_s scales linearly in $1/L$ toward a finite $D_s/\beta \sim 0.035$. In contrast, $b_0 > 0$ induces an exponential-like decay of $D_s \to 0$, at least for large enough $L > L^*$. This is closely related to the onset of the WD distribution and the effective breaking of the integrability. Here, L^* is presumably related to the transport mean-free

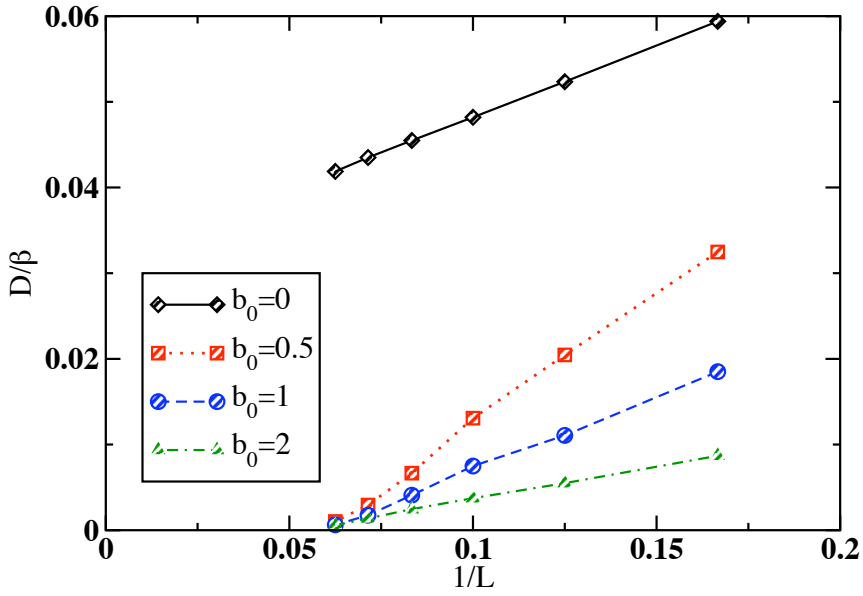

Figure 2.4: High temperature spin stiffness D_s/β vs $1/L$ for various values of the impurity field.

path, on the other hand such an interpretation is not straightforward. We expect that the exponential decay is generic for any finite $b_0 > 0$ although it would be difficult to establish numerically for weak b_0 due to L^* increasing beyond available system sizes L. Let us mention that we arrive at a similar behavior for the thermal stiffness as well.

2.5 Incoherent transport - High temperatures

Rapid (exponential) vanishing of D_s at $T > 0$ is the indication that the transport is not ballistic and becomes incoherent (resistive) beyond a characteristic L^* . In order to test this directly we evaluate dynamical spin and thermal conductivities from relations (A.5) (we repeat them here),

$$\sigma(z) = \frac{i}{zL}(\chi_0^s - \chi_{\jmath^s\jmath^s}(z)) \,, \quad \kappa(z) = \frac{i}{zTL}(\chi_0^\epsilon - \chi_{\jmath^\epsilon\jmath^\epsilon}(z)), \tag{2.22}$$

with the corresponding susceptibility of the operators $\hat{O}_p, \hat{O}_q$ defined as in Appx. A, Eq. (A.2),

$$\chi_{\hat{O}_p\hat{O}_q}(z) = i\int_0^\infty dt\, e^{izt}\, \langle [\hat{O}_p(t), \hat{O}_q(0)] \rangle \,, \quad z = \omega + i\eta \,. \tag{2.23}$$

$\chi_0^s, \chi_0^\epsilon$ can be expressed as the thermodynamic average of the "stress tensor" and the "thermal operator" respectively [29] or by taking the high frequency regime of the imaginary part of the corresponding conductivity (A.13).

For further discussion it is convenient to present and analyze also the corresponding spin M and energy N memory functions defined respectively as in Ref. [32] (cf. Appx. B as well)

$$\bar{\sigma}(z) = \frac{i(\chi_0^s/L)}{z + M(z)}\,, \quad \bar{\kappa}(z) = \frac{1}{T}\frac{i(\chi_0^\epsilon/L)}{z + N(z)}\,, \tag{2.24}$$

where the bars over the conductivities denote complex functions. Memory functions are complex functions as well with their real part being an antisymmetric function of frequency, while the imaginary part is symmetric.

Note that a finite component D represents the weight of the $\delta(\omega)$ contribution to the real part of conductivities, requiring the static limit of the respective susceptibility to be less than the respective χ_0, i.e.,

$$\chi_{\jmath^s\jmath^s}(\omega \to 0) < \chi_0^s\,, \qquad \chi_{\jmath^\epsilon\jmath^\epsilon}(\omega \to 0) < \chi_0^\epsilon\,.$$

Furthermore, for non-dissipative cases we can conclude from Eq. (2.24) that the static value of the imaginary part of the respective memory function will be zero ($M''(0) = 0$, $N''(0) = 0$). On the other hand, any finite value for $M''(0)$, $N''(0)$ denotes the finite decay rate of the spin, energy current and a finite dc conductivity as well, i.e., strictly $D_s, D_h = 0$.

We use further the advantage of studying closer the real part of the thermal conductivity, $\kappa(\omega) = \Re\bar{\kappa}(\omega)$, instead of the spin conductivity, $\sigma(\omega) = \Re\bar{\sigma}(\omega)$, since $\jmath^\epsilon$ is a conserved quantity in the pure AHM, hence $N(\omega) = 0$, and consequently $N(\omega) \neq 0$ appears only due to $b_0 \neq 0$. On the other hand, the spin current, $\jmath^s$, is not conserved in the pure system exhibiting a non-trivial ($M(b_0 = 0) = \mathcal{M} \neq 0$) memory function even in the absence of impurities. However, in the metallic regime ($\Delta < 1$) $\mathcal{M}(\omega = 0) = 0$ at any temperature as required to obtain $D_s(T) > 0$.

In the following paragraphs we evaluate spin and thermal conductivity in the high temperature regime ($T \gg J$) using the exact diagonalization technique (ED) for lattice sizes up to $L = 14$. δ-functions corresponding to the excitation spectra are summed in bins of width $\delta\omega = 0.01$ while we introduce an extra broadening $\gamma = 0.03$ using the Kramers-Kronig relations (A.23). The knowledge of the spin and thermal conductivity allows the evaluation of the respective memory functions $M(\omega), N(\omega)$ inverting Eq. (2.24).

For relatively weak perturbations ($b_0 < 1$) we also evaluate the energy memory function within the perturbative approach, Ref. [32], using the force-force correlation (B.11),

$$N_0(z) = \frac{1}{z\chi_0^\epsilon}(\chi_{f^\epsilon f^\epsilon}(z) - \chi_{f^\epsilon f^\epsilon}(0))\,, \qquad f^\epsilon = i[H, \jmath^\epsilon]\,, \tag{2.25}$$

where f^ϵ is the so called force operator, which is given by the time derivative of the respective current. In this perturbative approach the energy force operator is evaluated as $f^\epsilon \simeq i[H_0, \jmath_1^\epsilon] + i[H_1, \jmath_0^\epsilon]$, i.e., the energy force operator is linear in the field b_0 while the states of the pure Hamiltonian, Eq. (2.1), are used. An attempt for a similar perturbative approach for the spin transport would fail due to the non-conservation of the spin current and the domination of the bulk scattering, which is manifested in $\mathcal{M}$.

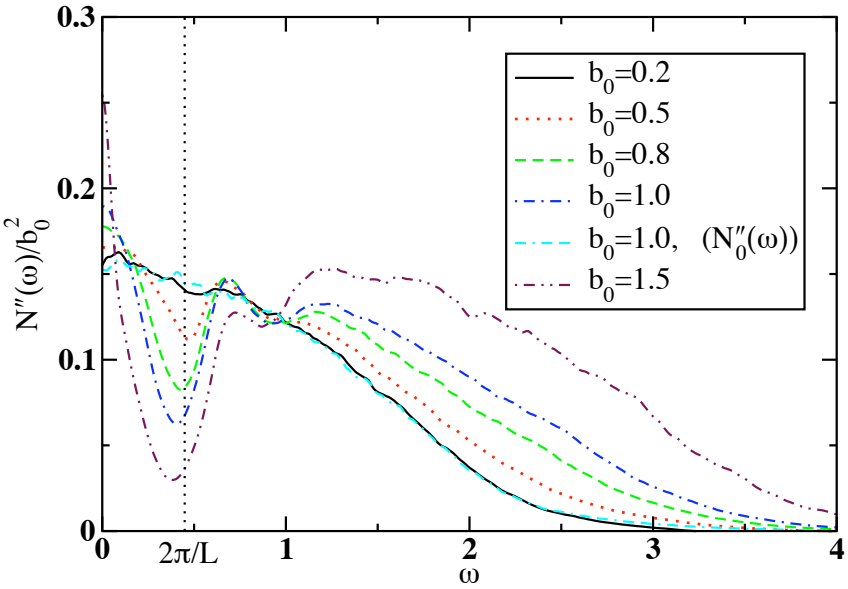

Figure 2.5: Frequency dependence of the imaginary part of the energy memory function divided by b_0^2, for various values of the impurity and $\Delta = 1$, $L = 14$, $T/J = 100$. The local minima are located at a frequency approximately equal to $\omega_m \simeq 2\pi/L$.

2.5.1 Memory function

Let us first discuss the spin memory function since we will focus on the thermal transport later on. One can discuss a possible decomposition of the spin memory function into two parts, one for each scattering mechanism according to Matthiessen's rule , $1/\tau = 1/\tau_{\rm bulk} + 1/\tau_{\rm imp}$, i.e.,

$$M(\omega \to 0) = \mathcal{M}(\omega \to 0) + \frac{1}{L}\tilde{M}(\omega \to 0)\,. \tag{2.26}$$

However, in the gapped phase $\Delta > 1$, we obtain from Eq. (2.26) a negative imaginary part for the memory function corresponding to the impurity scattering at low frequencies. In the gapless phase $\Delta \leq 1$, which is the metallic regime, memory function is positive at low frequencies, however, even for weak perturbations the agreement with the perturbative calculation $M_0(\omega)$ defined similarly to N_0 (with $f^s \sim [H_1, \jmath^s]$) is not satisfactory, indicating that such a decomposition would probably fail or that Matthiessen's rule holds as an inequality. The only case that the perturbative evaluation could be in agreement with the exact results would be for $\Delta = 0$ where $\mathcal{M} = 0$. However, this is not the case again since a single non-magnetic impurity does not destroy ballistic transport for a non-interacting system. The latter is in contrast to the magnetic impurity case where a single magnetic impurity renders coherent transport incoherent even for $\Delta = 0$, cf. sec. 3.3.3.

On the contrary, the relaxation rate for the energy current is induced solely by the impurity, as we have already mentioned, which makes the interpretation of the effect

of the single impurity on heat transport easier. In Fig. 2.5 we present results for the imaginary part of the energy memory function for a wide variety of the impurity field $b_0 = 0.2 - 1.5$. The lattice size is $L = 14$ and results are obtained using ED diagonalization at high temperatures $T/J \gg 1$. $N_0''(\omega)$, evaluated using the perturbation theory (2.25), for $b_0 = 1$ is plotted as well in Fig. 2.5 to compare the two methods. Although we present here results for the isotropic Heisenberg model, the behavior of $N''(\omega)$ is similar apart from the isotropic point.

From Fig. 2.5 one can claim that the energy memory function scales as $N(\omega) \sim b_0^2$ overall. However, it is also evident from Fig. 2.5 that the imaginary part of the energy memory function reveals some structure at higher frequencies, $\omega_m \sim 2\pi/L$, with the appearance of conspicuous local minima even for weak perturbations ($b_0 \gtrsim 0.5$). In addition the position of the minima is independent of the impurity, while it appears to shift towards lower frequencies as Δ is dwindled. Note that this structure cannot be revealed by perturbation theory since one has to include second order in concentration terms and moreover to let the system evolve in time with the full Hamiltonian $H = H_0 + H_1$, instead of H_0 to let this structure on.

Starting from the lowest value of b_0, $b_0 = 0.5$, in Fig. 2.5 we see that memory function approaches its zero frequency value $N''(\omega \to 0)$ with a minimal or even zero slope. This gives support to the argument that the imaginary part of memory function will provide a well defined, frequency independent, scattering rate, $1/\tau^\epsilon \sim N''(\omega \to 0)$, for weak perturbations, and thermal conductivity will be described from the standard Drude theory, exhibiting a Lorentzian form, i.e.,

$$\kappa(\omega) = \frac{\kappa_{dc}}{1 + (\omega\tau^\epsilon)^2} \,. \tag{2.27}$$

Considering a dilute concentration of impurities c_I, so that one can neglect correlations among impurities, the scattering rate will be proportional to the concentration $1/\tau \propto c_I$, as indicated by the memory function formalism (B.11) while for the single impurity case it will be $\tau^\epsilon \propto L$. Furthermore, perturbative results are in very good agreement with the exact ones for not so strong perturbations. However, perturbation theory starts to fail as this characteristic structure, the local minima at frequencies $\sim 2\pi/L$, becomes more and more pronounced.

So far we have ignored the contribution of the real part of the memory function to the conductivity (Eqs. (2.24), (2.27)). The complete form for the thermal conductivity written in terms of the real and the imaginary part of the energy memory function will be

$$\kappa(\omega) = \left(\frac{\chi_0^\epsilon}{LT}\right) \frac{N''(\omega)}{(\omega + N'(\omega))^2 + (N''(\omega))^2} \,. \tag{2.28}$$

For weak perturbations the real part will only renormalize the scattering time, with the renormalization constant being approximately equal to one. In Fig. 2.6 we show the more relevant quantity $\omega + N'(\omega)$, instead of $N'(\omega)$, for various values of the impurity $b_0 = 0.2 - 1.5$ and $L = 14$, $\Delta = 1$, $T/J \gg 1$. We can see that for relatively weak perturbations ($b_0 \sim 1$), at low frequencies ($\omega < 1$), curves scarcely deviate from the

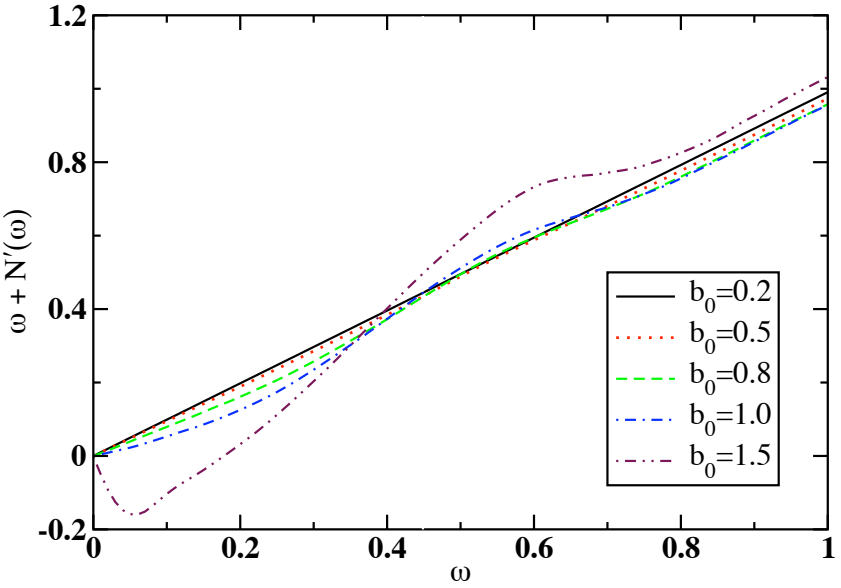

Figure 2.6: Frequency dependence of $\omega + N'(\omega)$ for various impurities b_0 and $\Delta = 1$, $L = 14$, $T/J = 100$.

linear behavior, illustrating the negligible contribution of the real part of the energy memory function to the thermal conductivity.

On the other hand, for strong perturbations we can see from Fig. 2.5 that the imaginary part of the memory function exhibits a rapid increase at low frequencies which inevitably will lead to a drastic reduction in the low frequency thermal conductivity. In addition the minimum value of the quantity $|\omega + N'(\omega)|$ (Fig. 2.6) for strong perturbations is not any more at zero frequency but at some finite frequency giving support to the argument that the thermal conductivity will not be a monotonic function of frequency. For strong perturbations we are led to the conclusion that the frequency dependent thermal conductivity will no more be a Lorentzian but rather a non-monotonic function of frequency. The maximum of the thermal conductivity will occur at some finite frequency, which actually is very close to the frequency where $\omega + N'(\omega) = 0$.

From all the above we would summarize that for weak perturbations ($b_0/J < 1$) and in the low frequency regime the real and imaginary part of the energy memory function will be

$$\omega + N'(\omega) \simeq \omega\,, \quad N''(\omega) \simeq N''(0) \simeq 1/\tau^{\epsilon}\,, \qquad (\omega \ll 1) \tag{2.29}$$

with the scattering time τ^{ϵ} being very close to the one obtained from the perturbation theory indicating that it scales—as it is clear from Eq. (2.25)—as $1/\tau^{\epsilon} \sim b_0^2/L$. More accurately, one can perform a Taylor expansion at low frequencies $\omega \ll 1$ for the

memory function to obtain

$$N'(\omega) = \left(\frac{d}{d\omega} N'(\omega) \Big|_{\omega=0} \right) \omega + \mathcal{O}(\omega^2) \,, \qquad N''(\omega) = N''(\omega = 0) + \mathcal{O}(\omega^2) \,. \tag{2.30}$$

In that case the Drude form (2.27) is still valid with the same κ_{dc},

$$\kappa_{dc} = \left(\frac{\chi_0^\epsilon}{TL} \right) \frac{1}{N''(0)} \,,$$

but the scattering time τ^ϵ will be renormalized as

$$1/\tau^\epsilon \to \alpha/\tau^\epsilon \,, \quad \alpha = 1 + \frac{d}{d\omega} N'(\omega) \Big|_{\omega=0} \,. \tag{2.31}$$

However, the renormalization constant is $\alpha \simeq 1$.

In contrast to the low frequency behavior of the memory function, which is structureless for the imaginary part and negligible for the real part, the high frequency behavior of the memory function exhibits a strong dependence on the frequency ω. Apparently the high frequency structure of the memory function will not be significant for the thermal conductivity in the sense that $\omega/N''(\omega) \ll 1$. Finally, the low frequency fluctuations of the imaginary part of the memory function are not significant to affect the behavior of the thermal conductivity as long as they are small in comparison to the magnitude of the memory function itself.

2.5.2 Thermal conductivity

Weak perturbations

In Fig. 2.7 we present results for the real part of the thermal conductivity, $T^2\kappa(\omega)$, for two values of the impurity field $b_0 = 0.5, 0.8$ using the ED technique at high temperatures ($T/J \gg 1$) for the isotropic Heisenberg model, $\Delta = 1$, and for $L = 14$ sites. The black solid lines with the label "exact", correspond to the thermal conductivity, calculated by the exact formula (A.10b) with the energy current given by (2.3b) with $J_l = J$ and $b_l = b_0 \delta_{l,0}$,

$$\kappa(\omega) = \frac{\pi\beta}{L} \frac{1 - e^{-\beta\omega}}{\omega} \sum_{\substack{n,m \\ (\epsilon_n \neq \epsilon_m)}} p_n |\langle n|j^\epsilon|m\rangle|^2 \delta(\epsilon_m - \epsilon_n - \omega) \,. \tag{2.32}$$

The red dotted curves with the label "perturbative" correspond to the thermal conductivity, extracted from

$$\kappa(\omega) = \frac{1}{T} \frac{i(\chi_0^\epsilon/L)}{\omega + N_0(\omega)} \,, \tag{2.33}$$

using for the perturbative calculation of the memory function Eq. (2.25), where the force operator is linear in the impurity field b_0—yielding trivially the behavior $N \sim b_0^2$. The green dashed lines, correspond to a two parameter Lorentzian fit.

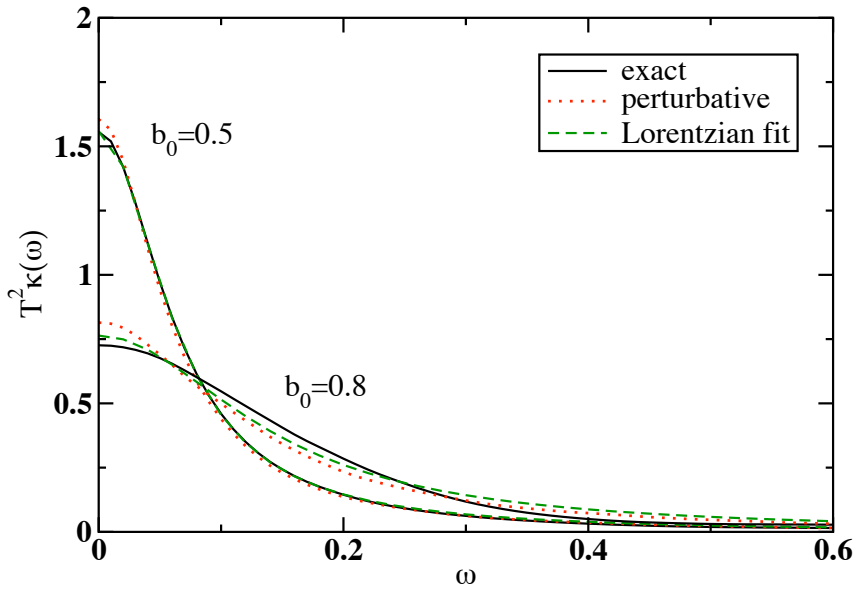

Figure 2.7: Frequency dependence of the real part of the thermal conductivity, $T^2\kappa(\omega)$, for two values of the impurity field $b_0 = 0.5, 0.8$ and $\Delta = 1$, $L = 14$, $T/J = 100$. In addition results from perturbation theory as well as a Lorentzian fit are also shown.

From the previous analysis for the respective energy memory function in the weak coupling regime we reached various conclusions for the thermal conductivity, which now are seen to be consistent with the numerical results. The thermal conductivity indeed exhibits a Lorentzian form for relatively weak perturbations and the scattering rate, $1/\tau^\epsilon$, is given by the zero frequency value of the memory function. For increasing impurity field, b_0, the thermal conductivity becomes a wider Lorentzian and its dc value is decreased. This can be quantified by exploiting the fact that if the thermal conductivity exhibits a Lorentzian form, Eq. (2.27), we can write for its dc value

$$\kappa_{dc} = \frac{\tau^\epsilon}{\pi} \int_{-\infty}^{\infty} \kappa(\omega) d\omega \,. \tag{2.34}$$

In the infinite temperature limit where the sumrule will be $\propto \kappa_0$, with κ_0 given by (1.19) taking $\langle b^2 \rangle = b_0^2/L$ for the single impurity problem.[1] On the other hand $1/\tau^\epsilon \sim b_0^2$ as it is implied by the memory function approach. Thus we conclude that the dc value of the thermal conductivity will scale with the impurity field, for weak perturbations (and a given lattice size), as

$$\kappa_{dc} \sim \frac{2}{L} + \left(1 + 2\Delta^2\right) \left(\frac{J}{b_0}\right)^2 \,. \tag{2.35}$$

[1] For a many but dilute impurity problem with a concentration c_I the same discussion is valid with $\langle b^2 \rangle = c_I b_0^2$.

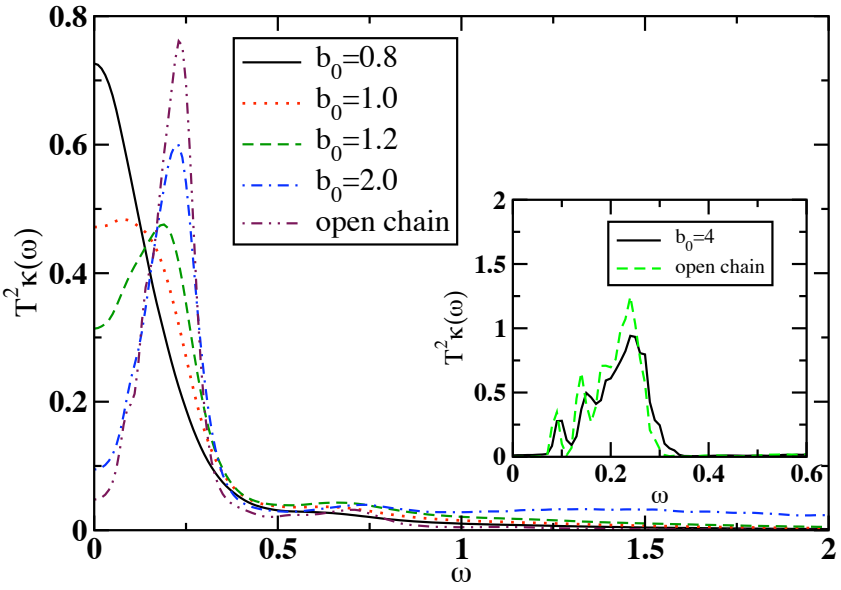

Figure 2.8: Frequency dependence of the thermal conductivity, $T^2\kappa(\omega)$, for various values of the local field, $b_0 = 0.5 - 2.0$ and $L = 14$, $\Delta = 1$, $T/J = 100$. In addition the thermal conductivity for an open chain is shown. Inset: frequency dependence of the thermal conductivity for a pure chain ($b_0 = 0$) with open boundary conditions as well with the un-smoothed data for a chain with an impurity $b_0 = 4$.

Taking into account that for these systems the thermal conductivity exhibits a trivial $1/T^2$ temperature dependence for $T \gtrsim J$, we could assume that the behavior shown in Eq. (2.35) is valid for a quite wide range of temperatures, and not only for the infinite temperature limit where it was evaluated.

We can also remark that while for $b_0 = 0.5$ the agreement is almost excellent between perturbation theory and exact results, for the higher field, $b_0 = 0.8$, in Fig. 2.7, some deviations appear indicating the limitations of the perturbative approach. Note that despite the term "weak perturbations" that we have coined for local fields up to $b_0 \sim 1$, due to the lorentzian shape of the thermal conductivity, the ratio of the impurity strength b_0 to the unit of energy of the system J is not so small that would justify the term "weak". Furthermore, the ratio of the impurity to the whole energy span is also not negligible, affecting a large part of the spectrum.

Strong perturbations

Leaving the weak coupling regime and entering into the strong one, we run into a totally different behavior. First of all, as it is expected in this regime perturbation theory breaks down. The thermal conductivity exhibits a depletion at low frequencies, the maximum is shifted at a finite frequency and it is not any more a monotonic function of frequency, which is exactly what was expected from the memory function analysis,

Fig. 2.8.

In Fig. 2.8 we show results for the thermal conductivity for different values of the local field $b_0 = 0.8-2.0$ obtained via ED at high temperatures $T/J \gg 1$ and for $L = 14$, $\Delta = 1$. For the lowest value of the impurity field, $b_0 = 0.8$, we can see that we are still in the weak coupling regime where the thermal conductivity exhibits a Lorentzian form. As the impurity field is increased a depletion appears at low frequencies and becomes more and more pronounced for a farther increase of the field b_0. Apparently due to local excitations of the impurity there will be some structure at higher frequencies $\omega \sim b_0$, nevertheless, the part that comes from the bulk of the chain will more and more tend to the curve of the open chain. Hence, the conclusion is that a significant part of the weight which was centered around the origin, $\omega = 0$, for weak perturbations, will be shifted at a finite frequency for stronger perturbations, with $\omega \sim \pi/L$ being a limiting frequency shift for very strong perturbations.

To verify this we show in the inset of Fig. 2.8 the thermal conductivity for a chain with open boundary conditions and the thermal conductivity for a ring in the presence of a severe perturbation, $b_0 = 4$. For very strong perturbations, like $b_0 \sim 4$, the un-smoothed spectra reproduce besides the dominant peak of the open chain and the smaller ones which are located at lower frequencies, indicating that the chain is cut. In the strong coupling limit the picture is that the bulk of the chain reproduces the thermal conductivity of a chain with open boundary conditions, while there is also some structure at frequencies $\omega \sim b_0$ due to local excitations attributed to the impurity. This is in agreement with the level statistics analysis where it was proposed that a very strong impurity cuts the chain leading to the integrable Heisenberg chain with open boundary conditions.

Let us clarify here a subtle point. So far we have plotted curves which were smoothed using the Kramers-Kronig relations (see Eq. (A.21) and discussion in Appx. C). Thus the finite dc value for the thermal conductivity that we obtain in Fig. 2.8 is only an artifact of the finite damping γ. This is verified in the inset where the dc value of the thermal conductivity vanishes for the un-smoothed data. Moreover, in the inset of Fig. 2.8 where we plot the thermal conductivity without implementing any smoothing procedure one can observe that the thermal conductivity of the ring in the presence of the impurity reproduces not only the overall shape of the open chain but the narrower secondary peaks as well, which correspond to the excitations of the open chain. Apparently, apart from the "integrable" points, $b_0 \to 0, \infty$, the smoothing procedure does not affect the results in a way that could lead to erroneous conclusions.

2.5.3 Anisotropy dependence

The next issue we would like to discuss is how results depend on the anisotropy parameter Δ. For the case of spin conductivity the anisotropy parameter plays a crucial role, changing dramatically the behavior of the spin conductivity from the gapless ($\Delta < 1$) to the gapped ($\Delta > 1$) phase. On the contrary, for the thermal conductivity where the thermal stiffness is finite in the pure AHM for any value of the anisotropy parameter Δ, the picture remains qualitatively similar to the isotropic point, which was discussed

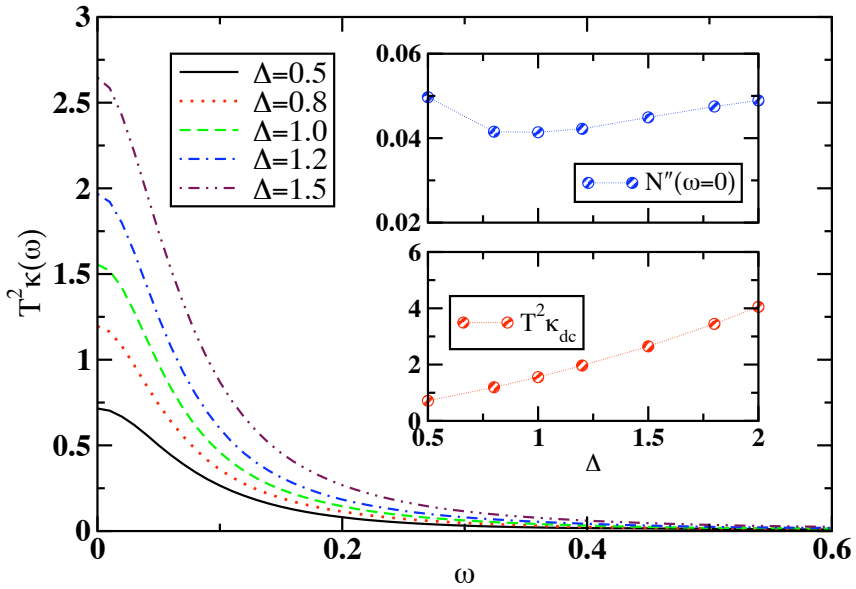

Figure 2.9: Frequency dependence of thermal conductivity for various values of the anisotropy parameter Δ and $b_0 = 0.5$, $L = 14$, $T/J = 100$. Inset top: The static limit of the imaginary part of the energy memory function, $N''(\omega \to 0)$, is shown as a function of the anisotropy Δ. Inset bottom: The dc thermal conductivity, $T^2\kappa_{dc}$, is shown as a function of the anisotropy parameter Δ.

previously. For a weak perturbation $b_0 = 0.5$ the thermal conductivity obtained via ED at high temperatures $T/J \gg 1$ for various values of the anisotropy parameter $\Delta = 0.5 - 1.5$ is shown in Fig. 2.9. In addition, two insets are included. In the one at the bottom the dc value of the thermal conductivity is plotted, while in the other one the zero frequency value of the imaginary part of the memory function—the scattering rate—is plotted. The picture is that for a given weak perturbation b_0 the behavior of the thermal conductivity remains qualitatively the same, i.e., the δ-function is broadened into a Lorentzian while quantitatively the results change significantly since the flux of the energy that is transfered changes with Δ.

However, Δ seems also to determine whether the perturbation is weak or strong for the system. The conclusion is that even for weak perturbations if $\Delta \lesssim b_0$ the thermal conductivity becomes a non-monotonic function of frequency, exhibiting a drop at low frequencies as it was mentioned in the previous paragraphs, which is an indication that the system is strongly disturbed by the impurity. For one thing, notice the increase of the scattering rate ($N''(\omega = 0)$) in the inset of Fig. 2.9 for $\Delta = 0.5$. Furthermore, compare the high temperature thermal conductivity in Figs. 2.8, 2.10 for $b_0 = 1$ but different anisotropy $\Delta = 1, 0.5$ respectively.

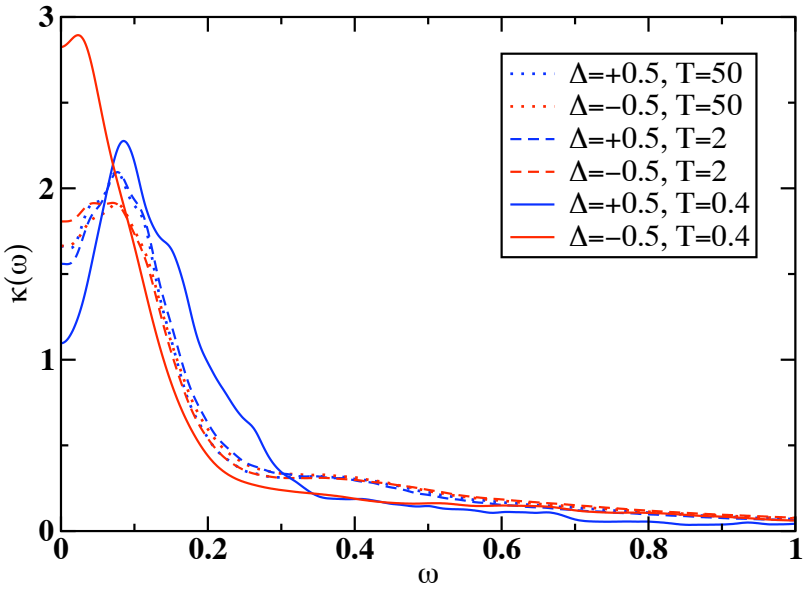

Figure 2.10: Frequency dependence of the normalized thermal conductivity for a relatively strong perturbation $b_0 = 1$ and for positive, $\Delta = +0.5$, and negative, $\Delta = -0.5$, anisotropy. The FTLM method is used and three temperatures $T = 0.4$, 2, 50 are shown for $L = 20$ sites.

2.6 Temperature dependence

The last issue we would like to explore is the temperature dependence of the transport properties of the Heisenberg model in the presence of a single non-magnetic impurity. The cutting-healing behavior that was proposed by Kane and Fisher (KF) [12, 33] can be investigated in the Heisenberg chain by letting the anisotropy parameter Δ to take positive and negative values as well. We have seen that the Jordan-Wigner transformation maps the spin system into a fermionic Luttinger liquid, with the interaction parameter V being proportional to the anisotropy parameter Δ, Eq. (1.6). Antiferromagnetic anisotropy ($\Delta > 0$) corresponds to repulsive interactions between fermions, ferromagnetic anisotropy ($\Delta < 0$) corresponds to attractive interactions between fermions, while $\Delta = 0$ corresponds to non-interacting tight binding fermions which is expected to be an intermediate situation, i.e., there will be a finite conductance but it will be reduced in comparison with the one of the pure model.

In order to investigate temperature dependent effects like the cutting or the healing of the host chain from the impurity, the finite temperature Lanczos method (FTLM) is used (Ref. [34]), to compute dynamical transport quantities in systems with $L > 16$. Typically, $N_L = 500$ Lanczos steps are used to obtain spectra with high frequency resolution, with an additional broadening, $\gamma = 0.03$.

Thermal conductivity

Before proceeding with the analysis of the temperature dependence let us summarize the conclusions that were obtained by the analysis in the previous sections. The thermal conductivity consists only of a δ-function located at the origin for vanishing impurity field. For weak perturbations the δ-function is broadened, where the role of the broadening parameter plays the scattering rate $1/\tau^{\epsilon}$, and the thermal conductivity exhibits a Lorentzian form. As we increase farther the perturbation, both level statistics and numerical results for the thermal conductivity and its memory function indicate that the chain is cut due to the impurity, for $\Delta \neq 0$, and the dc value of the thermal conductivity decreases with the development of a characteristic peak at a finite frequency; this behavior resembles the frequency dependence of a chain with open boundary conditions [35].

The strong dependence of the thermal conductivity on the temperature prevents definite conclusions for the cutting or the healing of the ring by looking only at $\kappa_{dc}(T)$ for a given value of the field b_0. However, the normalized dc value of the thermal conductivity, $\kappa_{dc}(T) \Big/ \int \kappa(\omega) d\omega$, or the static limit of the imaginary part of the memory function, $N''(\omega \to 0)$, could be more suitable since trivial temperature factors are eliminated making transparent the effect of the impurity on the system. On the other hand, the difference of the shape that we described in the previous paragraphs, monotonic for weak perturbations and non-monotonic for strong perturbations, can provide a valuable criterion for the cutting or the healing of the chain with lowering temperature. Let us become more specific. Suppose a given form for the thermal conductivity at a high temperature, either monotonic with the maximum at zero frequency or non-monotonic with the maximum at a finite frequency. An indication for the cutting behavior with decreasing temperature would be either the appearance of a depletion at low frequencies if it does not exist at high temperatures, or to become more pronounced in cases where it already exists at high temperatures. On the other hand, if the chain screens the impurity as the temperatures decreases we expect the depletion to disappear and the thermal conductivity to establish a Lorentzian behavior, characteristic for weak perturbations, or to retain its high temperature Lorentzian form. Unfortunately, for finite size systems limitations occur about the lowest achievable temperature with FTLM, where below the limiting temperature T_{fs} results are not to be trusted; we estimate $T_{fs}/J \simeq 0.3$. As a result, we are not able to observe the complete healing of the chain leading to a zero frequency δ-function but rather to observe the tendency for healing indicated as well by the opposite behavior for $\Delta \gtrless 0$. Finally, due to the sparse spectrum the zero temperature Lanczos method cannot offer anything to this discussion.

We would like now to exploit this different behavior of the form of the thermal conductivity depending on whether the system is in the strong or in the weak coupling limit. In Fig. 2.10 we present results for the normalized thermal conductivity, $\kappa(\omega) \Big/ \int \kappa(\omega) d\omega$, obtained for a system of $L = 20$ sites via the FTLM. The reason why we present the normalized thermal conductivity instead of the un-normalized one, is that we are interested in how the total weight of the thermal conductivity is distributed throughout the frequency range and how this distribution changes with temperature.

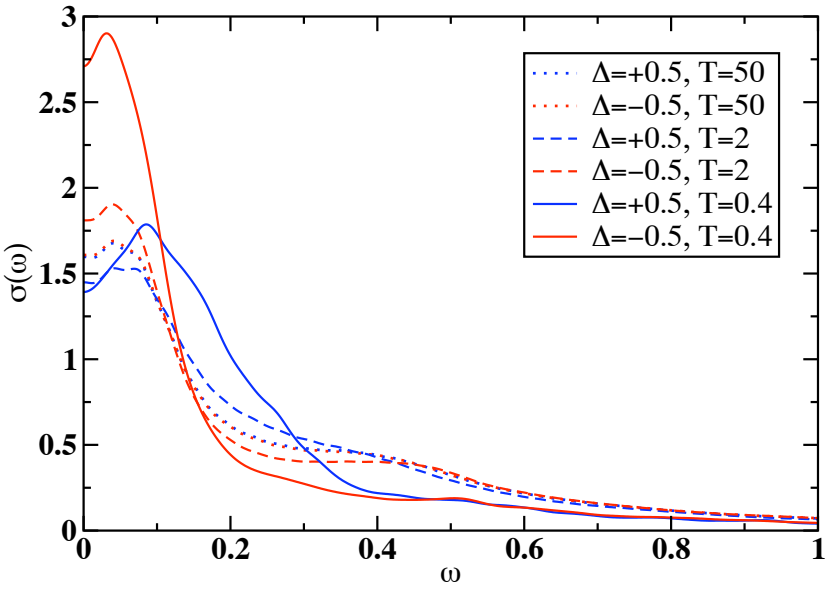

Figure 2.11: Frequency dependence of the normalized spin conductivity for a relatively strong perturbation $b_0 = 1$ and for positive, $\Delta = +0.5$, and negative, $\Delta = -0.5$, anisotropy. The FTLM method is used and three temperatures $T = 0.4$, 2, 50 are shown for $L = 20$ sites.

The exact magnitude of the conductivity is irrelevant for this approach. In Fig. 2.10 we consider an impurity field $b_0 = 1$ where it appears that for $\Delta = \pm 0.5$ we are in the strong coupling limit ($\Delta < b_0$) at high temperatures since the depletion is present. While at high temperature ($T/J = 50$) the curves for positive and negative Δ coincide, as the temperature is lowered ($T/J = 2$) they separate from each other. At the lowest temperature $T/J = 0.4$ the difference is more than sharp. While for positive (anti-ferromagnetic) Δ the systems couples stronger and stronger with the impurity as the temperature is reduced, in the ferromagnetic case the system seems to screen the impurity leaving from the strong coupling limit and entering into the weak one. Although a small depletion is still present at the lowest temperature, $T/J = 0.4$, for $\Delta < 0$ and consequently the thermal conductivity does not exhibit a Lorentzian form, the width of the curve as well with the contrast of the anti-ferromagnetic case ($\Delta > 0$) manifest the cutting-healing behavior.

Spin conductivity

So far we have used only the thermal conductivity as a probe for the cutting-healing effects due to its simple interpretation, since the only scattering mechanism is induced solely by the impurity. However, for a pure Heisenberg chain the spin conductivity exhibits a finite Drude weight in the metallic regime ($\Delta < 1$) despite the non-conservation of the spin current. We can again seek cutting-healing effects exploiting this Drude weight which could possible lead to a low frequency behavior for the spin conductivity

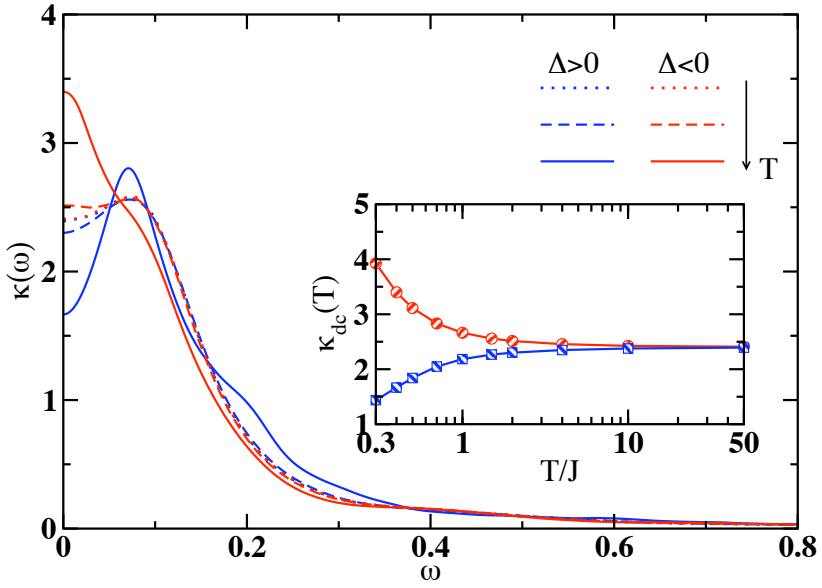

Figure 2.12: Frequency dependence of the normalized thermal conductivity for a single weak link $J'/J = 0.5$ and for a positive and negative anisotropy, $\Delta = \pm 0.8$. The FTLM method was used and three temperatures $T = 0.4,\ 2,\ 50$ are shown for $L = 20$ sites. Inset: The temperature dependence of the normalized dc thermal conductivity is shown in a semi log plot.

that would resemble the one of the thermal conductivity, despite the more complicated high frequency structure. Concentrating on the low frequency behavior of the spin conductivity we would expect the δ-function to be broadened into a Lorentzian-like form in the weak coupling regime while for strong couplings the low frequency depletion should appear similarly to the thermal conductivity. In Fig. 2.11 we indeed verify this behavior where the results are obtained via FTLM for a chain of $L = 20$ sites, $\Delta = \pm 0.5$, while three characteristic temperatures are presented, $T/J = 50, 2, 0.4$. For the highest temperature ($T/J = 50$) curves for ferromagnetic and anti-ferromagnetic anisotropy coincide, while as the temperature is lowered ($T/J = 2, 0.4$) curves separate from each other with the $\Delta > 0$ curves having the tendency to become wider with a more prominent depletion as well. On the other hand the curves for $\Delta < 0$, despite the fact that the depletion does not disappear, become narrower resembling the behavior of a Lorentzian who tends to become a δ-function.

2.6.1 Single weak link

Similarly to the local field perturbation the Heisenberg chain can be healed or cut by a single weak link as it was proposed by KF. We show this behavior in Fig. 2.12 where the normalized thermal conductivity is plotted. The Hamiltonian and the spin, energy currents are given by (2.1), (2.3) where $J_{l\neq 0} = J$ and $J_0 = J'$. In the present case

we have taken $J'/J = 0.5$ and $\Delta = \pm 0.8$. Moreover in the inset of Fig. 2.12 we plot the normalized dc thermal conductivity which could be seen as the scattering time $\tau^{\epsilon}(\omega \to 0)$ as well. The inset indicates that we cannot discuss a crossover temperature, below which the cutting-healing behavior occurs, since the curves incline to separate from very high temperatures already.

2.7 Conclusions

To summarize, we have primarily used numerical techniques to study the effect of a single non magnetic impurity on a Heisenberg chain. We have used as probes the level statistics analysis, studying particularly the parameters η (2.6) and Δ_3 (2.7), the spin stiffness D_s (2.11) in the metallic regime $\Delta < 1$ and the charge stiffness for $\Delta = 0$ (2.20) and finally the spin, thermal conductivities (2.22), and the corresponding spin, energy memory functions as well (2.24), (2.25). The conclusions are:

- We have shown that a single static impurity induces incoherent transport manifested in the level statistics analysis, the spin stiffness in the metallic regime and the well-defined energy current relaxation time. This should be contrasted with the case of noninteracting fermions in Eq. (2.20) where a single impurity only reduces the stiffness D_s but does not lead to current relaxation within the ring at any T. The fundamental difference seems to come from the umklapp processes which are revived by the impurity and lead to the decoherence between successive scattering events on the impurity.

- In this sense it is also plausible that for a finite but low concentration of static impurities, c_I, in a chain as relevant for experiments we expect that our results can be simply generalized as $1/\tau^{\epsilon} \propto c_I$, as it is evident also from the lowest-order perturbation theory, Eq. (2.25).

- Moreover as far as the temperature dependence is concerned, we explored the "cutting-healing" effects that were proposed theoretically for two models, a potential barrier and a single weak link. We indeed verify the proposed crossover behavior with lowering temperature for both models, proposing as a criterion the form of physical quantities like the spin (only for $|\Delta| < 1$) or the thermal conductivity. First, for the local barrier case, the spin chain is healed in the presence of the impurity for ferromagnetic anisotropy ($\Delta < 0$) in contrast to the antiferromagnetic case ($\Delta > 0$) where the impurity blocks the dc transport leading to a severe reduction of the low frequency conductivities. Second, for the AHM with a modified link, we again verify the cutting healing behavior depending on the sign of the anisotropy parameter Δ.

- Finally, finite size numerical limitations prevent us from discussing the limiting behavior $T \to 0$ as well as the existence of a crossover temperature below which the cutting-healing behavior occurs.

Bibliography

[1] X. Zotos and P. Prelovšek, Transport in one dimensional quantum systems, in *Strong interactions in low dimensions*, pages 347–382, Springer Netherlands, 2004.

[2] X. Zotos, Issues on the Transport of One Dimensional Quantum Systems, Journal of the Physical Society of Japan **74S**(Supplement), 173–180 (2005).

[3] C. Hess, Heat conduction in low-dimensional quantum magnets, The European Physical Journal - Special Topics **151**, 73–83 (2007).

[4] A. V. Sologubenko, T. Lorenz, H. R. Ott, and A. Freimuth, Thermal Conductivity via Magnetic Excitations in Spin-Chain Materials, Journal of Low Temperature Physics **147**, 387–403 (2007).

[5] X. Zotos, Finite Temperature Drude Weight of the One-Dimensional Spin- 1/2 Heisenberg Model, Physical Review Letters **82**(8), 1764–1767 (Feb 1999).

[6] H. Castella, X. Zotos, and P. Prelovšek, Integrability and Ideal Conductance at Finite Temperatures, Physical Review Letters **74**(6), 972–975 (Feb 1995).

[7] X. Zotos, F. Naef, and P. Prelovsek, Transport and conservation laws, Physical Review B **55**(17), 11029–11032 (May 1997).

[8] P. Mazur, Non-ergodicity of phase functions in certain systems, Physica **43**(4), 533 – 545 (1969).

[9] M. Suzuki, Ergodicity, constants of motion, and bounds for susceptibilities, Physica **51**(2), 277 – 291 (1971).

[10] J. Sirker, R. G. Pereira, and I. Affleck, Diffusion and Ballistic Transport in One-Dimensional Quantum Systems, Physical Review Letters **103**(21), 216602 (Nov 2009).

[11] P. Jung, R. W. Helmes, and A. Rosch, Transport in Almost Integrable Models: Perturbed Heisenberg Chains, Physical Review Letters **96**(6), 067202 (2006).

[12] C. L. Kane and M. P. A. Fisher, Transport in a one-channel Luttinger liquid, Physical Review Letters **68**(8), 1220–1223 (Feb 1992).

[13] A. Furusaki and N. Nagaosa, Single-barrier problem and Anderson localization in a one-dimensional interacting electron system, Physical Review B **47**(8), 4631–4643 (Feb 1993).

[14] A. Furusaki and T. Hikihara, Kondo effect in XXZ spin chains, Physical Review B **58**(9), 5529–5538 (Sep 1998).

[15] A. Metavitsiadis, X. Zotos, O. S. Barišić, and P. Prelovšek, Thermal transport in a spin- 12 Heisenberg chain coupled to a magnetic or nonmagnetic impurity, Physical Review B **81**(20), 205101 (May 2010).

[16] S. Rommer and S. Eggert, Spin- and charge-density oscillations in spin chains and quantum wires, Physical Review B **62**(7), 4370–4382 (Aug 2000).

[17] T. Giamarchi, Strong Correlations in Low Dimensional Systems, volume 846, pages 94–129, AIP, 2006.

[18] T. A. Brody, J. Flores, J. B. French, P. A. Mello, A. Pandey, and S. S. M. Wong, Random-matrix physics: spectrum and strength fluctuations, Reviews of Modern Physics **53**(3), 385–479 (Jul 1981).

[19] D. Poilblanc, T. Ziman, J. Bellissard, F. Mila, and G. Montambaux, Poisson vs. GOE Statistics in Integrable and Non-Integrable Quantum Hamiltonians, EPL (Europhysics Letters) **22**(7), 537 (1993).

[20] H. K. Owusu, K. Wagh, and E. A. Yuzbashyan, The link between integrability, level crossings and exact solution in quantum models, Journal of Physics A: Mathematical and Theoretical **42**(3), 035206 (2009).

[21] M. Di Stasio and X. Zotos, Connection between Low Energy Effective Hamiltonians and Energy Level Statistics, Physical Review Letters **74**(11), 2050–2053 (Mar 1995).

[22] D. A. Rabson, B. N. Narozhny, and A. J. Millis, Crossover from Poisson to Wigner-Dyson level statistics in spin chains with integrability breaking, Physical Review B **69**(5), 054403 (Feb 2004).

[23] P. Jacquod and D. L. Shepelyansky, Emergence of Quantum Chaos in Finite Interacting Fermi Systems, Physical Review Letters **79**(10), 1837–1840 (Sep 1997).

[24] B. Georgeot and D. L. Shepelyansky, Integrability and Quantum Chaos in Spin Glass Shards, Physical Review Letters **81**(23), 5129–5132 (Dec 1998).

[25] F. J. Dyson and M. L. Mehta, Statistical Theory of the Energy Levels of Complex Systems. IV, Journal of Mathematical Physics **4**(5), 701–712 (1963).

[26] O. Bohigas and M. J. Giannoni, Level density fluctuations and random matrix theory, Annals of Physics **89**(2), 393 – 422 (1975).

[27] A. Pandey, Statistical properties of many-particle spectra : III. Ergodic behavior in random-matrix ensembles, Annals of Physics **119**(1), 170 – 191 (1979).

[28] X. Zotos and P. Prelovšek, Evidence for ideal insulating or conducting state in a one-dimensional integrable system, Physical Review B **53**(3), 983–986 (Jan 1996).

[29] B. S. Shastry, Sum rule for thermal conductivity and dynamical thermal transport coefficients in condensed matter, Physical Review B (Condensed Matter and Materials Physics) **73**(8), 085117 (2006).

[30] T. Rejec and A. Ramšak, Conductance of interacting Aharonov-Bohm systems, Physical Review B **68**(3), 033306 (Jul 2003).

[31] T. Rejec and A. Ramšak, Formulas for zero-temperature conductance through a region with interaction, Physical Review B **68**(3), 035342 (Jul 2003).

[32] W. Götze and P. Wölfle, Homogeneous Dynamical Conductivity of Simple Metals, Physical Review B **6**(4), 1226–1238 (Aug 1972).

[33] C. L. Kane and M. P. A. Fisher, Transmission through barriers and resonant tunneling in an interacting one-dimensional electron gas, Physical Review B **46**(23), 15233–15262 (Dec 1992).

[34] M. W. Long, P. Prelovšek, S. El Shawish, J. Karadamoglou, and X. Zotos, Finite-temperature dynamical correlations using the microcanonical ensemble and the Lanczos algorithm, Physical Review B **68**(23), 235106 (Dec 2003).

[35] M. Rigol and B. S. Shastry, Drude weight in systems with open boundary conditions, Physical Review B **77**(16), 161101 (Apr 2008).

Chapter 3

Single magnetic impurity

3.1 Introduction

A (non) magnetic impurity coupled to a spin-1/2 Heisenberg chain is a prototype system that exemplifies "Kondo"-type effects in a correlated system. Starting with the proposal of Kane-Fisher [1], a weak link in a repulsive (attractive) Luttinger liquid was shown to lead to an insulating (transmitting) ground state. The cutting or healing of spin chains by a variety of (non) magnetic defects has also been established [2–5] as well as the effect of a magnetic impurity on the ground state of the anisotropic easy-plane Heisenberg chain [6]. Generically, a weak link or coupling to a magnetic impurity in a Heisenberg antiferromagnetic chain leads to a ground state corresponding to two open chains. In the exceptional case of two adjacent links or a ferromagnetic (attractive in the fermionic language) easy axis anisotropy a healing of the defect is conjectured [6]. This screening effect is characterized by a Kondo-like temperature and screening length [3, 4]. These phenomena have so far mostly been studied either as they are reflected on ground state properties, e.g. finite size gaps, entanglement or, somewhat indirectly, as a temperature dependent induced staggered susceptibility [3].

The thermal transport in the spin-1/2 Heisenberg chain is truly singular providing an exceptional physical probe to study these effects. Although the Heisenberg model describes a strongly correlated system, the thermal conductivity is purely ballistic as the energy current commutes with the Hamiltonian [7], a result that is related to the integrability of this model.[1] Thus the only scattering present is due to the defect and thus its frequency/temperature/coupling strength dependence can be isolated and clearly analyzed. In this context it was already found that a single potential impurity renders the thermal transport incoherent [8] (Ch. 2) with the frequency dependence of the thermal conductivity well described by a Lorentzian, at least for a weak impurity. This is in sharp contrast to the case of a non-interacting system where in spite of the impurity the transport remains coherent described within the Landauer formalism by a finite transmission coefficient through the impurity. Thus a single static impurity

[1] It should be noted that a tower of integrable Hamiltonians exist for every value of spin, where the energy current is a conserved quantity, but these Hamiltonians have no obvious physical realizations.

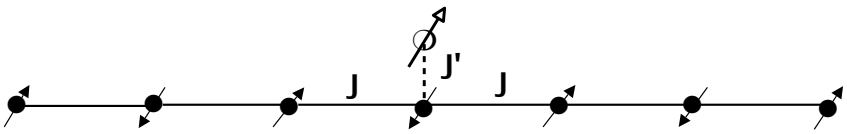

Figure 3.1: The Heisenberg spin-1/2 chain coupled to a spin-S magnetic impurity located out of the chain.

materializes the many-body character of scattering states.

Besides its theoretical interest, the effect of (non)magnetic impurities on the thermal transport of quasi-one dimensional materials as $SrCuO_2$, Sr_2CuO_3 and the ladder compound $La_5Ca_9Cu_{24}O_{41}$ has recently become possible to explore experimentally [9]. Particularly, evidence for ballistic transport was consolidated using samples of very high purity [10]. Moreover, the screening of the impurity by the chain [2], was verified in magnetic susceptibility measurements on Ni-doped Sr_2CuO_3 cuprate, Ref. [11].

3.2 Model

We consider two models where the pure one dimensional anisotropic spin-1/2 Heisenberg model (AHM) is disturbed by a single magnetic impurity. In the first case, we assume that a spin-S impurity is located out of the chain (SOC model) and it is coupled with only one of the spins of the chain—say the one at the zeroth site. The Hamiltonian which describes this model, which is depicted in Fig. 3.1, can be separated into two terms: one for the pure model and one for the local perturbation,

$$H = H_0 + H_1 \tag{3.1}$$

$$H_0 = J \sum_l \mathbf{s}_l \cdot \boldsymbol{\Delta} \cdot \mathbf{s}_{l+1} \,, \quad H_1 = J' \, \left(\mathbf{s}_0 \cdot \boldsymbol{\Delta}' \cdot \mathbf{S} \right) \tag{3.2}$$

where $\mathbf{s}$ are the chain spin-1/2 operators, $J > 0$ the in-chain magnetic exchange coupling, J' the chain-impurity coupling, Δ, Δ' the easy axis anisotropy parameters (cf. Ch. 1 and particularly Eq. (1.3)), and $\mathbf{S}$ a spin-S magnetic-impurity operator.[2] In addition, we assume periodic boundary conditions, $\mathbf{s}_L = \mathbf{s}_0$, and interactions only between nearest neighbors. We vary the anisotropy parameters Δ, Δ', with $\Delta = \Delta'$ in order to look for the cutting-healing of the chain effects mentioned above.

Spin $\jmath^s$, energy $\jmath^\epsilon$ currents are determined by the hydrodynamic $q \to 0$ limit of the respective continuity equation, $\dot{S}^z_q = -iq\jmath^s_q$, $\dot{H}_q = -iq\jmath^\epsilon_q$, with $\jmath^s = \jmath^s_{q\to 0}$, $\jmath^\epsilon = \jmath^\epsilon_{q\to 0}$ [12]. $\hat{O}_q$ is the q component of the Fourier transform of the local operator $\hat{O}_l$, with $\hat{O} = \sum_l \hat{O}_l$, given by

$$\hat{O}_q = \sum_l e^{-iql} \hat{O}_l \,, \tag{3.3}$$

[2]Recall that we use a system of units where the lattice constant a, the Planck and Boltzmann constants are a,$\hbar, k_B$=1. The quantity $\boldsymbol{\Delta} \cdot \mathbf{s}$ represents the vector $(s^x, s^y, \Delta s^z)$, cf. Ch. 1.

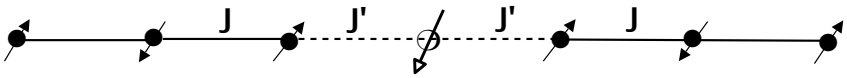

Figure 3.2: The Heisenberg spin-1/2 chain with an embedded spin-S magnetic impurity.

For the spin current we get

$$\begin{aligned} \dot{S}^z_q &\sim -iq\left(J\sum_l S^x_l S^y_{l+1} - S^y_l S^x_{l+1}\right), \\ \Rightarrow \quad \jmath^s &= \sum_l \jmath^s_l\,, \qquad \jmath^s_l = J(\mathbf{s}_l \times \mathbf{s}_{l+1})\cdot\hat{e}_z\,, \end{aligned} \tag{3.4}$$

where $\hat{e}_z$ is the unit vector along the z-axis. Similarly for the energy transport we arrive at

$$\jmath^\epsilon = \jmath^\epsilon_0 + \jmath^\epsilon_1\,, \tag{3.5a}$$

where,

$$\jmath^\epsilon_0 = \sum_l \jmath^\epsilon_l \qquad \text{with} \qquad \jmath^\epsilon_l = J^2\,\mathbf{s}_l\cdot(\boldsymbol{\Delta}\cdot\mathbf{s}_{l+1}\times\boldsymbol{\Delta}\cdot\mathbf{s}_{l-1})\,, \tag{3.5b}$$

$$\jmath^\epsilon_1 = \frac{JJ'}{2}\mathbf{s}_0\cdot(\boldsymbol{\Delta}'\cdot\mathbf{S}\times\boldsymbol{\Delta}\cdot\mathbf{s}_{L-1}) + \frac{JJ'}{2}\mathbf{s}_0\cdot(\boldsymbol{\Delta}\cdot\mathbf{s}_1\times\boldsymbol{\Delta}'\cdot\mathbf{S}). \tag{3.5c}$$

As a second model we consider the case where one of the spins of the chain is substituted by a spin-S magnetic impurity (SIC model) as shown in Fig. 3.2 (say the impurity is located at the $l=0$ site). The Hamiltonian in that case is

$$H = {\sum_l}' J\;(\mathbf{s}_l\cdot\boldsymbol{\Delta}\cdot\mathbf{s}_{l+1}) + J'_1\;(\mathbf{s}_1\cdot\boldsymbol{\Delta}'\cdot\mathbf{S}) + J'_{L-1}\;(\mathbf{s}_{L-1}\cdot\boldsymbol{\Delta}'\cdot\mathbf{S})\,, \tag{3.6}$$

where the prime at the sum denotes that the sum extends over the whole lattice except the sites $l=0, L-1$. We mostly take $J'_1 = J'_{L-1}$ except for the case of a single weak link, cf. Ch. 2. The corresponding spin, energy currents will be

$$\jmath^s = {\sum_l}' J(\mathbf{s}_l\times\mathbf{s}_{l+1})\cdot\hat{e}_z + J'_{L-1}(\mathbf{s}_{L-1}\times\mathbf{S})\cdot\hat{e}_z + J'_1(\mathbf{S}\times\mathbf{s}_1)\cdot\hat{e}_z \tag{3.7a}$$

$$\begin{aligned} \jmath^\epsilon &= {\sum_l}'' J^2\,\mathbf{s}_l\cdot(\boldsymbol{\Delta}\cdot\mathbf{s}_{l+1}\times\boldsymbol{\Delta}\cdot\mathbf{s}_{l-1}) + J'_1J'_{L-1}\mathbf{S}\cdot(\boldsymbol{\Delta}'\cdot\mathbf{s}_1\times\boldsymbol{\Delta}'\cdot\mathbf{s}_{L-1}) \\ &+ JJ'_{L-1}\,\mathbf{s}_{L-1}\cdot(\boldsymbol{\Delta}'\cdot\mathbf{S}\times\boldsymbol{\Delta}\cdot\mathbf{s}_{L-2}) + JJ'_1\,\mathbf{s}_1\cdot(\boldsymbol{\Delta}\cdot\mathbf{s}_2\times\boldsymbol{\Delta}'\cdot\mathbf{S})\,, \end{aligned} \tag{3.7b}$$

where the double prime at the sum means that the sum extends from $l=2$ to $l=L-2$.

Let us repeat here the linear response theory formulas for the real regular components of the spin σ, thermal κ conductivities (cf. Appx. A)

$$\sigma(\omega) = \Im\lim_{\eta\to 0^+}\frac{\chi_{\jmath^s\jmath^s}(z)}{z}\,, \quad \kappa(\omega) = \frac{1}{T}\Im\lim_{\eta\to 0^+}\frac{\chi_{\jmath^\epsilon\jmath^\epsilon}(z)}{z}\,, \tag{3.8}$$

with $z = \omega + i\eta$ and T the temperature. In addition, the susceptibility of the operators $\hat{O}_p$, $\hat{O}_q$ will be

$$\chi_{\hat{O}_p\hat{O}_q}(z) = \frac{i}{L}\int_0^\infty dt\, e^{izt}\,\langle[\hat{O}_p(t), \hat{O}_q]\rangle\,. \tag{3.9}$$

Notice that for posterior convenience the susceptibility is multiplied by an extra $1/L$ factor. The thermodynamic average for an operator $\hat{O}$, denoted by the angle brackets in (3.9), is given by

$$\langle\hat{O}\rangle = \frac{Tr\; e^{-\beta H}\hat{O}}{Tr\; e^{-\beta H}}\,, \qquad \text{with} \quad \beta = 1/T.$$

3.3 Spin out of the chain

3.3.1 High temperature limit

Starting from the high temperature ($\beta \to 0$) limit we can obtain a first impression on the behavior of the frequency dependence of $\sigma(\omega)$, $\kappa(\omega)$ from the respective 0th and 2nd moments given by,

$$\tilde{\sigma}_n = \int_{-\infty}^{\infty}\omega^n\sigma(\omega)\,d\omega\,, \qquad \tilde{\kappa}_n = \int_{-\infty}^{\infty}\omega^n\kappa(\omega)\,d\omega\,. \tag{3.10}$$

One can easily express the spin, energy moments as thermodynamic average of the respective current and its derivatives; whereupon the first two frequency moments will be given $\tilde{\sigma}_n = \pi\beta\sigma_n$, $\tilde{\kappa}_n = \pi\beta^2\kappa_n$ where (cf. Ch. 1 Eqs. (1.15)-(1.18))

$$\sigma_0 = \frac{1}{L}\langle\jmath^s\jmath^s\rangle\,, \quad \sigma_2 = \frac{1}{L}\langle f^s f^s\rangle\,, \quad f^s = i[H,\jmath^s] \tag{3.11a}$$

$$\kappa_0 = \frac{1}{L}\langle\jmath^\epsilon\jmath^\epsilon\rangle\,, \quad \kappa_2 = \frac{1}{L}\langle f^\epsilon f^\epsilon\rangle\,, \quad f^\epsilon = i[H,\jmath^\epsilon]\,. \tag{3.11b}$$

The operators f^s, f^ϵ are the so-called force operators. Performing an analytical calculation at the infinite temperature limit, $T \to \infty$, we get for the two lowest spin, energy frequency moments

$$\sigma_0 = \frac{J^2}{8} \tag{3.12a}$$

$$\sigma_2 = \frac{J^2}{16}\left[J^2\Delta^2 + \frac{1}{L}4\mathcal{B}^2(1+\Delta'^2)\right] \tag{3.12b}$$

$$\kappa_0 = \frac{J^2}{32}\left[J^2(1+2\Delta^2) + \frac{1}{L}2\mathcal{B}^2(1+\Delta^2+\Delta'^2)\right] \tag{3.12c}$$

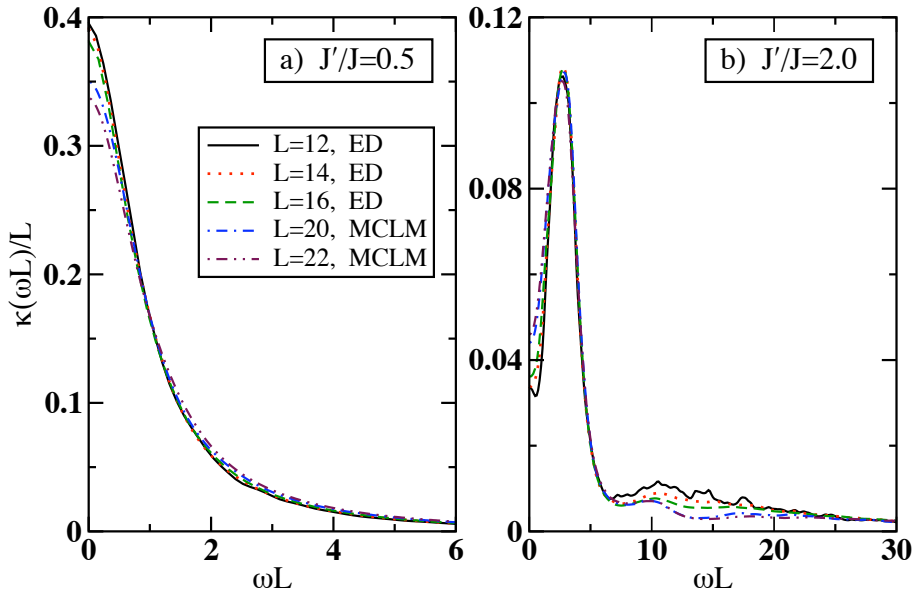

Figure 3.3: Frequency-dependent thermal conductivity in the high-T limit scaled as $\kappa(\omega L)/L$ for ($\Delta = 1$): (a) weak coupling $J' = 0.5J$, (b) strong coupling $J' = 2J$ (curves are normalized to unity).

$$\begin{aligned}\kappa_2 &= \frac{1}{L}\frac{J^4}{64}\mathcal{B}^2\Bigg[10 + 16\Delta^2 + 3\Delta'^2 + 10(\Delta\Delta')^2 - 12\Delta\Delta'\left(\frac{J'}{J}\right) \\ &+ \frac{1}{5}\left(-7 + 8\Delta^2 + 21\Delta'^2 - 3(\Delta\Delta')^2 - 4\Delta'^4\right)\left(\frac{J'}{J}\right)^2 \\ &+ \frac{3}{5}\left(16 + 16\Delta^2 + 12\Delta'^2 + 4(\Delta\Delta')^2 + 12\Delta'^4\right)\left(\frac{\mathcal{B}}{J}\right)^2\Bigg] \qquad (3.12d)\end{aligned}$$

where $\mathcal{B}^2 = (J'^2/3)S(S+1)$ is the characteristic impurity spin dependence.

As we have already mentioned there is no intrinsic scattering mechanism for the thermal transport in the pure Heisenberg model. Normal (incoherent) thermal transport is induced in the chain solely by defects and one could expect the 2nd moment to reflect the width of $\kappa(\omega)$ and thus to be related to the inverse scattering time $1/\tau$. We note that for this impurity problem an assumption of a Gaussian form $\kappa(\omega) = \kappa_{dc}\exp^{-(\omega\tau)^2}$ would imply from the L dependence of $\kappa_{0,2}$ that $\kappa_{dc} = \kappa(\omega \to 0)$ would scale as $\sqrt{L}$ and $1/\tau \sim 1/\sqrt{L}$. This is, however, incorrect as is also evident from the disagreement with higher moments, $n > 2$, which behave all as $\kappa_n \propto 1/L$. For weak-coupling cases, such as a single impurity weakly coupled to the host chain, we should therefore rather expect a Lorentzian-like frequency dependence with a static $\kappa(0) \propto L$ and a characteristic frequency width $1/\tau \propto 1/L$.

In Fig. 3.3 we show the frequency dependence of the thermal conductivity, normalized and appropriately scaled with system size. Note that in the high-T ($\beta \to 0$)

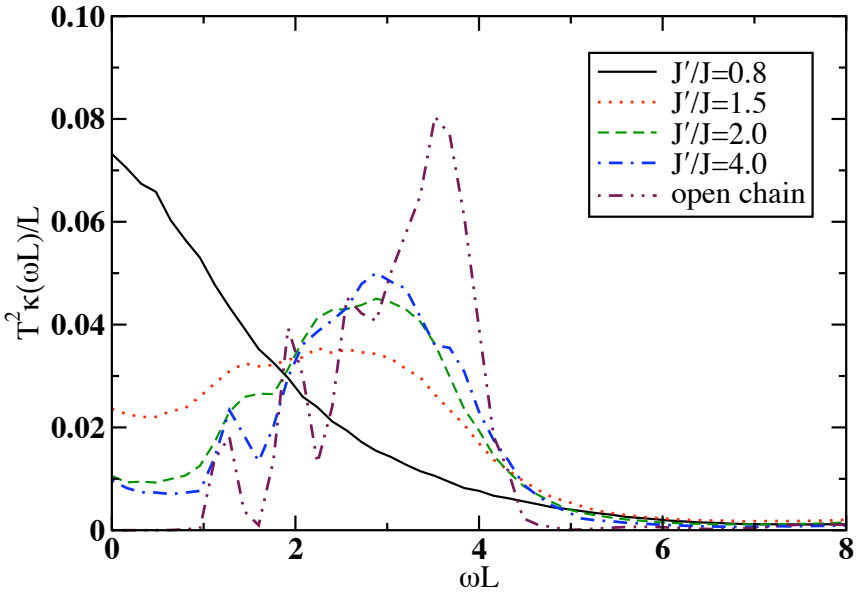

Figure 3.4: Frequency dependence of the thermal conductivity $T^2\kappa(\omega L)/L$ in the high temperature limit for various values of the coupling $J'/J = 0.8 - 4.0$ and $\Delta = 1.0$.

limit the relevant (but still nontrivial) quantity is $T^2\kappa(\omega)$ which is implicitly extracted by the normalization. We thus present results of the normalized $\kappa(\omega L)/L$ for a weak, $J' = 0.5J$ and strong, $J' = 2J$ coupling case respectively. The data up to $L = 16$ were obtained by (full) exact diagonalization (ED) while for $L = 18 - 22$ the Microcanonical Lanczos method (MCLM) was used [13] in the $S_z = 0$ subsector. The $\delta-$peaks at the excitation frequencies are binned in windows $\delta\omega = 0.01$, which also gives the frequency resolution of the spectra. An additional broadening $\eta \simeq 0.03$ is introduced using the Kramers-Kroning relations (A.23). For $J' = 0.5J$ we find a simple Lorentzian form while in the strong coupling case the behavior is nonmonotonic with a maximum at a finite frequency $O(1/L)$. In both cases the proposed L scaling is indeed realized.

Next we would like to show how the system flows from the weak coupling regime into the strong one, with increasing the perturbation parameter J'/J, and eventually how the behavior of the thermal conductivity resembles the behavior of the thermal conductivity of a chain with open boundary conditions. In Fig. 3.4 we present results for the thermal conductivity of a chain of $L = 16$ sites obtained using ED in the high temperature limit for various couplings J' and $S = 1/2$. In addition we show the thermal conductivity of a uniform chain with open boundary conditions. Fig. 3.4 illustrates the flow of the system from a Drude like behavior (weak coupling) to a chain with open boundary conditions (strong coupling), which was already proposed for a single non-magnetic impurity (a local field) from the level statistics analysis [8] (cf. Ch. 2). We choose to present the jagged results, i.e., without implementing any smoothing procedure, in order not to wash out the development of the narrow peaks corresponding

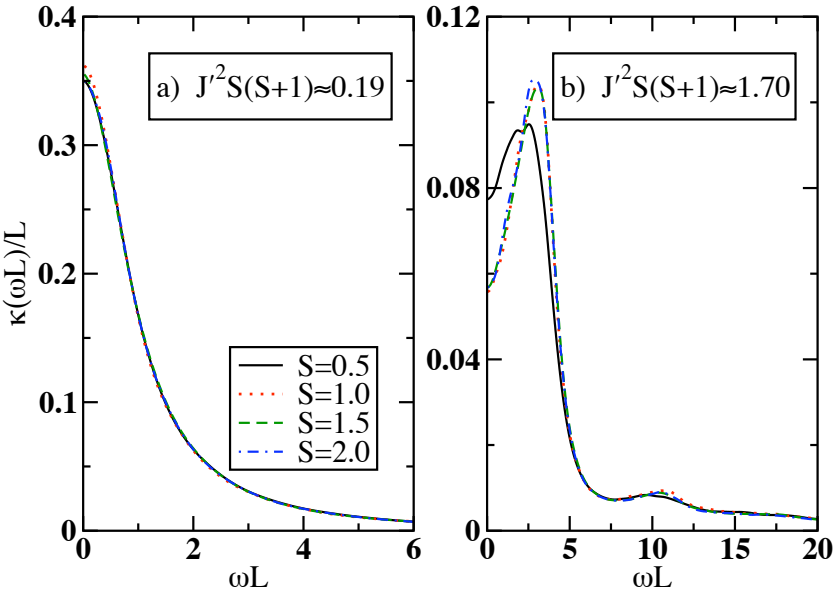

Figure 3.5: Frequency dependence of the normalized thermal conductivity $\kappa(\omega L)/L$ in the high-T limit for a variety of impurity spin values $S = 1/2, 1, 3/2, 2$ and for: (a) $J'/J = 0.5, 0.3, 0.22, 0.18$ corresponding to the weak coupling $\mathcal{B}^2 = (J'^2/3)S(S+1) \simeq 0.06$, (b) $J'/J = 1.5, 0.92, 0.67, 0.53$ corresponding to the stronger coupling $\mathcal{B}^2 \simeq 0.57$.

to the excitations of the open chain. For the strong coupling cases there is some rather significant structure at frequencies $\omega \sim J'$ which correspond to local excitations of the impurity. However, these excitations are irrelevant for the effect of the impurity on the chain which is studied here.

As for the scaling with impurity spin S suggested by the proportionality of the 2nd moment to $\mathcal{B}^2 = (J'^2/3)S(S+1)$ we show in Fig. 3.5 MCLM results for $\kappa(\omega L)/L$ for a series of S-values and couplings J' so that the effective perturbation strength $\mathcal{B}^2$ retains its value. The lattice size is $L = 19, 20$ depending on whether we have a half-integer or an integer spin-S magnetic impurity. For the strong coupling case the thermal conductivity exhibits a depletion at low frequencies characteristic of the strong coupling of the chain with the impurity and the effective cutting of the former. We find indeed that at both weak as well as strong coupling the scaling is well obeyed, giving a wider applicability to our results. They can be applied to a range of impurity spin values becoming directly relevant in the interpretation of experiments.

The spin conductivity on the other hand is more complicated due to the non-conservation of the spin current in the pure model—$[H_0, \jmath^s] \neq 0$ as long as $\Delta \neq 0$, see σ_2 (3.12b)—which is the dominant scattering mechanism at least for not so strong perturbations. Similarly to Fig. 3.5 we present in Fig. 3.6 the frequency dependence of the normalized spin conductivity obtained for different magnetic impurities in the strong coupling limit $\mathcal{B}^2 \simeq 0.57$. Not only is the $\mathcal{B}^2$ scaling obeyed by $\sigma(\omega)$ but in

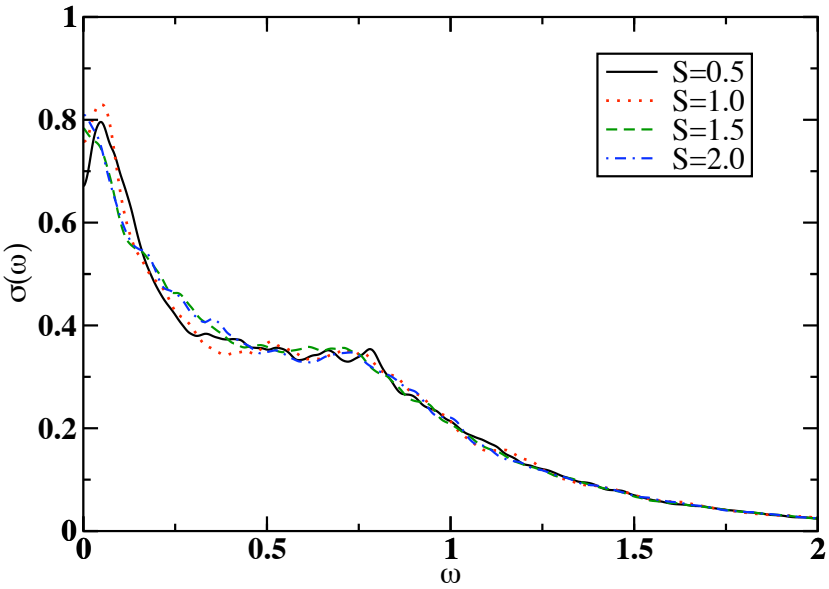

Figure 3.6: Frequency dependence of the normalized spin conductivity $\sigma(\omega)$ in the high-T limit for a variety of impurity spin values $S = 1/2, 1, 3/2, 2$ and for $J'/J = 1.5, 0.92, 0.67, 0.53$ corresponding to the stronger coupling $\mathcal{B}^2 \simeq 0.57$.

addition it changes only slightly within a wide range of values of the parameter $\mathcal{B}^2$ (not shown). Clearly even a strong perturbation scarcely affects the spin conductivity since it is only a $1/L$ effect, in contrast to the thermal conductivity whose behavior is entirely determined by the perturbation of the magnetic impurity due to the absence of any other scattering mechanisms.

In order to illustrate the effect of the magnetic impurity on the spin conductivity we present in Fig. 3.7 ED results for $T\sigma(\omega)$ (un-smoothed spectra) for an $S = 1/2$ impurity out of the chain and host-impurity couplings $J'/J = 0, 0.2, 1$ ($L = 14$, $\beta \to 0$). Although results for $J' = 0$ are not to be trusted at low frequencies, since $\Delta = 1$ is a long standing problem for the spin conductivity, we can see that the impurity does not affect at all the high frequency behavior. At low frequencies, whether a finite stiffness exists or not, the impurity washes out the singularities (like the δ-function at zero frequency or a sharp drop in the regular part) leading to a rather smooth low frequency regime.

3.3.2 Lattice size scaling

Now let us focus again only on the thermal conductivity and address the generic $L \to \infty$ behavior. We can discuss it by considering the memory function $N(\omega)$ representation defined via the general complex function $\bar{\kappa}(\omega)$,

$$\bar{\kappa}(\omega) \quad = \quad i\beta \frac{\chi_0}{\omega + N(\omega)}, \quad \chi_0 = \chi(\omega \to 0). \tag{3.13}$$

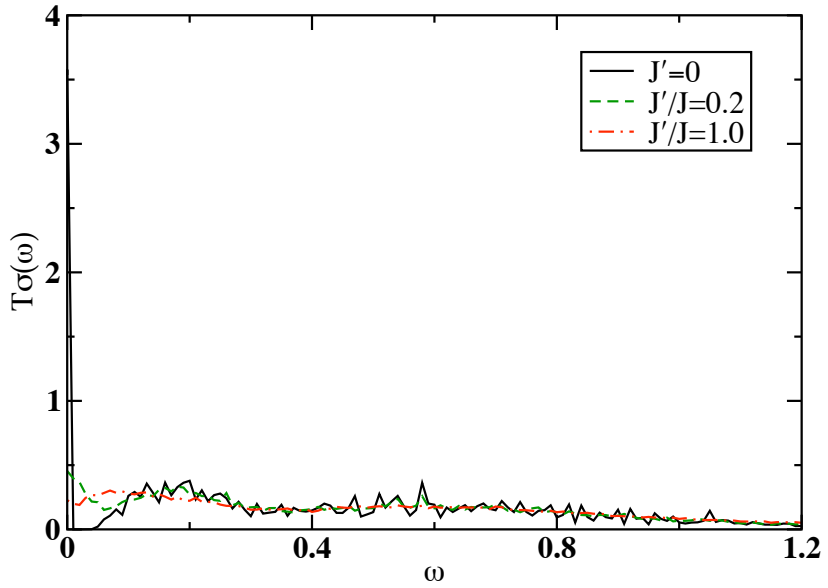

Figure 3.7: Frequency dependence of the spin conductivity $T\sigma(\omega)$ in the high-T limit for a spin $S = 1/2$ impurity and for $J'/J = 0, 0.2, 1$.

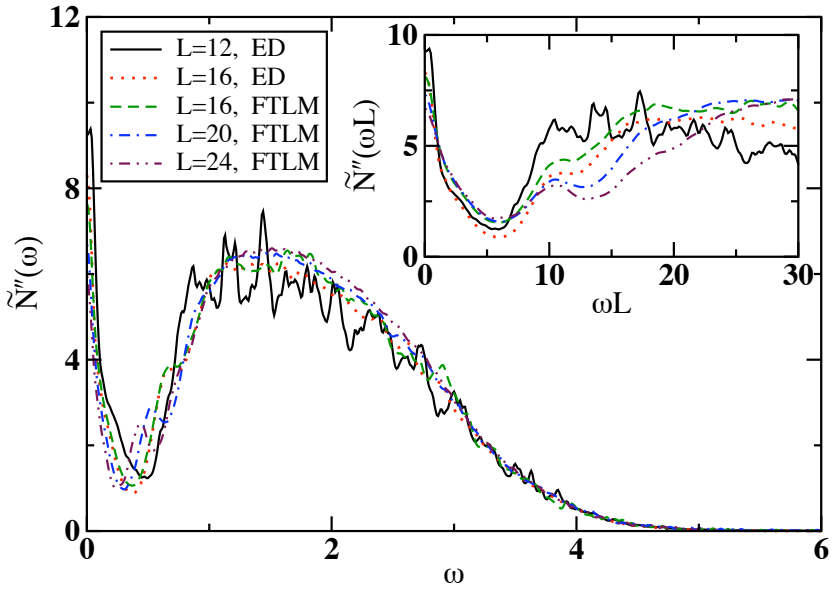

Figure 3.8: Memory function $\tilde{N}''(\omega)$ for a strong coupling $J' = 2J$ and for various lattice sizes $L = 12 - 24$, using both ED and FTLM. Inset: the scaled function $\tilde{N}''(\omega L)$ is shown at low frequencies.

where the real $\kappa(\omega) = \bar{\kappa}'(\omega)$ and $N''(\omega) \sim 1/\tau$ plays the role of the (frequency dependent) thermal-current relaxation rate. The lowest moments κ_n can be evaluated (in

principle) exactly in the high-T limit [14] on a finite size lattice of L sites. Involving only local quantities, at least for $0 < n < L/2$, they should behave as $\kappa_n = \tilde{\kappa}_n/L$ whereby $\tilde{\kappa}_n$ is size independent for $n < L/2$. It is plausible that also higher moments, $n > L/2$, behave as $\kappa_n \propto 1/L$. If $\tilde{\kappa}_n$ for $n > L/2$ would be also size independent, then this would imply the scaling $N(\omega) = \frac{1}{L}\tilde{N}(\omega)$, with a universal (size independent) $\tilde{N}(\omega)$. Consequently

$$\bar{\kappa}(\omega) = \frac{i\beta\chi_0 L}{(\omega L) + \tilde{N}(\omega)}, \tag{3.14}$$

with the real part $\kappa(\omega)$ for $L \to \infty$ and $\omega \to 0$ obeying the Lorentzian scaling relation,

$$\frac{\kappa(\omega L)}{L} = \frac{\beta\chi_0 \tilde{N}''(\omega \to 0)}{(\omega L)^2 + \tilde{N}''(\omega \to 0)^2}, \tag{3.15}$$

provided that $N''(\omega \to 0)$ is finite. This is, however, clearly not what we observe in Fig. 3.3, where from the non-Lorentzian shape we must conclude that the memory function also scales as $\tilde{N}(\omega L)$ and thus,

$$\frac{\kappa(\omega L)}{L} = \frac{\beta\chi_0 \tilde{N}''(\omega L)}{(\omega L + \tilde{N}'(\omega L))^2 + \tilde{N}''(\omega L)^2}. \tag{3.16}$$

This is not in contradiction with the moments argument, since the higher moments, $n > L/2$, determine the low frequency behavior. So we can argue that at high frequencies $\tilde{N}(\omega)$ scales as ω while at low frequencies as ωL. This scenario is indeed verified in Fig. 3.8 at the low/high frequency regimes, where $N(\omega)$ is extracted from the $\kappa(\omega)$ data. The Finite temperature Lanczos method (FTLM) [15] is used for lattice sizes $L \geq 16$ with $M_L = 500$ Lanczos steps and smoothed with an additional frequency broadening $\eta \simeq 0.03$. On the other hand, we can also explain the observed general $\kappa(\omega L)/L$ scaling with the similarity to a noninteracting system—with an impurity. In the latter case, the characteristic scaling $L\omega$ is signature of "free" oscillations in the system.

3.3.3 Perturbative memory function approach

In this section we would like to compare results for the spin, thermal conductivities obtained in the full system described by the Hamiltonian H (3.1) with the corresponding conductivities extracted from the spin M_0, energy N_0 memory functions which are evaluated using the eigenstates of the Hamiltonian H_0 (3.2) of the unperturbed system [16] (cf. Appx. A); the relevant formulas are

$$\tilde{M}_0(z) = \frac{1}{z\chi_0^s}(\chi_{f^s f^s}(z) - \chi_{f^s f^s}(0)), \qquad \left(\tilde{M}_0(z) = LM_0(z)\right) \tag{3.17a}$$

$$\tilde{N}_0(z) = \frac{1}{z\chi_0^\epsilon}(\chi_{f^\epsilon f^\epsilon}(z) - \chi_{f^\epsilon f^\epsilon}(0)), \qquad \left(\tilde{N}_0(z) = LN_0(z)\right) \tag{3.17b}$$

with the force operators being linear in the perturbative coupling J' and conductivities are extracted using

$$\bar{\sigma}(z) = i\frac{\chi_0^s}{z + M_0(z)}, \quad \bar{\kappa}(z) = \frac{i}{T}\frac{\chi_0^\epsilon}{z + N_0(z)}. \tag{3.18}$$

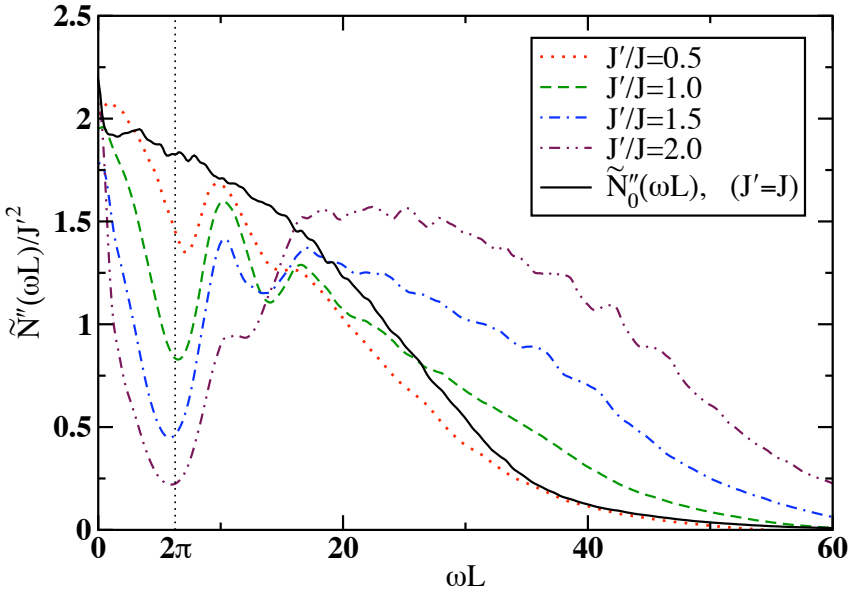

Figure 3.9: Impurity coupling J' dependence of scaled $\tilde{N}''(L\omega)/J'^2$ and the comparison with the perturbative result. Results are obtained for $\Delta = 1$ and $L = 16$ via ED.

To study the crossover from weak to strong coupling regime we show in Fig. 3.9 the evolution of the relaxation-rate function $\tilde{N}''(\omega L)$ with impurity coupling J' along with a perturbative evaluation $\tilde{N}''_0(\omega L)$. It is interesting that the memory function shows an increasingly pronounced structure with minima at approximately the same frequencies, multiples of $2\pi/L$ *independently of* J' and which are not present in the perturbative calculation. In particular the characteristic frequency of the minima decreases as the anisotropy parameter Δ decreases and thus it is apparently related to the velocity of elementary excitations (spinons) in the system. We can conjecture that this peak structure is due to a resonant mode, created by multiple forward/backward scattering on the impurity, characteristic of an noninteracting system. It is remarkable that this happens even in this high temperature limit. This effect has already been seen in integrable systems where a perturbation seems to affect the totality of the energy spectrum [14]. Now the picture is clear, $\tilde{N}''(\omega)$ increases as J'^2, scales as ωL at low frequencies and at the same time develops a structure that dominates the behavior of $\kappa(\omega L)$ turning the Lorentzian weak-coupling shape to a nontrivial one at strong coupling.

As long as the perturbation is not very strong, roughly speaking $J' \lesssim 0.8J$ for a spin-1/2 impurity, the perturbative approach is in good agreement with the exact results. We illustrate the validity of the memory function approach in Fig. 3.10 where the results were obtained using the ED technique for a system with $L = 16$, $J'/J = 0.5$, $\Delta = 1.0$, $\beta \to 0$. The thermal conductivity obtained with the exact numerical calculation (Eq.

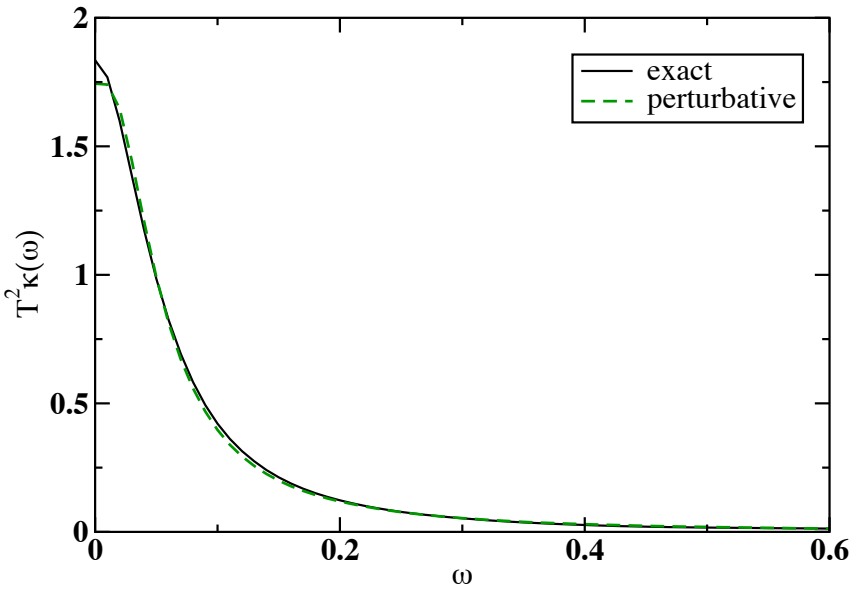

Figure 3.10: Frequency dependence of the thermal conductivity $T^2\kappa(\omega)$ calculated in the full system via Eq. (3.8) (black solid line or extracted from the perturbative memory function Eq. (3.18) (green dashed line) where $L = 16$, $J'/J = 0.5$, $\Delta = 1.0$, $\beta \to 0$.

(3.8)) is labeled as "exact" while the thermal conductivity which is extracted from the perturbative memory function (Eq. (3.18)) is labeled as "perturbative". The agreement between the two approaches is remarkably good. This can be also justified from Fig. 3.9 where for the lowest J' coupling the memory function is quite smooth despite some structure which does not affect $\kappa(\omega)$. The occurrence of this structure in the memory function as extracted from the thermal conductivity is not significant since the deviations are negligible with respect to its magnitude. Moreover for the real part of the memory function, we obtain a similar behavior as we did in Ch. 2 for the local field case, Fig. 2.6; hence a Drude-like behavior is established for weak perturbations.

On the other hand the behavior of the spin conductivity is completely different since the spin current relaxation is dominated by the bulk scattering and the anisotropy parameter Δ plays the major role in its behavior. Nevertheless, for $\Delta = 0$ the spin current commutes with the unperturbed Hamiltonian $H_0(\Delta = 0)$ and the memory function approach becomes applicable. An important attribute of the magnetic impurity, which is in sharp contrast to the non-magnetic impurity (e.g. the case of one local field), is that even for $\Delta = 0$ the spectrum of the system retains its many body features. Thus the level spacing is exponentially small $\sim e^{-L}$ and we obtain smooth curves for the finite system we study. Recall that for the XY model even in the presence of a single non-magnetic impurity ballistic transport is not destroyed, manifested in a finite Drude weight. From Fig. 3.11, where the spin conductivity ($\sigma(\omega)$) is shown, it can be inferred that a magnetic impurity renders ballistic transport incoherent even for $\Delta = 0$. For Fig. 3.11 we have used the ED technique for a system with $L = 16$, $J'/J = 0.5$, $\Delta = 0$

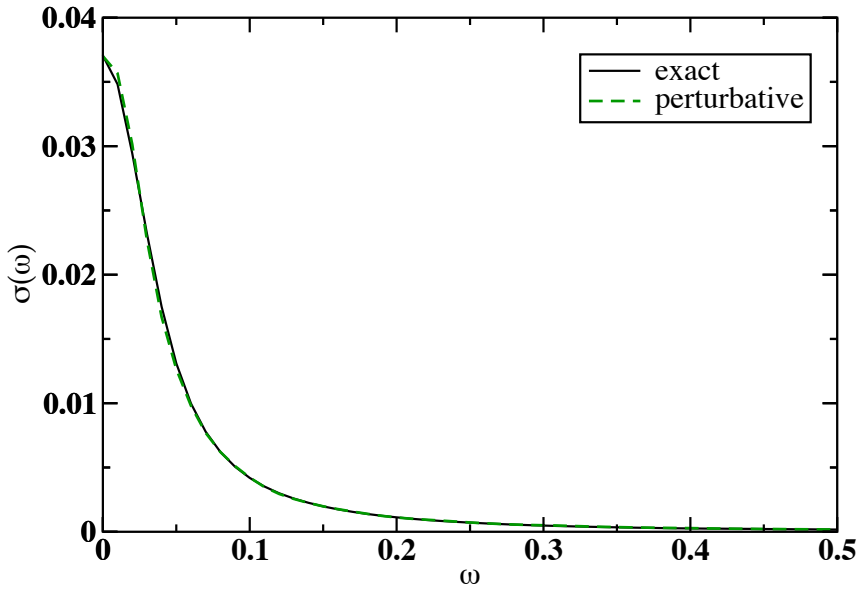

Figure 3.11: Frequency dependence of the spin conductivity $\sigma(\omega)$ calculated in the full system via Eq. (3.8) (black solid line) or extracted from the perturbative memory function Eq. (3.18) (green dashed line) where $L = 16$, $J'/J = 0.5$, $\Delta = 0$, $\beta \to 0$.

and $\beta \to 0$. Moreover we present the perturbative spin conductivity as extracted from the memory function M_0 which clearly is in very good agreement with the exact results. Let us mention here that while for the spin conductivity the agreement between exact and perturbative results deteriorates as $|\Delta|$ is increased, for the thermal conductivity case the agreement is contingent only on the perturbation strength and the anisotropy parameter does not affect its qualitative behavior.

3.3.4 Finite temperature

Now we can study the effect of lowering the temperature on the scattering by a magnetic impurity. According to Eggert and Affleck (EA) [2] it leads to cutting the chain at $T = 0$ irrespective of the sign of J'. This proposal was extended by Furusaki and Hikihara [6] to the anisotropic spin chain $-1 < \Delta \leq 1$ where they furthermore proposed that for $-1 < \Delta < 0$ (attractive case in the fermionic language) there is "healing" of the impurity.

In the Kondo problem the characteristic temperature in the weak coupling limit is given by $T_K \sim v \exp(-c/J')$ with c being a constant, v the velocity of spin excitations and J' the Kondo coupling. In the case of a spin-1/2 chain it was shown [17] that the exponential dependence is replaced by $T_K \sim \exp(-\pi\sqrt{1/J' - (S' + 1/2)^2})$ and a next-nearest neighbor coupling $J_2 \simeq 0.2412$ is needed to recover the traditional Kondo case. We should note that in the model studied the impurity spin is attached only at the end of the chain - in contrast to our model - but plausibly the behavior is

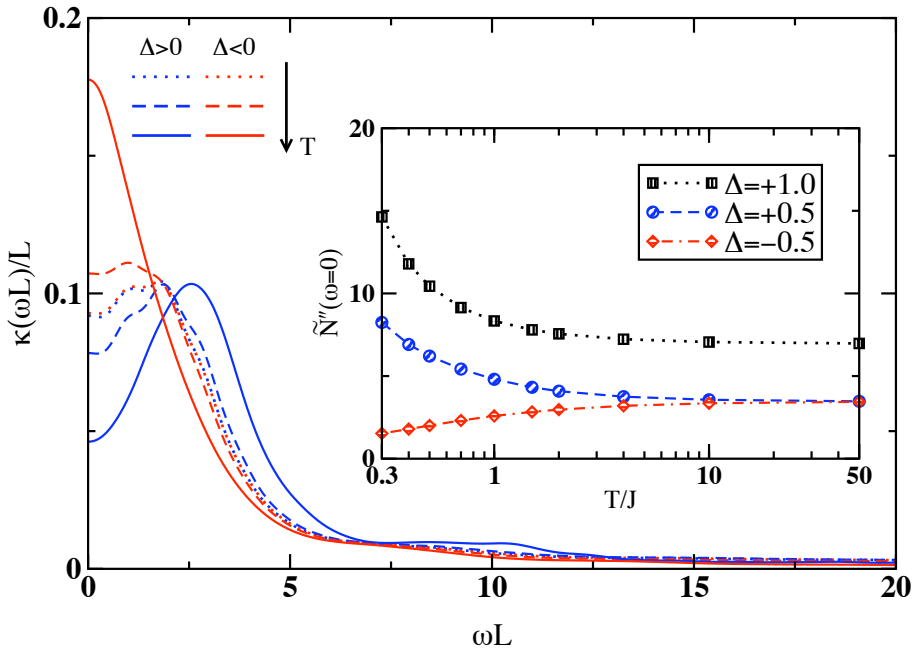

Figure 3.12: Frequency dependent normalized thermal conductivity $\kappa(\omega L)/L$ for strong coupling $J' = 2J$, $\Delta = \pm 0.5$ and three $T/J = 50, 2, 0.4$. Inset: T-dependence of $N''(0)$ for $\Delta = \pm 0.5$ and $\Delta = +1$.

qualitatively similar. To get a qualitative idea of orders of magnitude for our problem [5] for $J' = 0.3J$, $T_K \sim 0.014$, $\xi_K \sim 40$, for $J' = 0.6J$, $T_K \sim 0.388$, $\xi_K \sim 4$ and $J' = J$, $\xi_K = 0.65$. As in our study we are limited to $T \geq 0.4$ in order to see a "Kondo" crossover we must consider a coupling $J' \geq 0.5J$ and thus we are in the relatively strong coupling regime, with typical screening length of the order $\xi_K \sim 1$.

In Fig. 3.12 we show $\kappa(\omega L)/L$ for a chain of $L = 22$ sites at strong coupling $J' = 2J$ and two representative cases $\Delta = \pm 0.5$ as we lower the temperature. Indeed we find at low frequencies the gradual development of the corresponding "cutting/healing" behavior which we exemplify in the inset by $\tilde{N}''(0)$ as a function of temperature both for $\Delta = \pm 0.5$ and the most typical isotropic case $\Delta = +1.0$. It is remarkable that the tendency to increase-decrease the scattering time is already evident from high T, presumably due to the local character of the effect because of the strong J' coupling. We note in passing that the ωL scaling is found not just at high T but rather at all T (not shown).

Next in Fig. 3.13 we show $\tilde{N}''(0)$ as a function of T for a series of increasing J' couplings. The "cutting" effect for the repulsive case $\Delta = +0.5$ is present for all values of J' with no easily distinguishable "Kondo" temperature. We are always dealing with screening lengths well less than the system size where presumably no subtle many-body effects come into play. On the other hand, in the attractive case $\Delta = -0.5$, we do not observe "healing" for the weakest coupling $J' = +0.5$ where the screening length is

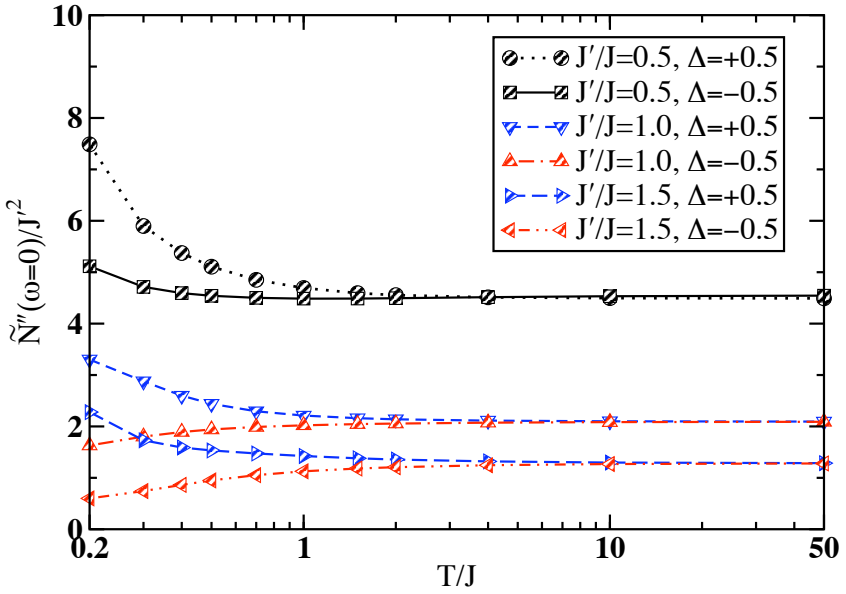

Figure 3.13: $\tilde{N}''(0)$ vs. T for the repulsive (attractive) case $\Delta = +0.5(-0.5)$ for different $J'/J = 0.5, 1.0, 1.5$.

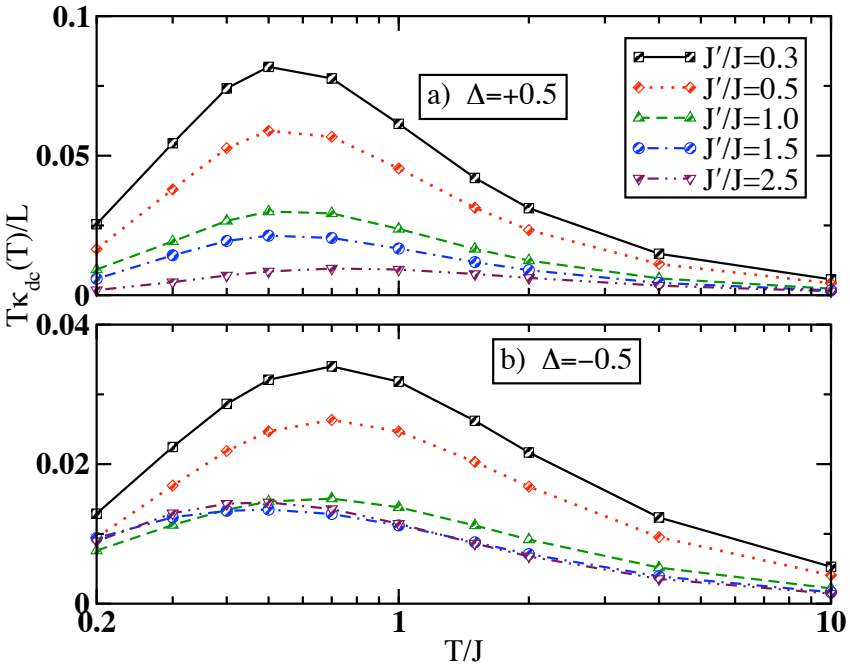

Figure 3.14: Temperature dependence of κ_{dc}/L for a variety of impurity couplings J' and for: (a) repulsive $\Delta = +0.5$, (b) attractive $\Delta = -0.5$.

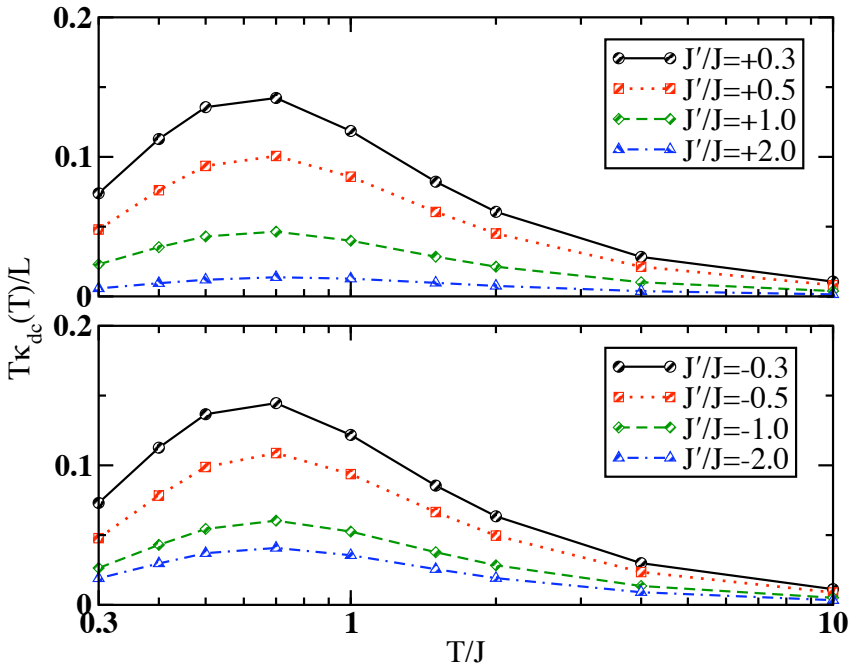

Figure 3.15: Temperature dependence of κ_{dc}/L for a variety of impurity couplings J', $\Delta = 1$ and for: anti-ferromagnetic couplings (top), ferromagnetic couplings (bottom).

expected to be several lattice sites.

Finally, in Fig. 3.14 we summarize the T-dependence of κ_{dc}/L for a variety of coupling strengths J'/J and $\Delta = \pm 0.5$. The experimentally most interesting case $\Delta = +1$ corresponding to isotropic antiferromagnetic as well as ferromagnetic impurity coupling is shown in Fig. 3.15. For $\Delta > 0$ we observe in Fig. 3.14a and Fig. 3.15 a continuous decrease of the κ_{dc} with increasing J'. This can be explained with the formation of a local singlet, at least for $T < J'$ which blocks the current through the impurity region. On the other hand, the $\Delta < 0$ case in Fig. 3.14b reveals a saturation of κ_{dc} with J', at least for intermediate large J'. However, for severe perturbations ($J' \gg J$) the impurity cannot be healed by the chain leading inevitably to a further decrease of the κ_{dc}.

3.4 Weak links - finite temperature

Next, we would like to proceed with the study of the Heisenberg spin-1/2 chain in the presence of two consecutive modified bonds. This model can be considered as a special case of the SIC model. For one thing, the substitution of an ion of the chain with another one of different species with spin $S = 1/2$ could lead to a spin-1/2 Heisenberg chain but with two altered bonds. Thus, the Hamiltonian and the current operators will be given by Eqs. (3.6) and (3.7) with $J'_{L-1} = \tilde{J} = J'_1$. In addition it is interesting

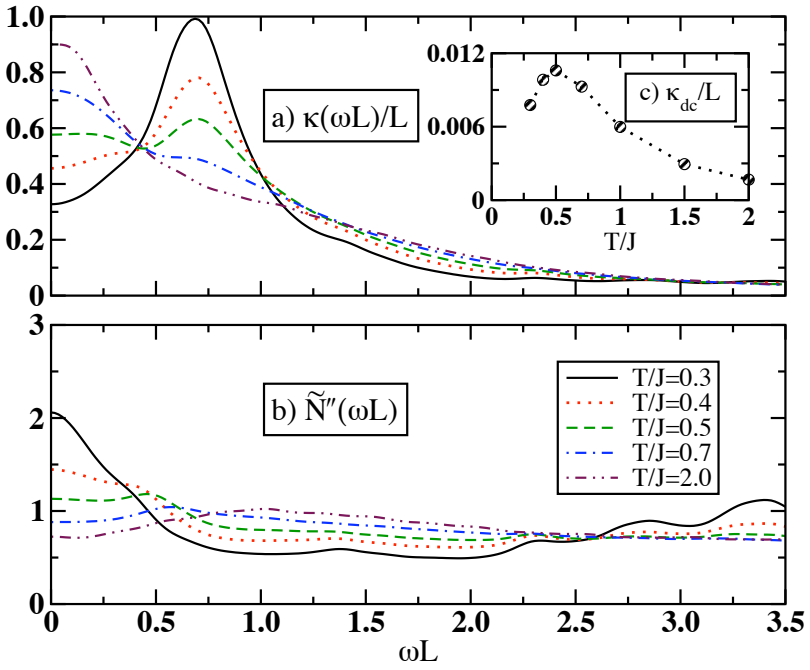

Figure 3.16: Frequency dependence of: (a) the normalized thermal conductivity $\kappa(\omega L)/L$, (b) the extracted memory function $\tilde{N}''(\omega L)$, for a chain of $L = 22$ sites with one weak link $\tilde{J} = 0.7J$ and various $T/J = 0.3 - 2.0$. (c) Temperature dependence of $\kappa_{dc}(T)/L$.

to compare the behavior of the the thermal conductivity as we lower the temperature for this model with the case where only one link is modified. In Ch. 2 it was shown that in the presence of a single modified link the chain is healed for a ferromagnetic ($\Delta < 0$) anisotropy while it is cut for antiferromagnetic ($\Delta > 0$). Particularly for the isotropic model, Kane-Fisher [1] for a Luttinger liquid and Eggert and Affleck [2] for the isotropic spin-1/2 Heisenberg chain, proposed that a weak link leads to an open chain (cutting) in the low energy limit. In contrast, a defect of two adjacent weak links is "healed" leading to a uniform chain at $T = 0$ [3]. To analyze this effect we consider the isotropic Heisenberg chain with only one weak link, i.e., the operators are given again by Eqs. (3.6) and (3.7) but this time $J'_{L-1} = J$ and $J'_1 = \tilde{J}$. In what follows we attempt to analyze the different influence of a single versus two adjacent modified links on the thermal conductivity of the spin-1/2 Heisenberg chain.

The characteristic Kane-Fisher temperature is given in the weak coupling limit by $T_{KF} \sim (J-\tilde{J})^2/J$. In Fig. 3.16a we show the corresponding $\kappa(\omega L)/L$ for $\tilde{J} = 0.7J$ and a series of temperatures. The data are obtained using the FTLM method for a chain of $L = 22$ spins, by $M_L = 2000$ Lanczos steps and smoothed by an additional frequency broadening $\eta \simeq 0.007$. From Fig. 3.16a we notice that $\kappa(\omega L)/L$ develops a strongly nonmonotonic frequency dependence by lowering the temperature, with a maximum

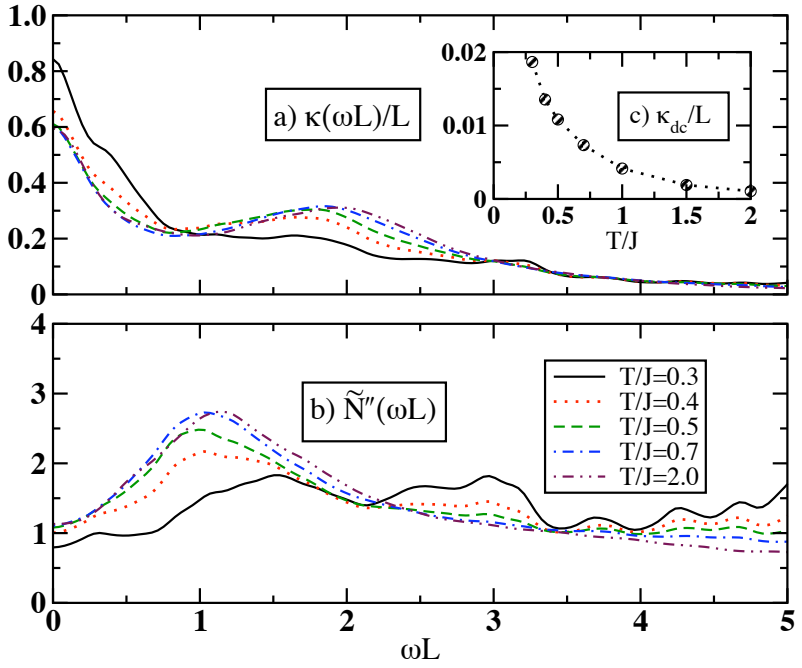

Figure 3.17: Frequency dependence of: (a) the normalized thermal conductivity $\kappa(\omega L)/L$, (b) the extracted memory function $\tilde{N}''(\omega L)$ for a chain of $L = 22$ sites with two adjacent weak links $\tilde{J} = 0.7J$ and various $T/J = 0.3 - 2.0$. (c) Temperature dependence of $\kappa_{dc}(T)/L$.

at a finite frequency that suggests a flow to the strong coupling limit similar to the one discussed before by increasing J'. In Fig. 3.16b, the extracted $\tilde{N}''(\omega L)$ for various T is presented, with the development of a characteristic structure that explains the nonmonotonic behavior of $\kappa(\omega)$. The increasing value of $\tilde{N}''(0) \sim 1/\tau$ with decreasing temperature indeed corresponds to the effect of "cutting" of the chain.

Nonmonotonic is also the frequency dependence of $\kappa(\omega L)/L$ for the case of two adjacent equal weaker links, $J'_{L-1} = J'_1 = \tilde{J} = 0.7J$, as shown in Fig. 3.17a. However, in this case we observe in Fig. 3.17b the opposite behavior of $\tilde{N}''(\omega)$. Namely "healing" of the double defect deduced by the decreasing $\tilde{N}''(0)$ as the temperature is lowered in agreement with theoretical prediction [2]. We should note that both cutting/healing are low frequency effects at frequencies ωL $O(1)$.

To summarize the observed behavior we show in Fig. 3.18, the T-dependence of the relaxation rate $\tilde{N}''(0)$ for two different couplings $\tilde{J}/J = 0.5, 0.7$, for one and two weak links, respectively. The presented results confirm the existence of the cutting behavior at low T for a single link, as well as the healing by lowering T for two adjacent and equal links. As expected, both effects appear only at low $T/J < 1$ while the dependence of the characteristic T_{KF} on $\tilde{J}/J$ is less pronounced.

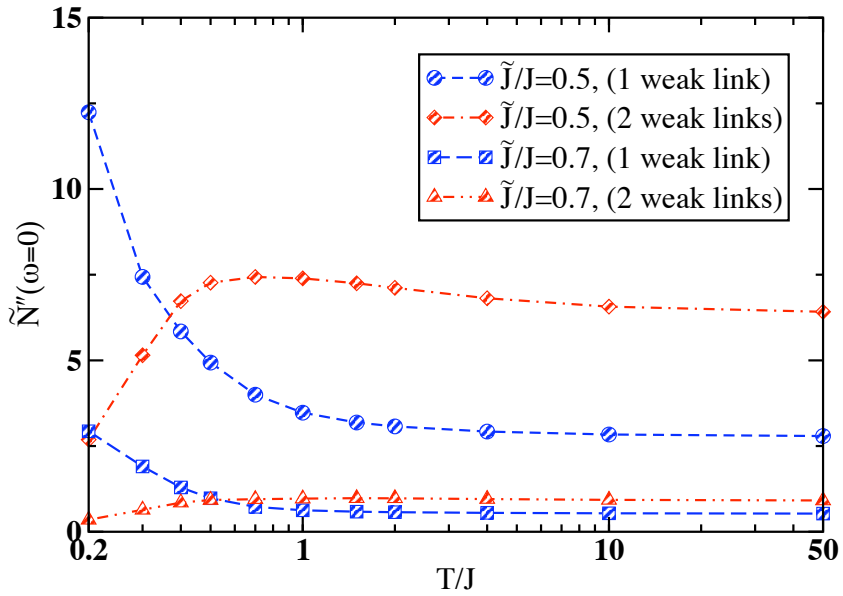

Figure 3.18: Temperature dependence of $\tilde{N}''(0)$ for $\tilde{J} = 0.5, 0.7J$ showing cutting/healing behavior for one and two weak links.

3.5 Spin-1 impurity in the chain

Let us now proceed with the generic spin-S magnetic impurity embedded in the spin-1/2 chain and particularly start with the spin-1 case, which is the most appealing doping—besides spin-1/2 impurities—for experiments. The Hamiltonian and the spin, energy current operators are given by (3.6), (3.7) with $S = 1$, $J'_{L-1} = J' = J'_1$ and we consider the case where $\Delta = \Delta'$.

In Fig. 3.19 we present results obtained via ED for a spin $S = 1$ impurity and for the isotropic ($\Delta = 1$) Heisenberg model. On the left part of Fig. 3.19 we present the frequency dependence of the thermal conductivity $T^2\kappa(\omega)$ where the impurity is coupled with the spin-1/2 chain with a host-impurity coupling $J' = 0.8J$, for which the dc thermal conductivity, $\kappa_{dc} = \kappa(\omega \to 0)$, exhibits its maximum value, see the inset of the left part of Fig. 3.19. In addition, in the same figure a Lorentzian fit is presented which signifies that the thermal conductivity exhibits a Lorentzian behavior. The thermal conductivity retains its Lorentzian behavior,

$$\kappa(\omega) = \frac{\kappa_{dc}}{1 + (\omega\tau^{\epsilon})} ,$$

roughly, in the interval of values of the host-impurity coupling, $0.6 \lesssim J'/J \lesssim 1.0$. Using the FTLM method we obtain the same Lorentzian behavior, with a constant scattering time, for temperatures as low as T_{fs}, where T_{fs} is the temperature for a finite system below which FTLM results become unreliable; we estimate this temperature to be approximately $T_{fs}/J \simeq 0.3$ for these systems. Although for a spin-1 impurity

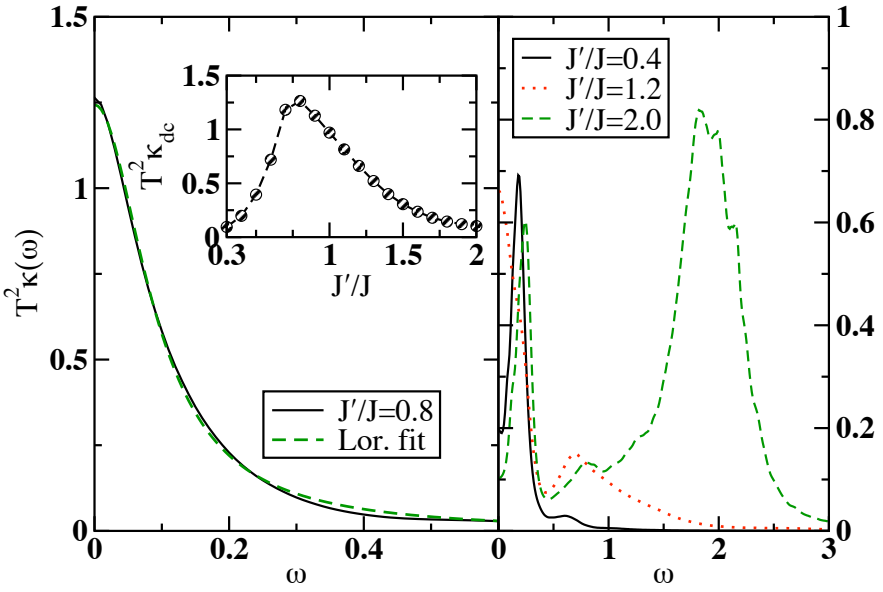

Figure 3.19: Frequency dependence of the thermal conductivity $T^2\kappa(\omega)$ of the isotropic ($\Delta = 1$) Heisenberg model in the presence of a spin-1 magnetic impurity at high temperatures, $\beta \to 0$. On the left part of the figure the thermal conductivity for a perturbative coupling $J'/J = 0.8$ is shown in addition with a Lorentzian fit. In the inset of the left part of the figure the dc value of the thermal conductivity is shown as a function of the ratio J'/J. On the right part of the figure the thermal conductivity for $J'/J = 0.4, 1.2, 2.0$ is shown.

and $J' = 1.2J$, Fig. 3.19 (right), the low frequency depletion—characteristic of the strong coupling regime—is not present, the Lorentzian behavior is destroyed by the conspicuous local excitations of the impurity.

For extreme values of the coupling J', either strong or weak, the thermal conductivity exhibits a strongly non-monotonic behavior, Fig. 3.19 (right). The non-monotonic behavior, as it is insinuated by the results for the spin out of chain (SOC) or the weak link (WL) models, is an indication that the system has flown to the strong coupling regime, while a Lorentzian form of $\kappa(\omega)$ is an indication of a weak perturbation. From Fig. 3.19 (right) it can be inferred that the system couples strongly with the impurity for extreme values of the host-impurity coupling. Whereupon, the low frequency behavior, corresponding to an open-like chain, is the same for a strong as well as for a weak J'—notice the difference, $|J' - J| = 0.6J$, from the uniform coupling in the weak coupling case. On the other hand, the high frequency behavior of the thermal conductivity for a weak and a strong J' is strikingly different due to the emergence of a conspicuous secondary structure, Fig. 3.19(b). The frequency of this structure shifts with J', indicating that its origin is local excitations of the impurity. Moreover, the larger the J' the more weight is accumulated in this structure, which becomes

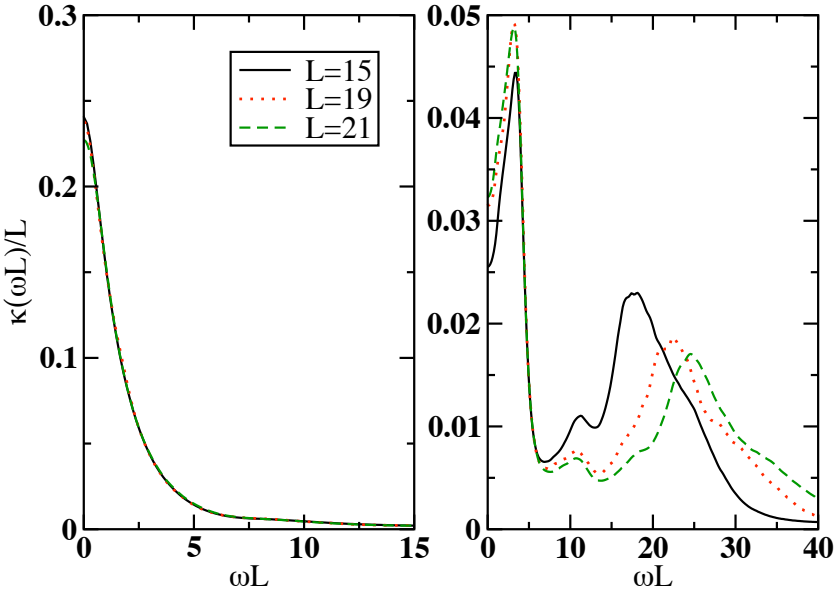

Figure 3.20: Frequency dependence of the normalized thermal conductivity scaled with the lattice size as $\kappa(\omega L)/L$ in the presence of a spin-1 impurity for $L = 15, 19, 21$ and for: a weak $J'/J = 0.8$ (left) and a strong $J'/J = 1.5$ (right) perturbation.

the prevalent contribution to the thermal conductivity for fairly strong couplings (Fig. 3.19(b) $J' = 2J$) despite being only a $1/L$ effect.

Taking all the above into account we could infer that a spin-1 impurity in the chain is a relatively weak perturbation for the thermal transport yielding a Drude-like behavior as long as the coupling of the impurity with the chain J' extends within a certain range of values.

3.5.1 Lattice size scaling

As far as the lattice size scaling of the thermal conductivity for the SIC model is concerned, we examine the scaling $\kappa(\omega L)/L$ similarly to the SOC model, sec. 3.3.1. For the latter, we have seen that the thermal conductivity exhibits a universal scaling with L and $\kappa(\omega L)/L$ is the size independent quantity. For the SIC model, a Lorentzian $\kappa(\omega)$, like the one on the left part of Fig. 3.20, obeys trivially a universal L scaling, since $\kappa_{dc}, \tau^{\epsilon} \sim L$, and the size independent quantity is again $\kappa(\omega L)/L$. On the other hand for strong J', the prominent impurity contribution at $\omega \sim J'$, which is $\mathcal{O}(1)$, does not scale with L, Fig. 3.20 (right).[3] Nonetheless, the low frequency, $\omega \sim 1/L$, bulk contribution to $\kappa(\omega)$ obeys the scaling $\kappa(\omega L)/L$ even in the strong perturbation

[3] Note that for the SOC model, one has to assume a very strong host-impurity coupling to yield a conspicuous secondary structure at high frequencies which will not obey the scaling with the lattice size L.

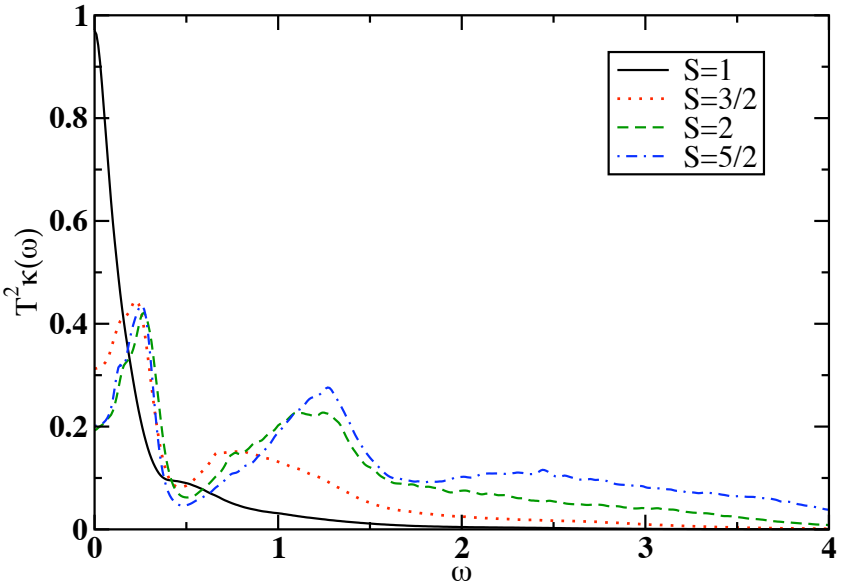

Figure 3.21: Frequency dependence of the thermal conductivity $T^2\kappa(\omega)$ for different magnetic impurities, $S = 1, 3/2, 2, 5/2$ and $J' = J$, $\Delta = 1$, at high temperatures, $\beta \to 0$.

regime. Moreover, Fig. 3.20 (right) signifies that the contribution of a single impurity dwindles with respect to the bulk contribution with increasing L, becoming negligible in the limit $L \to \infty$. However, in an experimental realization with a finite but dilute impurity concentration c_I, so that correlations among impurities can be neglected, one could plausibly assume that $\kappa(\omega)$ will obey the same scaling behaviors, in the weak and strong perturbation regimes, with the substitution $1/L \to c_I$.

3.6 Spin-S impurity in the chain

So far we have presented some basic properties of the spin-1/2 Heisenberg chain with an embedded spin-1/2 and spin-1 magnetic impurity. Let us now present how a generic spin-S magnetic impurity affects the transport properties of the spin-1/2 Heisenberg chain.

To start with, a spin-S magnetic impurity with $S > 1$ constitutes a strong perturbation for the Heisenberg chain. For any value of the host-impurity coupling J' the low frequency depletion is present yielding a non-Lorentzian behavior. Moreover, as we have seen from the spin-1 impurity, when the chain is strongly coupled to the impurity the thermal conductivity exhibits a conspicuous high frequency structure at frequencies $\omega \sim J'$. Similarly with the spin-1 impurity this structure is present for spin-S impurities with $S > 1$, and moreover the larger the impurity spin S the more prominent it becomes. In Fig. 3.21 we plot as an illustrative example the frequency dependence of

the thermal conductivity $T^2\kappa(\omega)$ for the isotropic Heisenberg model ($\Delta = 1$), $J' = J$, $S = 1, 3/2, 2, 5/2$, in the high temperature regime ($\beta \to 0$), using the ED technique. For the lowest impurity spin, $S = 1$, the thermal conductivity is roughly described by a Lorentzian despite the subtle presence of a secondary structure. As the impurity spin S is increased this structure gains more weight which becomes comparable with the weight at low frequencies which arises from the bulk contribution of the chain. Eventually, for stronger perturbations, whose strength is given by the parameter $\mathcal{B}^2 = \frac{J'^2}{3}S(S+1)$, the secondary structure will become the prevalent contribution to the thermal conductivity despite being a $1/L$ effect.

The fact that the contribution of a $1/L$ effect to thermal conductivity surpasses the bulk contribution may seem quite bizarre, however, we can comprehend the origin of this effect from the analytical expression of the sumrule of $\kappa(\omega)$, $\tilde{\kappa}_0 = \pi\beta^2\kappa_0$, where κ_0 is given by[4]

$$\kappa_0 = \left(1 - \frac{3}{L}\right)\frac{J^4}{32}(1+2\Delta^2) + \frac{4}{L}\left(2\frac{J^2}{32}(1+\Delta^2+\Delta'^2)\mathcal{B}^2 + \frac{J'^2}{32}(1+2\Delta'^2)\mathcal{B}^2\right), \quad (3.20)$$

as evaluated at the infinite temperature limit, $\beta \to 0$. The bulk contribution to κ_0, manifested by the J^4 term, is compensated by the impurity contribution, $\propto J'^2\mathcal{B}^2 \propto J'^4$, for a coupling $J' > J^*$, where J^* is given by

$$J^* = \sqrt[4]{\frac{3}{4}\frac{L-3}{S(S+1)}}. \quad (3.21)$$

Note that we took into account only the local energy current term

$$\tilde{j^\epsilon} = J'^2\mathbf{S}\cdot(\boldsymbol{\Delta}'\cdot\mathbf{s}_1 \times \boldsymbol{\Delta}'\cdot\mathbf{s}_{L-1}), \quad (3.22)$$

which is $\propto J'^2$. The evaluation of J^* implies that for finite systems like the ones studied here via ED J^* would be $J^* \simeq 1.45$ for $S = 1, L = 15$ and $J^* \simeq 1.05$ for $S = 2, L = 13$. Hence, for a spin $S = 2$ impurity and a coupling $J' \simeq J$ the dominant contribution to the thermal conductivity for a finite system of $L = 13$ sites will come from terms which involve transitions between states $\sim J'$. Thus, as the host-impurity coupling J' is increased, the excitations at $\omega \sim J'$ will separate from the bulk contribution located at $\omega \sim 1/L$, while the corresponding weight accumulated at $\omega \sim J'$ will surpass the bulk contribution creating resonant modes at frequencies $\omega \sim J'$.

On the other hand the spin conductivity seems to be less sensitive than the thermal conductivity to the presence of the magnetic impurity, especially for $\Delta \geq 1$. A significant change in the spin conductivity becomes perceptible only for strong couplings or high impurity spin S due to the high frequency contribution of the impurity. In Fig.

[4]The sumrule of the spin conductivity $\tilde{\sigma}_0$ is given by

$$\tilde{\sigma}_0 = \pi\beta\left(\frac{J^2}{8}\left(1 - \frac{2}{L}\right) + \frac{\mathcal{B}^2}{L}\right) \quad (3.19)$$

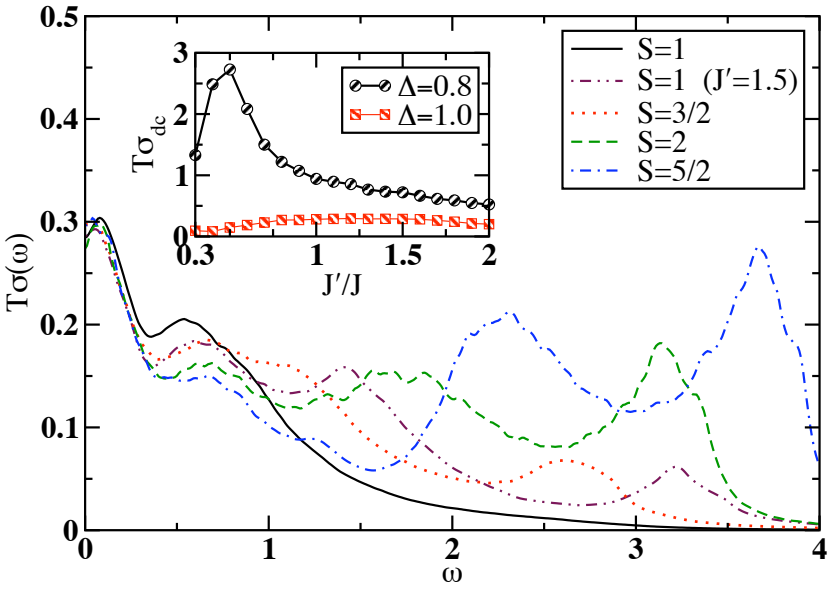

Figure 3.22: Frequency dependence of the spin conductivity $T\sigma(\omega)$ for different magnetic impurities, $S = 1, 3/2, 2, 5/2$ and $J' = J$, as well with the case $S = 1, J' = 1.5$ for $\Delta = 1$ at high temperatures, $\beta \to 0$ via ED. Inset: The dc spin conductivity $T\sigma_{dc}$ for $S = 1$ is shown as a function of the perturbation coupling J'.

3.22 we present ED results for the frequency dependent spin conductivity obtained at the high temperature limit ($\beta \to 0$), at the isotropic point ($\Delta = 1$), for $J' = J$ and various impurities, $S = 1 - 5/2$. In addition, for $S = 1$ the $J' = 1.5J$ case is shown. Moreover, in the inset we present the dc value of the spin conductivity, $\sigma_{dc} = \sigma(\omega \to 0)$, for an $S = 1$ impurity as a function of the ratio J'/J for $\Delta = 0.8, 1$.

Despite the conspicuous high frequency contribution of the impurity to the spin conductivity the low frequency $\sigma(\omega \to 0)$ remains virtually unaffected for $\Delta = 1$ for a wide range of couplings J' and/or impurity spin S, Fig. 3.22. In the gapless regime, Fig. 3.22 ($\Delta = 0.8$) the behavior of the dc spin conductivity resembles qualitatively the behavior of κ_{dc}, Fig. 3.19, as a function of the ratio J'/J. However, the maximum of σ_{dc} is obtained for a quite weak host-impurity coupling, $J' = J/2$. Another difference between spin and thermal conductivities is that for the range of values of the J' coupling, shown in the inset of Fig. 3.22, the former changes less than three times from its minimum to its maximum value while the latter changes more than ten times.

For $S = 1$, $\Delta = 0.8$ and $J' = J/2$ where the spin conductivity exhibits its maximum dc value, we show in Fig. 3.23 the frequency dependence of the spin conductivity. In addition, we present for the same J' the spin conductivity of different magnetic impurities including the $S = 1/2$ case. The results are obtained via ED in the high temperature regime. It is interesting that the $S = 1$ case exhibits the highest σ_{dc}, even higher than the $S = 1/2$ case.

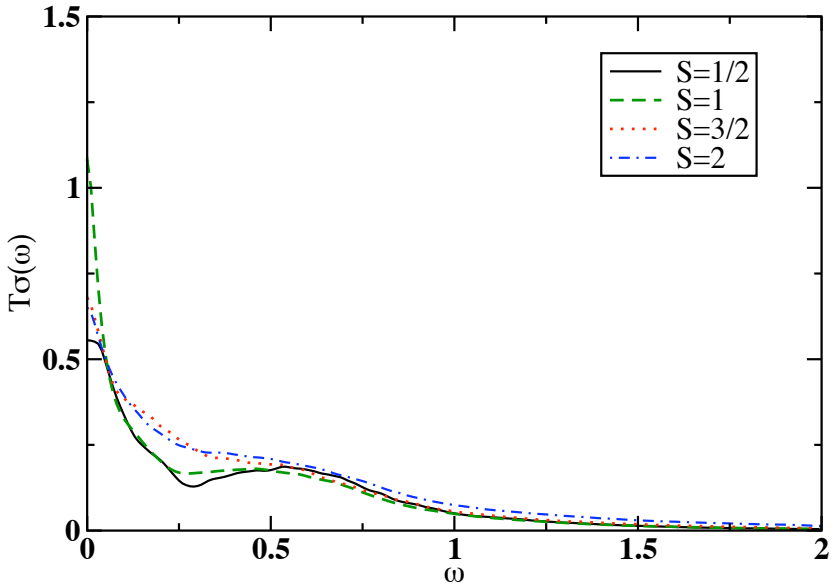

Figure 3.23: Frequency dependence of the spin conductivity $T\sigma(\omega)$ for different magnetic impurities, $S = 1/2, 1, 3/2, 2$ and $J' = 0.5J$ for $\Delta = 0.8$ at high temperatures, $\beta \to 0$, obtained via ED

3.6.1 Strong coupling limit

The high frequency structure that emerges, in both the spin and the thermal conductivity, due to a strong perturbation $\sim \mathcal{B}^2$, $\sim J'^2\mathcal{B}^2$, respectively, can be well understood by taking the limit $J' \to \infty$. Starting from Eq. (3.6) for the isotropic point ($\Delta = 1$) and taking $J = 0$ we arrive at the local Hamiltonian describing the system consisting of the impurity and its two nearest neighbors

$$\mathcal{H} = J'(\mathbf{s}_{L-1} + \mathbf{s}_1) \cdot \mathbf{S} \,. \tag{3.23}$$

Since the Heisenberg Hamiltonian conserves the total S_z component we can diagonalize (3.23) analytically separating it into different S_z subsectors. In the maximum total S_z subsector for the three spin system, $S_z = S + 1$, there is only one state, $|\uparrow S \uparrow\rangle$, where the first and the second arrows denote the z-component of the $\mathbf{s}_{L-1}, \mathbf{s}_1$ spin-1/2 operators respectively while between these two arrows the z-component of the impurity is denoted by S.

The second highest $S_z = S$ subsector is a 3-dimensional subspace consisting of the states $|S, 1\rangle = |\uparrow S - 1 \uparrow\rangle$, $|S, 2\rangle = |\uparrow S \downarrow\rangle$, $|S, 3\rangle = |\downarrow S \uparrow\rangle$. The eigenvalues of the Hamiltonian (3.23) within the $S_z = S$ subsector are

$$\epsilon_0 = 0 \,, \quad \epsilon_\pm = \frac{J'}{2}(S - 1 \pm (S + 1)) \,, \tag{3.24}$$

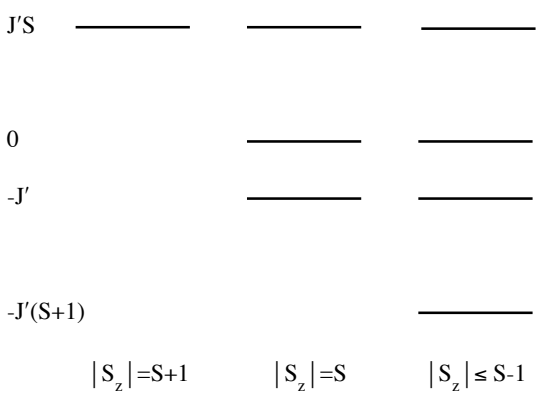

Figure 3.24: The energy spectrum of the 3-spin system at the isotropic point.

while the eigenstates have the form

$$|S,\epsilon_0\rangle = \frac{1}{\sqrt{2}}\left(|S,2\rangle - |S,3\rangle\right) \ , \quad |S,\epsilon_\pm\rangle = c_1'|S,1\rangle + c_2'\left(|S,2\rangle + |S,3\rangle\right) \tag{3.25}$$

with $c_{1,2}'$ being functions of the impurity spin S.

Let us focus on the thermal transport and particularly on the matrix elements of the local energy current operator $\tilde{j^\epsilon}$ (3.22). The form of the eigenstates imposes that there are no energy current matrix elements of the operator $\tilde{j^\epsilon}$ between the $|S,\epsilon_\pm\rangle$ states. Particularly for the isotropic ($\Delta = 1$) local Hamiltonian 3.23 there in not a transition between $|S,\epsilon_-\rangle$ and $|S,\epsilon_0\rangle$ hence, the only non-vanishing transition is between the states $|S,\epsilon_0\rangle$, $|S,\epsilon_+\rangle$ which is a transition of an energy difference $\delta\epsilon = \pm J'$. Apparently the same conclusions hold for the corresponding $S_z = -(S+1), -S$ subsectors.

The rest $2\tilde{S}+1$ S_z subsectors, with $\tilde{S} = S-1$, are 4-dimensional spaces consisting of the states $|S_z,1\rangle = |\uparrow\ S_z - 1\ \uparrow\rangle$, $|S_z,2\rangle = |\uparrow\ S_z\ \downarrow\rangle$, $|S_z,3\rangle = |\downarrow\ S_z\ \uparrow\rangle$, $|S_z,4\rangle = |\downarrow\ S_z + 1\ \downarrow\rangle$, leading to the following eigenvalues

$$\epsilon_{2=} - J', \quad \epsilon_3 = 0, \quad \epsilon_{1,4} = -\frac{J'}{2}\left(1 \pm (2S+1)\right) \tag{3.26}$$

where the + sign corresponds to the lowest ϵ_1 eigenstate and the − sign to ϵ_4. The ground state of the 3-spin system is $\epsilon_g = \epsilon_1$; the energy spectrum for the isotropic point is shown in Fig. 3.24.

The Hamiltonian of the 4-dimensional subspaces imposes that the eigenstates will be

$$|S_z,\epsilon_n\rangle = \begin{cases} \dfrac{1}{\sqrt{2}}\left(|S_z,2\rangle - |S_z,3\rangle\right) & \text{for} \quad \epsilon_n = 0\ , \\ c_1|S_z,1\rangle + c_2\left(|S_z,2\rangle + |S_z,3\rangle\right) + c_4|S_z,4\rangle & \text{for} \quad \epsilon_n \neq 0\ , \end{cases} \tag{3.27}$$

with $c_{1,2,4}$ being functions of S, S_z.

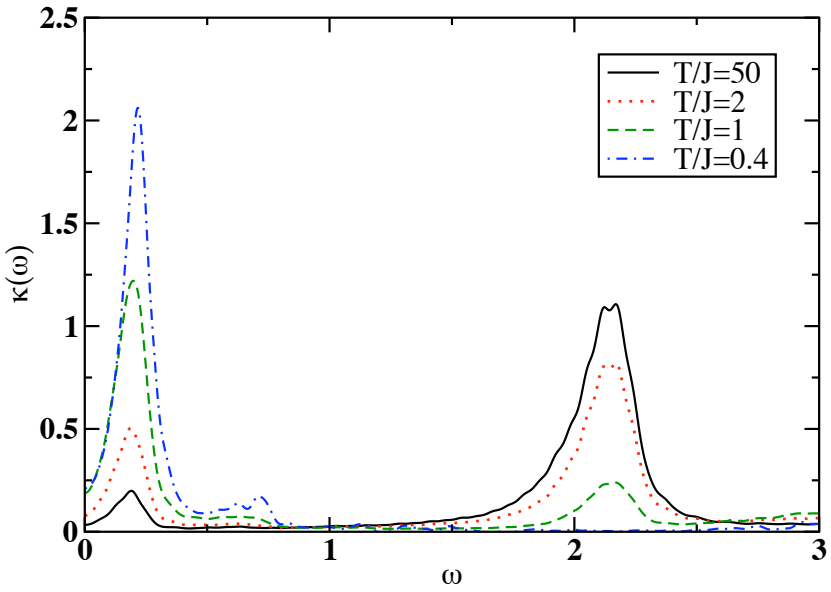

Figure 3.25: Frequency dependence of the normalized thermal conductivity $\kappa(\omega)$ obtained via the FTLM for a strong perturbation $S = 2, J' = 2J$, for $\Delta = 1$ and various temperatures, $T/J = 50, 2, 1, 0.4$.

Likewise the 3-dimensional subspaces, the matrix elements of $\tilde{j}^{\epsilon}$ are zero except $\langle S_z, \epsilon_2|\tilde{j}^{\epsilon}|S_z, \epsilon_3\rangle$ which is again a transition of energy $\delta\epsilon = \pm J'$. Note that for the anisotropic Heisenberg Hamiltonian ($\Delta \neq 1$) the matrix elements of the energy current operator $\tilde{j}^{\epsilon}$ vanish only for transitions between states which correspond to non-zero eigenvalues, similarly to the $S_z = \pm S$ subspaces. Thus the property that there will be non-zero energy current matrix elements only between states that correspond to transitions of energy $\delta\epsilon = \pm J'$ is a unique property of the *isotropic* Heisenberg model.

The previous conclusions are depicted in Fig. 3.25 were the frequency dependence of the normalized thermal conductivity $\kappa(\omega)$ is shown for various temperatures. The results were obtained using the FTLM method for a strong perturbation $S = 2, J' = 2J$, a system of $L = 19$ sites and $\Delta = 1$. At high temperatures there is a significant weight centered at $\omega = J'/J$ as it is expected from the analysis of the 3-spin model. Moreover, the position of this resonant mode at $\omega = J'/J$ is independent of the spin of the impurity, as indicated by the previous analysis for the strong J' coupling, Figs. 3.19 ($S = 1$), 3.25 ($S = 2$). As the temperature is decreased and the system flows to the ground state the peak at $\omega = J'/J$ vanishes gradually. This is expected since the transitions that yield the peak at $\omega = J'/J$ are between elevated eigenstates which will not be occupied as the temperature is decreased. For $\Delta \neq 1$ where there are fewer forbidden transitions there will be more than one high frequency peaks; see for example Fig. 3.27. For the spin current there are more allowed transitions than for the energy current, Fig. 3.22; particularly there are transitions involving the ground state, thus, at

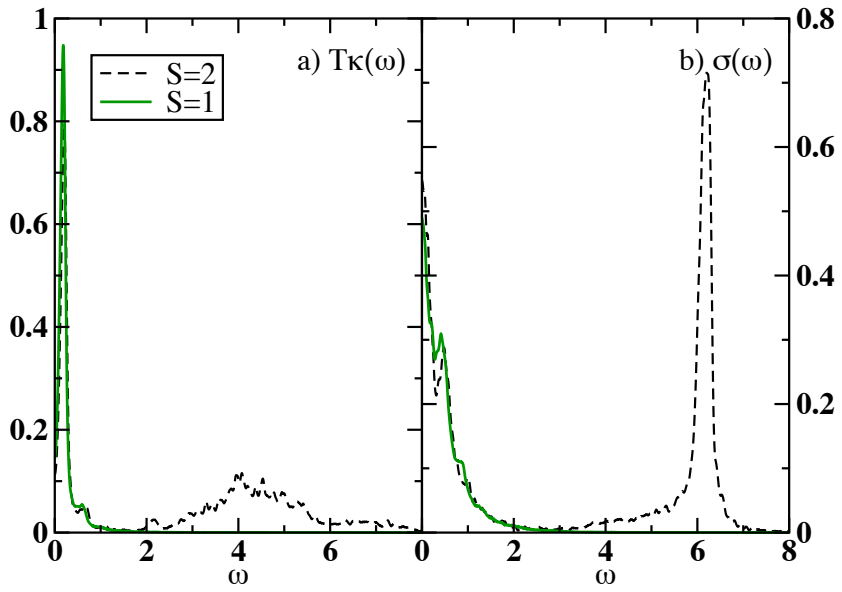

Figure 3.26: Comparison of the frequency dependent thermal conductivity $T\kappa(\omega)$ (left) and the spin conductivity $\sigma(\omega)$ (right) at a low temperature $T/J = 0.7$ for $S = 1, J'/J = -0.25$ and $S = 2, J'/J = 2$ ($L = 19$, $\Delta = 1$).

low temperatures there will be resonant modes at the corresponding frequencies, Fig. 3.26. Let us remark here that Fig. 3.25 may lead to the erroneous conclusion that the high frequency weight is shifted at lower frequencies, but this is an artifact only due to the unit integral of the curves.

At low energies the properties of the system will be described by the ground state which is $(2\tilde{S}+1)$-fold degenerate implying that the degrees of freedom of the 3-spin system, at low energies, will be described by a pseudo spin $\tilde{S} = S - 1$ coupled with the chain with an effective coupling $\tilde{J}$ [2]. Thus, at low energies one can assume that the system will be described by states of the form $|S_z, \epsilon_g\rangle \otimes |\text{chain}\rangle$ where $|S_z, \epsilon_g\rangle$ is given by (3.27), while $|\text{chain}\rangle$ represents the state of the rest $L-3$ spins. One can evaluate the effective coupling $\tilde{J}$ of the pseudo spin $\tilde{S}$ with the chain by considering the matrix element $\langle S'_z, \epsilon_g| \otimes \langle \text{chain}'|J\mathbf{s}_1 \cdot \mathbf{s}_2|S_z, \epsilon_g\rangle \otimes |\text{chain}\rangle$ [18] to obtain

$$\tilde{J}_z = \frac{c_1(S_z)^2 - c_4(S_z)^2}{2S_z}\,, \tag{3.28a}$$

$$\tilde{J}_+ = \frac{c_2(S_z)c_1(S_z+1) + c_2(S_z+1)c_4(S_z)}{\sqrt{S(S-1) - S_z(S_z+1)}}\,, \tag{3.28b}$$

$$\tilde{J}_- = \frac{c_2(S_z-1)c_1(S_z) + c_2(S_z)c_4(S_z-1)}{\sqrt{S(S-1) - S_z(S_z-1)}}\,, \tag{3.28c}$$

with $\tilde{J}_z = \tilde{J} = \tilde{J}_\pm$ wherever they are defined and the coefficients $c_{1,2,4}$ are given by

$$c_1(S_z) = \frac{1}{N(S_z)} \frac{2a_-}{\epsilon_g - b_-} , \quad c_2(S_z) = \frac{1}{N(S_z)} , \quad c_4(S_z) = \frac{1}{N(S_z)} \frac{2a_+}{\epsilon_g - b_+} , \tag{3.29}$$

where,

$$N(S_z) = \sqrt{2 + \left(\frac{2a_-}{\epsilon_g - b_-} \right)^2 + \left(\frac{2a_+}{\epsilon_g - b_+} \right)^2} \tag{3.30}$$

and

$$a_\pm = \sqrt{S(S+1) - S_z(S_z \pm 1)} , \qquad b_\pm = -2(1 \pm S_z) . \tag{3.31}$$

For a spin-2 magnetic impurity coupled with the Heisenberg chain we obtain a *ferromagnetic* effective coupling $\tilde{J} = -0.25J$ for $\Delta = 1$. Note that the higher the spin of the impurity the smaller the effective coupling with the rest of the chain. In Fig. 3.26 the comparison of the thermal conductivity $T\kappa(\omega)$ (left) and spin conductivity $\sigma(\omega)$ (right) for a spin-2 magnetic impurity strongly coupled with the chain ($J' = 2J$) and an impurity $S = 1$ coupled with a ferromagnetic coupling $J' = -0.25J$ at a low temperature $T/J = 0.7$ are shown; the lattice size is $L = 19$ and $\Delta = 1$. We have also tested stronger couplings $J'/J = 3, 4$ and we obtain the same results, implying that $J' = 2J$ is already a very strong perturbation. We observe that while the low frequency part for the transport quantities shown in Fig. 3.26 is in good agreement for the two impurities, the high frequency part is striking different. This can be understood easily since a strong host-impurity coupling yields a conspicuous high frequency structure $\omega \sim J'$, at least for a finite system, which cannot be reproduced by the weak effective coupling $|\tilde{J}| \ll |J'|$ that we obtain.[5] Thus, the picture of the effective spin fails to describe the transport quantities in the whole frequency range, at least for a single impurity in a finite system or a finite concentration of impurities in the thermodynamic limit.

Finally we have seen for the SOC model, the single weak link and the local field that the chain is healed for $\Delta < 0$ while it is cut for $\Delta > 0$ [1, 6, 19]. Thus, we investigate whether or not the cutting-healing behavior occurs as well for a spin-S magnetic impurity embedded in the chain. In Figs. 3.27 for the thermal conductivity, and 3.28 for the spin conductivity we present FTLM results, where the normalized corresponding quantity is plotted for $\Delta = \pm 0.5$ and three temperatures $T/J = 50, 2, 0.4$. Both figures signify that the cutting-healing occurs for an $S = 1$ impurity while we observe this behavior for higher $S > 1$ as well (not shown). For the spin conductivity case—where the spin current is not conserved in the pure AHM—the accumulated weight at $\omega = 0$ for the lowest temperature $T/J = 0.4$ is reminiscent of the δ-function located at zero frequency for the pure model.

[5] The high frequency structure of the thermal conductivity in Fig. 3.26 comes from the $\sim JJ'$ terms of the energy current (3.7) and not from the $\tilde{j}^\epsilon$ that we discussed before.

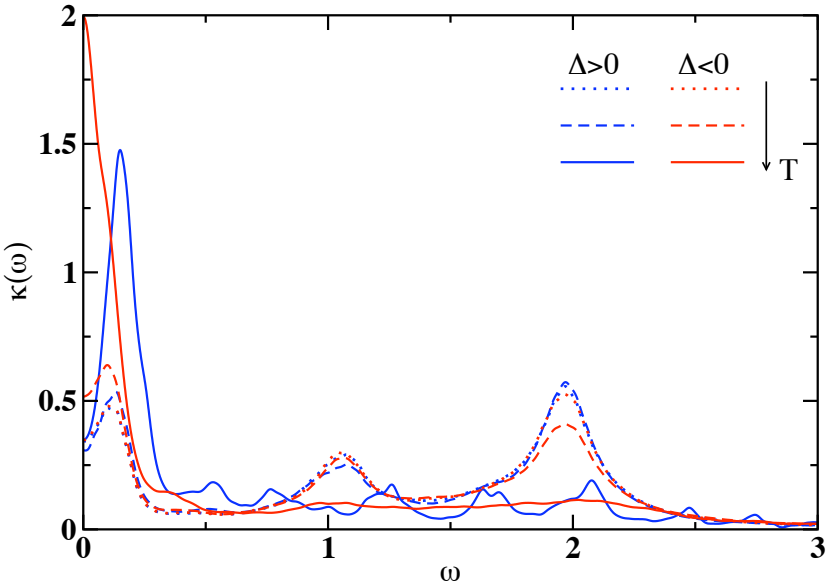

Figure 3.27: Frequency dependence of the normalized thermal conductivity $\kappa(\omega)$ for three temperatures $T/J = 50, 2, 0.4$, a magnetic impurity $S = 1$ and $L = 19$, $J'/J = 2.0$ and two values of the anisotropy $\Delta = \pm 0.5$.

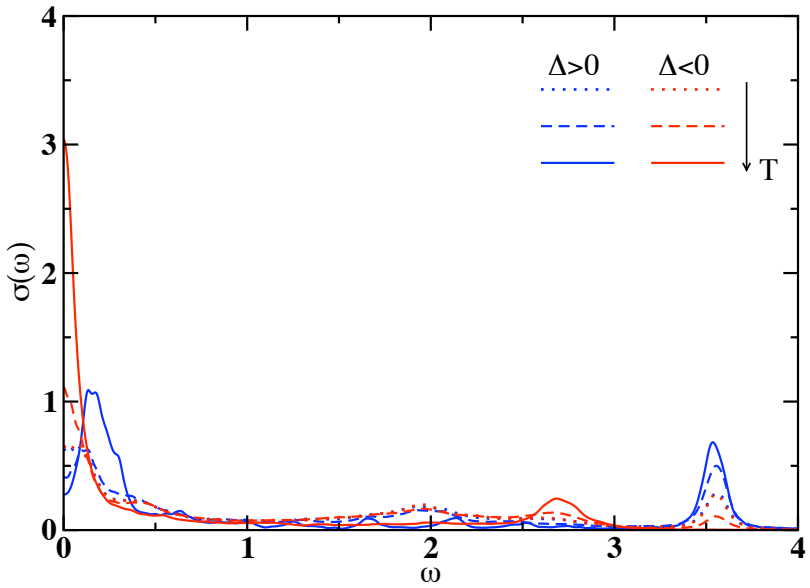

Figure 3.28: Frequency dependence of the normalized spin conductivity $\kappa(\omega)$ for three temperatures $T/J = 50, 2, 0.4$, a magnetic impurity $S = 1$ and $L = 19$, $J'/J = 2.0$ and two values of the anisotropy $\Delta = \pm 0.5$

3.7 Conclusions

In conclusion, by analyzing the unique behavior of the thermal conductivity (mostly) and the spin conductivity as well of the spin-1/2 Heisenberg model several effects of the local static and dynamical impurities have been established:

- A single local impurity, either static as the local field [8] and weak link, or dynamical as a magnetic impurity coupled to the chain turn the dissipationless thermal conductivity into an incoherent one. Numerical results for the dynamical conductivities, best studied at high-T, reveal that a single impurity in a system of L sites shows a universal scaling form $\kappa(\omega L)/L$ at least in the low-ω regime. For weak perturbation, as weakly coupled spins outside the chain or $S = 1$ impurity embedded in the chain for a certain range of host-impurity couplings J', the scaling form is of the simple Lorentzian type. On the contrary large local perturbation can lead to a nontrivial form with the maximum response at $\omega > 0$. Any magnetic impurity embedded in the chain with $S > 1$ is a strong perturbation for the thermal conductivity.

- In contrast to the thermal conductivity, the spin conductivity, which has intrinsic spin current relaxation mechanisms, is less sensitive to the $1/L$ effect of the impurity, especially its low frequency part.

- Furthermore, universal oscillations in the dynamical relaxation rate $N''(\omega)$—studied for the magnetic impurity out of the chain—become visible, from the weak coupling regime already, with the period $\omega \propto 1/L$ being a remnant of the impurity multiple-scattering phenomena in a noninteracting system.

- For the magnetic impurity embedded in the chain the contribution of the impurity to the transport properties dominates quite easily over the bulk contribution. Since the bulk contribution occurs at frequencies $\omega \sim 1/L$ while the impurity contribution is at $\omega \sim J'/J$ the two contributions are well separated for strong J'. The combination of these two properties yields resonant modes, at least at high temperatures and a finite system. Using the strong coupling limit $J' \gg J$ and analyzing the properties of the 3-spin system (3.23), it was shown that the resonant modes diminish with decreasing temperature if they do not involve transitions with the ground state of this local model.

- Our results confirm the existence of Kondo-type effects of impurities on lowering the temperature. In the case of weak links and for the isotropic Heisenberg model cutting and healing effects are observed at lower T for a single weak link and a pair of identical weaker links, respectively, in accordance with theoretical predictions [1, 3]. In the case of a spin coupled to the chain the cutting/healing effects at low T depend on the sign of the anisotropy Δ. For ferromagnetic anisotropy ($\Delta < 0$), the chain screens the impurity and the system enters the weak coupling regime as the temperature is decreased. The opposite behavior is

obtained for antiferromagnetic anisotropy ($\Delta > 0$), where the system flows to the strong coupling limit at lower temperatures.

- The picture of the formation of an effective spin $\tilde{S} = S - 1$ for a strong J' was shown to fail to describe the whole frequency range of the transport properties, at least for a finite system, Fig. 3.26—although it may be sufficient for their static limit or for thermodynamic quantities.
- Obtained data can be used to model the behavior observed in experiments on materials with spin chains doped with magnetic and nonmagnetic impurities [9].

Bibliography

[1] C. L. Kane and M. P. A. Fisher, Transport in a one-channel Luttinger liquid, Physical Review Letters **68**(8), 1220–1223 (Feb 1992).

[2] S. Eggert and I. Affleck, Magnetic impurities in half-integer-spin Heisenberg antiferromagnetic chains, Physical Review B **46**(17), 10866–10883 (Nov 1992).

[3] S. Rommer and S. Eggert, Spin- and charge-density oscillations in spin chains and quantum wires, Physical Review B **62**(7), 4370–4382 (Aug 2000).

[4] E. S. Srensen, M.-S. Chang, N. Laflorencie, and I. Affleck, Impurity entanglement entropy and the Kondo screening cloud, Journal of Statistical Mechanics: Theory and Experiment **2007**(01), L01001 (2007).

[5] N. Laflorencie, E. S. Srensen, and I. Affleck, The Kondo effect in spin chains, Journal of Statistical Mechanics: Theory and Experiment **2008**(02), P02007 (2008).

[6] A. Furusaki and T. Hikihara, Kondo effect in XXZ spin chains, Physical Review B **58**(9), 5529–5538 (Sep 1998).

[7] X. Zotos, F. Naef, and P. Prelovsek, Transport and conservation laws, Physical Review B **55**(17), 11029–11032 (May 1997).

[8] O. S. Barišić, P. Prelovšek, A. Metavitsiadis, and X. Zotos, Incoherent transport induced by a single static impurity in a Heisenberg chain, Physical Review B **80**(12), 125118 (Sep 2009).

[9] C. Hess, Heat conduction in low-dimensional quantum magnets, The European Physical Journal - Special Topics **151**, 73–83.

[10] N. Hlubek, P. Ribeiro, R. Saint-Martin, A. Revcolevschi, G. Roth, G. Behr, B. Büchner, and C. Hess, Ballistic heat transport of quantum spin excitations as seen in $SrCuO_2$, Physical Review B **81**(2), 020405 (Jan 2010).

[11] A. V. Mahajan and N. Venkataramani, Magnetic properties of Ni-doped Sr_2CuO_3, Physical Review B **64**(9), 092410 (Aug 2001).

[12] X. Zotos, High Temperature Thermal Conductivity of Two-Leg Spin-1/2 Ladders, Physical Review Letters **92**(6), 067202 (Feb 2004).

[13] M. W. Long, P. Prelovšek, S. El Shawish, J. Karadamoglou, and X. Zotos, Finite-temperature dynamical correlations using the microcanonical ensemble and the Lanczos algorithm, Physical Review B **68**(23), 235106 (Dec 2003).

[14] P. Prelovšek, S. E. Shawish, X. Zotos, and M. Long, Anomalous scaling of conductivity in integrable fermion systems, Physical Review B **70**(20), 205129 (Nov 2004).

[15] J. Jaklič and P. Prelovšek, Finite-temperature properties of doped antiferromagnets, Advances in Physics **49**, 1–92 (2000).

[16] W. Götze and P. Wölfle, Homogeneous Dynamical Conductivity of Simple Metals, Physical Review B **6**(4), 1226–1238 (Aug 1972).

[17] H. Frahm and A. A. Zvyagin, The open spin chain with impurity: an exact solution, Journal of Physics: Condensed Matter **9**(45), 9939 (1997).

[18] W. Zhang, J. Igarashi, and P. Fulde, Magnetic impurity coupled to a Heisenberg chain: Density-matrix renormalization-group study, Physical Review B **56**(2), 654–660 (Jul 1997).

[19] A. Metavitsiadis, X. Zotos, O. S. Barišić, and P. Prelovšek, Thermal transport in a spin- $\frac{1}{2}$ Heisenberg chain coupled to a magnetic or nonmagnetic impurity, Physical Review B **81**(20), 205101 (May 2010).

Appendix A

Linear response theory

The aim of this appendix is to function as a reference guide for many relations that are used throughout this manuscript and moreover to present them in a more detailed way.

A.1 Spin and thermal conductivities

To start with, we consider the definition of the susceptibility in the linear response theory framework. Let us assume that a time dependent perturbation $V(t)$ is switched on at some initial time $t_0 = 0$ and disturbs our system which initially was described by the Hamiltonian H. Given that the perturbation is the product of an operator $\hat{O}_q$ times a function $y(t)$, which carries the time dependence, i.e.,

$$V(t) = -\hat{O}_q y(t) \,, \tag{A.1}$$

the frequency dependent complex susceptibility of an observable $\hat{O}_p$ due to this perturbation will be [1]

$$\chi_{\hat{O}_p\hat{O}_q}(z) = \frac{i}{\hbar}\int_0^{+\infty} dt\, e^{izt}\, \langle[\hat{O}_p(t), \hat{O}_q(0)]\rangle \,, \quad z = \omega + i\eta \,, \tag{A.2}$$

which is a holomorphic function in the upper complex plane and decays as $\sim 1/z$ at high frequencies, $|z| \gg 1$. Let us explain the notation used above. The square brackets denote the commutator of the two enclosed operators and the angle brackets the thermodynamic average, which for an operator $\hat{O}$ is given by

$$\langle\hat{O}\rangle = \frac{Tr\, \hat{O}\, e^{-\beta H}}{Tr\, e^{-\beta H}} \,, \qquad \text{with} \qquad \beta = \frac{1}{k_B T} \,. \tag{A.3}$$

$\hbar$, k_B are the Planck, Boltzmann constants respectively, T is the temperature and Tr stands for the trace of the respective operator. The Heisenberg picture is used for the time evolution of the operators, where the time evolution of an operator $\hat{O}$ is obtained by the unitary transformation

$$\hat{O}(t) = U^\dagger(t)\hat{O}\, U(t) \,, \quad \text{with} \quad U(t) = \exp(-iHt/\hbar) \,. \tag{A.4}$$

Complex conductivities, spin and thermal,[1] are defined using the corresponding current-current susceptibility for the spin $\jmath^s$ and the energy $\jmath^\epsilon$ current respectively (cf. Refs. [3–5]) via the relations

$$\sigma(z) = \frac{i}{zL}(\chi_0^s - \chi_{\jmath^s\jmath^s}(z)) \,, \quad \kappa(z) = \frac{i}{zTL}(\chi_0^\epsilon - \chi_{\jmath^\epsilon\jmath^\epsilon}(z)) \,. \tag{A.5}$$

L is the lattice size and χ_0^s, χ_0^ϵ coincide with the static limit of the respective susceptibility for dissipative cases (see below). Using the eigenvalues ϵ_n and the eigenstates $|n\rangle$ of the Hamiltonian H,

$$H|n\rangle = \epsilon_n|n\rangle \,, \tag{A.6}$$

to express the thermodynamic average, Eq. (A.3), it is straightforward to show that the spin conductivity will be given by (real parts of complex quantities are denoted with a single prime and imaginary parts with a double prime)

$$\sigma'(\omega) = 2\pi D_s\delta(\omega) + \sigma'_{\rm reg}(\omega) \,, \qquad D_s = \frac{1}{2}\lim_{\omega\to 0}\omega\sigma''(\omega) \,, \tag{A.7a}$$

$$\sigma'_{\rm reg}(\omega) = \frac{\pi}{L}\mathcal{P}\left(\frac{1-e^{-\beta\hbar\omega}}{\omega}\right)\sum_{n,m} p_n|\langle n|\jmath^s|m\rangle|^2\delta(\epsilon_m-\epsilon_n-\hbar\omega) \,, \tag{A.7b}$$

$$\sigma''(\omega) = \frac{1}{L}\mathcal{P}\left(\frac{1}{\omega}\right)\left(\chi_0^s - \mathcal{P}\sum_{n,m}|\langle n|\jmath^s|m\rangle|^2\frac{p_n-p_m}{\epsilon_m-\epsilon_n-\hbar\omega}\right) \,. \tag{A.7c}$$

$\delta(\omega)$ is the Dirac δ-function and $\mathcal{P}$ denotes the principal value which have emerged from the identity

$$\lim_{\eta\to 0}\frac{1}{x\pm i\eta} = \mathcal{P}\left(\frac{1}{x}\right) \mp i\pi\delta(x) \,, \tag{A.8}$$

while p_n are the corresponding Boltzmann weights

$$p_n = \exp(-\beta\epsilon_n)/Z \,, \qquad Z = \sum_n \exp(-\beta\epsilon_n) \,. \tag{A.9}$$

Similarly we will have for the thermal conductivity

$$\kappa'(\omega) = 2\pi D_h\delta(\omega) + \kappa'_{\rm reg}(\omega) \,, \qquad D_h = \frac{1}{2}\lim_{\omega\to 0}\omega\kappa''(\omega) \,, \tag{A.10a}$$

$$\kappa'_{\rm reg}(\omega) = \frac{\pi}{TL}\mathcal{P}\left(\frac{1-e^{-\beta\hbar\omega}}{\omega}\right)\sum_{n,m} p_n|\langle n|\jmath^\epsilon|m\rangle|^2\delta(\epsilon_m-\epsilon_n-\hbar\omega) \,, \tag{A.10b}$$

$$\kappa''(\omega) = \frac{1}{LT}\mathcal{P}\left(\frac{1}{\omega}\right)\left(\chi_0^\epsilon - \mathcal{P}\sum_{n,m}|\langle n|\jmath^\epsilon|m\rangle|^2\frac{p_n-p_m}{\epsilon_m-\epsilon_n-\hbar\omega}\right) \,. \tag{A.10c}$$

[1] The thermal conductivity is a more peculiar case since a temperature gradient, which is what causes the energy current flow, is a thermodynamic quantity while linear response theory is based on the fact that a mechanical force disturbs the system. However, the difficulty was overcome by Luttinger who introduced the coupling with a pseudo gravitational field [2] enabling the use of linear response theory for the thermal conductivity as well.

Let us elaborate on the formulas above. The spin $D_s(T)$ and thermal $D_h(T)$ stiffness express whether coherent transport exists in the system or not and particularly for which transport modes, spin and/or thermal. In other words the system is an ideal conductor with respect to the corresponding transport modes if the respective stiffness is finite. Spin and energy stiffnesses could both be finite or vanish, or one of them remains finite while the other one vanishes. On the other hand the dc conductivity, the dissipative part of the real part of the conductivity, is obtained by the $\omega \to 0$ limit of the regular component of real part of the respective conductivity

$$\sigma_{dc}(T) = \lim_{\omega\to 0} \sigma_{\rm reg}(\omega)\,, \qquad \kappa_{dc}(T) = \lim_{\omega\to 0} \kappa_{\rm reg}(\omega)\,. \tag{A.11}$$

Furthermore, we can observe from Eqs. (A.7), (A.10) that

$$\chi_0^s - \chi_{\jmath^s\jmath^s}(\omega\to 0) \geq 0\,, \qquad \chi_0^\epsilon - \chi_{\jmath^\epsilon\jmath^\epsilon}(\omega\to 0) \geq 0\,, \tag{A.12}$$

since the imaginary part of the conductivity is an odd function and the real part an even and positive function of the frequency ω. The equality holds for dissipative cases where coherent transport vanishes. One can obtain the value of χ_0^s, χ_0^ϵ from the imaginary part of the respective conductivity by taking the limit $z \to \infty$ where the susceptibility decays as $\sim 1/z$. Thus, neglecting second order terms we have

$$\sigma''(\omega) \simeq \frac{\chi_0^s}{\omega L}\,, \qquad T\kappa''(\omega) \simeq \frac{\chi_0^\epsilon}{\omega L}\,, \qquad |\omega| \to \infty\,. \tag{A.13}$$

A.2 Non-interacting case

In the case of a non-interacting fermionic system Eqs. (A.7b), (A.7c) and (A.10b), (A.10c) could be properly modified. Let as assume that the particle and the energy currents are given from the generic single particle operators

$$\jmath = \sum_{p,q} \jmath_{pq} c_p^\dagger c_q\,, \qquad \jmath^\epsilon = \sum_{p,q} \jmath^\epsilon_{pq} c_p^\dagger c_q \tag{A.14}$$

where $\jmath_{pq}, \jmath^\epsilon_{pq}$ are the corresponding matrix elements and $c_p^\dagger(c_p)$ creates(annihilates) a particle at the single particle eigenstate with energy ϵ_p,

$$H|p\rangle = \epsilon_p|p\rangle\,. \tag{A.15}$$

For instance, for the tight binding model—cf. sec. 1.6 Eqs. (1.20), (1.28), (1.29)—the matrix elements would be

$$\jmath_{pq} = -\frac{iat}{\hbar}\sum_l \psi_p(l)\psi_q^*(l+1) - \psi_p(l+1)\psi_q^*(l)\,, \tag{A.16a}$$

$$\jmath^\epsilon_{pq} = +\frac{iat^2}{\hbar}\sum_l \psi_p(l-1)\psi_q^*(l+1) - \psi_p(l+1)\psi_q^*(l-1)\,, \tag{A.16b}$$

where a is the lattice constant, t the hopping amplitude and $\psi_p(l)$ are the eigenfunctions.

Starting from the relation (A.5) for the spin conductivity, plugging into it Eq. (A.14) for the spin current and using Wick's theorem [6–8] we arrive at

$$\sigma'_{\rm reg}(\omega) = \frac{\pi}{L}\mathcal{P}\left(\frac{1}{\omega}\right)\sum_{p,q}|\jmath_{pq}|^2(f_p-f_q)\delta(\epsilon_q-\epsilon_p-\hbar\omega)\,, \tag{A.17a}$$

$$\sigma''(\omega) = \frac{1}{L}\mathcal{P}\left(\frac{1}{\omega}\right)\left(\chi_0-\mathcal{P}\sum_{p,q}|\jmath_{pq}|^2\frac{f_p-f_q}{\epsilon_q-\epsilon_p-\hbar\omega}\right)\,, \tag{A.17b}$$

where f_p is the Fermi-Dirac distribution

$$f_p=\frac{1}{e^{\beta(\epsilon_p-\mu)}+1}\,, \tag{A.18}$$

with μ being the chemical potential. Similarly, for the thermal conductivity we arrive at

$$\kappa'_{\rm reg}(\omega) = \frac{\pi}{TL}\mathcal{P}\left(\frac{1}{\omega}\right)\sum_{p,q}|\jmath^{\epsilon}_{pq}|^2(f_p-f_q)\delta(\epsilon_q-\epsilon_p-\hbar\omega)\,, \tag{A.19a}$$

$$\kappa''(\omega) = \frac{1}{LT}\mathcal{P}\left(\frac{1}{\omega}\right)\left(\chi^{\epsilon}_0-\mathcal{P}\sum_{p,q}|\jmath^{\epsilon}_{pq}|^2\frac{f_p-f_q}{\epsilon_q-\epsilon_p-\hbar\omega}\right)\,. \tag{A.19b}$$

A.3 Analytic properties

Finally we would like to proceed with a few analytic properties for the conductivities, which are very useful and provide valuable information. We define two new quantities for each conductivity from the relations

$$\sigma_{\pm}(\omega)\equiv\lim_{\eta\to0}\frac{\sigma(z)\pm\sigma(z^*)}{2}\,,\quad \kappa_{\pm}(\omega)\equiv\lim_{\eta\to0}\frac{\kappa(z)\pm\kappa(z^*)}{2}\,. \tag{A.20}$$

It is not hard to observe from Eqs. (A.7), (A.10) that the complex spin and thermal conductivities will be given with the aid of the new quantities $\sigma_{\pm},\kappa_{\pm}$ by the integrals

$$\sigma(z)=\frac{i}{\pi}\int_{-\infty}^{\infty}\frac{\sigma_{\pm}(\omega')}{z-\omega'}d\omega'\,,\qquad \kappa(z)=\frac{i}{\pi}\int_{-\infty}^{\infty}\frac{\kappa_{\pm}(\omega')}{z-\omega'}d\omega'\,. \tag{A.21}$$

Virtually the quantities $\sigma_{\pm},\kappa_{\pm}$ are the real and the imaginary part of the conductivities (modulo the imaginary unit for the imaginary part)

$$\sigma_-(\omega) = \sigma'(\omega)\,,\qquad \sigma_+(\omega)=i\sigma''(\omega) \tag{A.22a}$$

$$\kappa_-(\omega) = \kappa'(\omega)\,,\qquad \kappa_+(\omega)=i\kappa''(\omega)\,. \tag{A.22b}$$

Combining Eqs. (A.21), (A.22) we arrive at the celebrated Kramers-Kronig relations which hold for any analytic complex function $f(z) = f'(z) + if''(z)$ and relate its real and imaginary parts (cf. Refs. [6, 7])

$$f(\omega) = \lim_{\eta\to 0} \frac{1}{i\pi} \int_{-\infty}^{+\infty} d\omega' \frac{f'(\omega')}{\omega' - \omega - i\eta} \tag{A.23a}$$

or

$$f(\omega) = \lim_{\eta\to 0} \frac{1}{\pi} \int_{-\infty}^{+\infty} d\omega' \frac{f''(\omega')}{\omega' - \omega - i\eta} \,. \tag{A.23b}$$

Kramers-Kronig relations are very important since the knowledge of only one part of a complex function, the real or the imaginary, is enough to determine the whole complex function.

The last property we would like to discuss, is the short time or high frequency expansion. Starting from (A.21) and taking $z \gg \omega'$ we can expand in powers of the small quantity ω'/z, arriving at

$$\sigma(z) = \frac{i}{\pi z} \sum_{n=0}^{\infty} \frac{\tilde{\sigma}_n}{z^n} \,, \qquad \kappa(z) = \frac{i}{\pi z} \sum_{n=0}^{\infty} \frac{\tilde{\kappa}_n}{z^n} \,, \tag{A.24}$$

where

$$\tilde{\sigma}_n = \int_{-\infty}^{\infty} \omega^n \sigma_{\pm}(\omega) d\omega \,, \qquad \tilde{\kappa}_n = \int_{-\infty}^{\infty} \omega^n \kappa_{\pm}(\omega) d\omega \,. \tag{A.25}$$

The meaning of the last relations is that in the high frequency regime, the complex conductivities are fully described by the frequency moments of either the real (even moments) or the imaginary (odd moments) part of the respective conductivity. Apparently the validity of this expansion over the frequency range depends on how many terms of it are taken into account.

Appendix B

Memory function approach

In this appendix we present in some detail the memory function perturbative approximation [4, 9, 10].

Assume a pure system, interacting or not, which is described by a Hamiltonian H_0 disturbed by a number of impurities. The total Hamiltonian of the system in the presence of impurities will be the sum of the unperturbed Hamiltonian and the perturbation one, say H_1, namely,

$$H = H_0 + H_1 \,. \tag{B.1}$$

We can define the memory function $\mathcal{M}(z)$ for a current $\jmath$, which denotes the decay rate of this current, using the susceptibility $\chi_{\jmath\jmath}(z)$ Eq. (A.2) as (cf. Ref. [4])

$$\mathcal{M}(z) \equiv z \frac{\chi_{\jmath\jmath}(z)}{\chi_0 - \chi_{\jmath\jmath}(z)} \,. \tag{B.2}$$

To express conductivities using memory functions we invert the formula above to obtain the susceptibility and substitute it into the definition for the spin(or particle for the non interacting case), energy conductivities (A.5). From this follows that the spin, energy conductivities can be written using the memory functions $M(z)$, $N(z)$ as

$$\sigma(z) = \frac{i(\chi_0^s/L)}{z + M(z)} \,, \quad \kappa(z) = \frac{1}{T} \frac{i(\chi_0^\epsilon/L)}{z + N(z)}, \tag{B.3}$$

where $M(z)$, $N(z)$ are defined from the spin, energy current susceptibility respectively. Note that Eqs. (B.3) are exact since we have not used any approximations. The knowledge of the real part of the conductivities Eqs. (A.7b), (A.10b) with the aid of the Kramers-Kronig relations (A.23a) enables the extraction of the memory function from the conductivity by inverting (B.3).

If the respective current is a constant of motion in the pure system and the system is weakly coupled with the perturbation we expect a smooth imaginary part for the memory function at low frequencies where ω is comparable with the magnitude of $\mathcal{M}$ and approximately equal with its static limit $\mathcal{M}(\omega) \simeq \mathcal{M}(\omega \to 0)$,

$$\frac{1}{\tau^s} \sim M''(\omega \to 0) \,, \qquad \frac{1}{\tau^\epsilon} \sim N''(\omega \to 0) \,, \tag{B.4}$$

where $1/\tau^{s,\epsilon}$ are the corresponding scattering rates. In addition, at low frequencies the real part is not expected to have a substantial contribution to the conductivity, viz.,

$$\omega + M'(\omega) \simeq \omega \,, \qquad \omega + N'(\omega) \simeq \omega \,. \tag{B.5}$$

Combining Eqs. (B.3), (B.4), (B.5) one arrives at a Lorentzian form for the conductivities and a Drude-like behavior, i.e.,

$$\sigma'(\omega) = \frac{\sigma_{dc}}{1 + (\omega\tau^s)^2} \,, \qquad \kappa'(\omega) = \frac{\kappa_{dc}}{1 + (\omega\tau^\epsilon)^2} \,. \tag{B.6}$$

Assume again the generic current operator $\jmath$ which is a conserved quantity in the unperturbed system described by the Hamiltonian H_0. It is evident from the definition of the susceptibility that it vanishes in the absence of impurities and so does the corresponding memory function. Assuming a dilute concentration of impurities c_I and neglecting higher order in concentration terms in equation (B.2) we have

$$z\chi_{\jmath\jmath}(z) = \chi_0 \mathcal{M}(z) + \mathcal{O}(c^2) \,. \tag{B.7}$$

Using twice the equation of motion for the susceptibility $\chi_{\hat{O}_p\hat{O}_q}(z)$,

$$iz\chi_{\hat{O}_p\hat{O}_q}(z) = -\frac{i}{\hbar}\langle[\hat{O}_p, \hat{O}_q]\rangle - \chi_{f^p\hat{O}_q}(z) \,, \tag{B.8}$$

where the force operator f, is the time derivative of the operator $\hat{O}$,

$$f = \frac{i}{\hbar}[H, \hat{O}], \tag{B.9}$$

we have the expression for the current-current susceptibility

$$\chi_{\jmath\jmath}(z) = \frac{1}{z^2}\left(\chi_{ff}(z) - \chi_{ff}(0)\right) \,. \tag{B.10}$$

In first order we can evaluate the force-force susceptibility for a single impurity, which will be chosen to be located at the origin of the lattice, and then multiply it with the number of impurities $N_I = c_I L$. Finally, using (B.7) and (B.10) we will have for the memory function

$$\mathcal{M}_0(z) = \frac{N_I}{z\chi_0}(\chi_{ff}(z) - \chi_{ff}(0)) + \mathcal{O}(c^2) \,, \tag{B.11}$$

where force-force correlations are calculated in the unperturbed system, therefrom the subscript 0 at the memory function.

It is expected that the perturbation theory breaks down in cases where the perturbation is coupled strongly with the system even if the concentration is small. Another case where the perturbation theory fails is when the current $\jmath$ is not a constant of motion in the unperturbed system since the expansion (B.7) will not be valid.

Appendix C

Numerical techniques

Numerical diagonalization techniques like the (full) exact diagonalization (ED) [11] , the microcanonical Lanczos method (MCLM) [12] and the finite temperature Lanczos method (FTLM) [13] are used in order to compute the transport quantities described in Appx. A, B. In this appendix we discuss briefly the numerical techniques that are used.

In order to evaluate transport quantities like conductivities or memory functions we need to know the energy spectrum, the whole or part of it, and the matrix elements of the corresponding operators. In order to proceed we construct the quantum mechanical operators using the S^z operator's eigenstates

$$S^z|m\rangle = m|m\rangle \,,$$

which are represented with a $(2S+1)$-base number. For instance for a spin $S = 1/2$ we have two states, 0 for spin down and 1 for spin up. More generally for a many spin system these states will be a binary string, viz.,

$$|S + m_1, S + m_2, \ldots\rangle \,.$$

Using these many spin states we construct the operators that we are interested in and diagonalize the Hamiltonian to obtain the energy spectrum and the corresponding energy eigenstates. ED is the most trivial case, where the full diagonalization of the Hamiltonian provides the whole spectrum and the complete set of eigenstates. On the contrary, Lanczos methods (FTLM, MCLM) provide eigenvalues in a truncated space thus we obtain only a part of the spectrum. While with FTLM one can obtain dynamical quantities at finite temperatures in the canonical ensemble, MCLM functions in the microcanonical ensemble targeting on an eigenstate λ which energy would be equal with the mean value of the Hamiltonian at a given temperature. MCLM works better at high temperatures while FTLM at intermediate-finite temperatures.

The major problem of a many body system to be handled numerically is the rapid increase of the Hilbert space. In the minimal case of L spins-1/2 the dimension of the Hilbert space increases with the lattice sites as $\mathcal{D}_H = 2^L$. A consequence of this is that small lattices already exhaust the computational limitations. Considering only

states that belong in the $S^z_{\rm total} = 0$ subsector, where we have the largest number of states, enables us to diagonalize a little larger systems. Within this subsector we can fully diagonalize systems up to $L = 16$ spin-1/2 for which the number of states is of the order of $\mathcal{N} \sim 10^4$, while with Lanczos methods we can go up to $L = 24$ spin-1/2 corresponding to a number of states of the order $\mathcal{N} \sim 10^6$.

Finally, to obtain quantities that characterize the transport properties of the spin system we calculate the regular part of the real part of the conductivities from (A.7b), (A.10b) and perturbative memory function from an analogous formula that we obtain starting from (B.11). To handle the δ-functions we bin the excitation frequencies in windows of width $\delta\omega$; typically $\delta\omega \simeq 0.01$. Next, using the Kramers-Kronig relations (A.23) we obtain both parts of the complex function that we are interested in. Kramers-Kronig relations except of allowing to calculate the unknown part of a complex function have an effect also in the known part, the one that is used in the integrand. This effect is that it introduces a smoothing which could be rather useful and necessary as well for jagged spectra, but also dangerous since narrow peaks could be washed out. Finally, we use (B.3) to obtain either memory function for the full system or conductivities from perturbation theory. The quantities $\chi^s_0, \chi^\epsilon_0$ can be evaluated either by (A.13) or from the thermodynamic average of the squared current at high temperatures.

Bibliography

[1] R. Kubo, Statistical-Mechanical Theory of Irreversible Processes. I. General Theory and Simple Applications to Magnetic and Conduction Problems, Journal of the Physical Society of Japan **12**(6), 570–586 (1957).

[2] J. M. Luttinger, Theory of Thermal Transport Coefficients, Physical Review **135**(6A), A1505–A1514 (Sep 1964).

[3] B. S. Shastry, Sum rule for thermal conductivity and dynamical thermal transport coefficients in condensed matter, Physical Review B **73**(8), 085117 (2006).

[4] W. Götze and P. Wölfle, Homogeneous Dynamical Conductivity of Simple Metals, Physical Review B **6**(4), 1226–1238 (Aug 1972).

[5] X. Zotos and P. Prelovšek, Evidence for ideal insulating or conducting state in a one-dimensional integrable system, Physical Review B **53**(3), 983–986 (Jan 1996).

[6] E. N. Economou, *Green's Functions in Quantum Physics*, Springer, July 2006.

[7] G. C. Psaltakis, *Quantum Many-Particle Systems*, Crete University Press, November 2008, (published in greek).

[8] S. Doniach and E. Sondheimer, *Green's functions for solid state physicists*, Imperial College Press, 2004.

[9] H. Mori, Transport, Collective Motion, and Brownian Motion, Progress of Theoretical Physics **33**(3), 423–455 (1965).

[10] H. Mori, A Continued-Fraction Representation of the Time-Correlation Functions, Progress of Theoretical Physics **34**(3), 399–416 (1965).

[11] S. E. Koonin and D. C. Meredith, *Computational Physics*, Redwood City, CA, USA, 1990.

[12] M. W. Long, P. Prelovšek, S. El Shawish, J. Karadamoglou, and X. Zotos, Finite-temperature dynamical correlations using the microcanonical ensemble and the Lanczos algorithm, Physical Review B **68**(23), 235106 (Dec 2003).

[13] J. Jaklič and P. Prelovšek, Finite-temperature properties of doped antiferromagnets, Advances in Physics **49**, 1–92 (2000).

The NOVMAG project

This work was financially supported by the FP6-032980-2 NOVMAG[†] project (full title: *Novel magnetic mode heat transport for thermal management in microelectronics*). The NOVMAG project is a consortium of several European research teams aiming to investigate a novel heat transport mode, namely, heat transport via magnetic excitations.

More particularly, magnetic heat transport occurs in a wide variety of materials. It appears that some of these materials—at least the ones that the NOVMAG participants are mostly interested in—exhibit a very high and anisotropic thermal conductivity. As a matter of fact, the thermal conductivity along one crystal axis is of metallic order, or even higher, while in the transverse directions is orders of magnitude smaller. The origin of the anisotropy of the thermal conductivity and its high value is attributed to the formation of low dimensional spin structures, i.e., heat transport occurs via localized magnetic moments. The anisotropy in heat transport holds for a wide range of temperatures, including room temperature. Moreover, the nature of this novel transport mode, the fact that heat propagates via localized moments, makes tunable thermal transport viable using mechanical means. Last but not least, we mention that these materials are electric insulators; hence, unlike the ordinary electronic contribution, they exhibit thermal conductivity of metallic order while on the other hand they are electric insulators.

The combination of the characteristics described above, viz.:

a) high and anisotropic thermal conductivity

b) electric insulator

c) origin: localized magnetic moments

makes these materials very promising for technological applications. One such application could be the effective removal of parasitic heat in electronic devices generated by integrated semiconductor circuits. As shown in Fig. C.1, these materials could be placed as substrates underneath a hotspot, since they are electric insulators, to carry away the generated heat preventing diffusion throughout the device. This could lead either to the reduction of the volume of electronic devices or to increase the density of integrated circuits per volume, or to prolong the time of life of the electronic circuits.

[†]http://www.novmag.eu

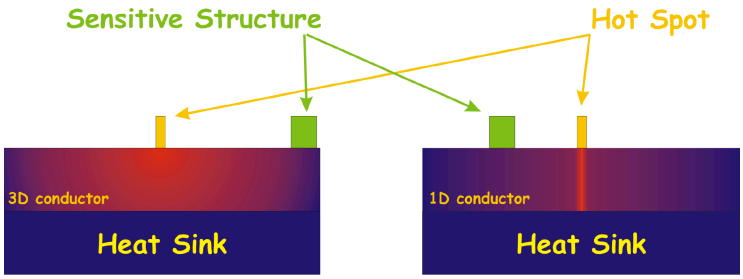

Figure C.1: Schematic illustration of parasitic heat removal via a conventional 3D conductor (left) and a novel quasi-one-dimensional conductor (right).

Furthermore, besides its technological interest these systems offer a fertile ground for fundamental research, both theoretical and experimental. In order to explore the new mode of heat transport and moreover to exploit the unconventional thermal transport properties of these systems the NOVMAG project comprises experimental and theoretical teams. The expertise of the research participants in addition with fruitful collaborations which have arisen during the past few years have led to several publications [1–16] and [17–19]. Below we give the list of the partners participating in the NOVMAG project and a brief description of their field of research.

1. Leibniz Institute for Solid State and Materials Research Dresden, Germany
   - thermal conductivity studies and temperature profile measurements on bulk samples and thin films
   - *url* : http://www.ifw-dresden.de *Leader* : Dr. Christian Hess*
2. Univerité Paris Sud, France
   - single crystal growing of novel quasi-one-dimensional materials
   - *url* : http://www.u-psud.fr *Leader* : Prof. Alexandre Revcolevschi
   - fabrication of epitaxial thin films and thermal conductivity measurements
   - *url* : http://www.ucy.ac.cy *Leader* : Prof. John Giapintzakis
3. Rijksuniversiteit Groningen, Netherlands
   - optical, magneto-optical measurements, local temperature profile measurements, heat and magnetization transport measurements
   - *url* : http://www.rug.nl *Leader* : Prof. Paul van Loosdrecht
4. Foundation of Research and Technology - Hellas, Greece
   - analytical and numerical studies in microscopic level

*coordinating partner

- *url* : http://www.forth.gr *Leader* : Prof. Xenophon Zotos

5. Jožef Stefan Institute, Slovenia

   - analytical and numerical studies in microscopic level, development of numerical techniques, theoretical studies of optical properties
   - *url* : http://www.ijs.si *Leader* : Prof. Peter Prelovšek

6. ASCOMP GmbH, Switzerland

   - large scale heat transport simulations
   - *url* : http://www.ascomp.ch *Leader* : Dr. Djamel Lakehal

NOVMAG publications

[1] C. Hess, Heat conduction in low-dimensional quantum magnets, The European Physical Journal - Special Topics **151**, 73–83 (Dec 2007).

[2] M. S. Hawkins, M. W. Long, and X. Zotos, Long-time asymptotics and conservation laws in integrable systems, ArXiv e-prints (Dec 2008), cond-mat.str-el/0812.3096.

[3] A. R. Kolovsky, Atomic current in optical lattices: Reexamination of the Esaki-Tsu equation, Physical Review A **77**(6), 063604 (Jun 2008).

[4] A. R. Kolovsky, Interplay between Anderson and Stark Localization in 2D Lattices, Physical Review Letters **101**(19), 190602 (Nov 2008).

[5] M. Pervolaraki, G. Athanasopoulos, R. Saint-Martin, A. Revcolevschi, and J. Giapintzakis, KrF pulsed laser deposition of $La_5Ca_9Cu_{24}O_{41}$ thin films on various substrates, Applied Surface Science **255**(10), 5236 – 5239 (2009), Laser and Plasma in Micro- and Nano-Scale Materials Processing and Diagnostics - Proceedings from the European Material Research Society Spring Meeting 2008 - Symposium B.

[6] A. R. Kolovsky, Conductivity with cold atoms in optical lattices, Journal of Statistical Mechanics: Theory and Experiment **2009**(02), P02018 (2009).

[7] M. Otter, V. Krasnikov, D. Fishman, M. Pshenichnikov, R. Saint-Martin, A. Revcolevschi, and P. van Loosdrecht, Heat transport imaging in the spin-ladder compound $Ca_9La_5Cu_{24}O_{41}$, Journal of Magnetism and Magnetic Materials **321**(7), 796 – 799 (2009), Proceedings of the Forth Moscow International Symposium on Magnetism.

[8] J. Kokalj and P. Prelovšek, Finite-temperature dynamics with the density-matrix renormalization group method, Physical Review B **80**(20), 205117 (Nov 2009).

[9] N. Hlubek, P. Ribeiro, R. Saint-Martin, A. Revcolevschi, G. Roth, G. Behr, B. Büchner, and C. Hess, Ballistic heat transport of quantum spin excitations as seen in $SrCuO_2$, Physical Review B **81**(2), 020405 (Jan 2010).

[10] N. Hlubek, M. Sing, S. Glawion, R. Claessen, S. van Smaalen, P. H. M. van Loosdrecht, B. Büchner, and C. Hess, Heat conductivity of the spin-Peierls compounds TiOCl and TiOBr, Physical Review B **81**(14), 144428 (Apr 2010).

[11] X. Zotos, On the nonlinear response of a particle interacting with fermions in a 1D lattice, ArXiv e-prints (Apr 2010), cond-mat.str-el/1004.4353.

[12] J. H. Jefferson, A. Ramak, and T. Rejec, Entanglement and transport anomalies in nanowires, Journal of Physics: Condensed Matter **20**(16), 164206 (2008).

[13] G. Athanasopoulos, E. Svoukis, M. Pervolaraki, R. Saint-Martin, A. Revcolevschi, and J. Giapintzakis, Thermal conductivity of Ni, Co, and Fe-doped La5Ca9Cu24O41 thin films measured by the 3ω method, Thin Solid Films **518**(16), 4684 – 4687 (2010), Proceedings of the EMRS 2009 Spring Meeting Symposium H: Synthesis, Processing and Characterization of Nanoscale Multi Functional Oxide Films II.

[14] D. Lakehal, Advances in Computational Heat Transfer & Two-Phase Flow based on Direct Interface Tracking, 5th Int. Conf. Transport Phenomena in Multiphase Systems -HEAT5, 2009.

[15] M. Pervolaraki, J. Giapintzakis, G. Socol, N. Stefan, F. Sima, C. G. Ristoscu, I. Mihailescu, A. M. Vlaicu, R. Saint-Martin, and R. A., Epitaxial like thin films of $La_5Ca_9Cu_{24}O_{41}$ grown on MgO and $SrTiO_3$ substrates using PLD, Proceedings of Symposium I, Functional and Structural Ceramic and Ceramic Matrix Composites, E-MRS 2008 Fall Meeting, September 15-19, 2008, Warsaw, Poland.

[16] G. I. Athanasopoulos, E. C. Svoukis, M. Pervolaraki, and J. Giapintzakis, Thermal conductivity measurements of $La_5Ca_9Cu_{24}O_{41}$ thin films using the 3ω method, Proceedings of Symposium I, Functional and Structural Ceramic and Ceramic Matrix Composites, E-MRS 2008 Fall Meeting, September 15-19, 2008, Warsaw, Poland.

[17] O. S. Barišić, P. Prelovšek, A. Metavitsiadis, and X. Zotos, Incoherent transport induced by a single static impurity in a Heisenberg chain, Physical Review B **80**(12), 125118 (Sep 2009).

[18] A. Karahalios, A. Metavitsiadis, X. Zotos, A. Gorczyca, and P. Prelovšek, Finite-temperature transport in disordered Heisenberg chains, Physical Review B **79**(2), 024425 (Jan 2009).

[19] A. Metavitsiadis, X. Zotos, O. S. Barišić, and P. Prelovšek, Thermal transport in a spin- $\frac{1}{2}$ Heisenberg chain coupled to a magnetic or nonmagnetic impurity, Physical Review B **81**(20), 205101 (May 2010).

List of Figures

Index